Identification and chemogenetic profiling of two antimicrobial auranofin analogs in *B. cenocepacia* K56-2

by

Dustin Troy Nelson Maydaniuk

A Thesis submitted to the Faculty of Graduate Studies of the University of Manitoba in partial fulfilment of the requirements of the degree of

MASTER OF SCIENCE

Department of Microbiology

University of Manitoba

Winnipeg, Manitoba, Canada

ABSTRACT

The *Burkholderia cepacia* complex (Bcc), a group of Gram-negative multi-drug resistant pathogens are notorious for causing persistent lung infections in people with cystic fibrosis and new antibiotics are needed to treat these infections. One way to find new antimicrobials is to repurpose old drugs for a new use. One such example of this auranofin, which has antimicrobial activity against Gram-positive bacteria, with low to no activity against Gram-negatives. Thus, to create novel antimicrobials for Gram-negatives, specifically *Burkholderia cenocepacia*, we synthesized chemical analogs of auranofin. I hypothesize auranofin analogs that will be bactericidal against *B. cenocepacia* K56-2 and other CF pathogens and that the mechanism of action of these antimicrobials can be determined through randomly barcode transposon sequencing (BarSeq). Two auranofin analogs with bactericidal activity against *B. cenocepacia* determined their mechanism of action. The two auranofin analogs are bactericidal, do not select for resistance, kill persisters, and are well-tolerated by *C. elegans* and *Galleria* in toxicity tests. They also inhibit the enzyme thioredoxin reductase. Interestingly, they do not inhibit the structurally and functionally similar protein glutathione reductase. The compounds also cause an increase in reactive oxygen species upon exposure. BarSeq identified the mechanism of action of these compounds include the glutathione system, potentially by protecting from the increase in reactive oxygen species, and purine metabolism, by altering the metabolic state of the bacterium. Thus, we have determined the mechanism of action of these novel therapeutics. We have also shown that BarSeq is able to determine the mechanism of action of novel antimicrobials.

ACKNOWLEDGEMENTS

I want to start by saying a huge thank you to my supervisor Dr. Silvia Cardona. Silvia, you have always supported every decision I made and allowed me to pursue every idea I had in my research and for that I will be forever grateful. We have learned a lot about each other throughout my time in your lab and have talked about a lot of serious issues and our relationship has definitely grown because of it. Thank you is not enough.

I would also like to thank my amazing and supportive committee members, Dr. Gerd Prehna, Dr. Frank Schweizer, and Dr. Denice Bay. You have given me a lot of guidance and help throughout my journey. I would also like to thank our collaborator at the University of Massachusetts Lowell, Dr. Mingdi Yan.

To the present and past Cardona lab members. You made going into the lab each day a fun time and I am going to miss spending every day with all of you. Thank you to Dr. Andrew Hogan for training me when I first got to the lab and for the constant guidance and advice, you have definitely made me into the scientist I am today. Thank you to Dr. Anna Motnenko, Zisan Rahman, Zhong Ling Yap, Becca Lohmann, Zayra Batun, and Jules Novomisky Nechcoff for the countless hours of question-and-answer sessions and everything in between. To the two undergrads I mentored, Brielle Martens and Sarah Iqbal, thank you for questioning me at every step, as this helped me grow as a scientist. Again, to everyone in my Cardona Lab family, thank you and I will forever cherish our time together and all the times we played Wordle and Squardle in the lunchroom, y'all will always be in my heart.

To everyone in the Department of Microbiology who I asked for help, borrowed equipment, borrowed chemicals, and everything else, thank you so much. This is such an amazing department with a bunch of brilliant people. I am truly lucky to know every one of you.

I would also like to thank my funding sources that have made this work possible over the years: CIHR, Cystic Fibrosis Canada, UofM Faculty of Science and Faculty of Graduate Studies.

To my family and friends who listened to me talk about my research, thank you for supporting me and being there for me through the good and bad times. I could not have been able finish this journey without each and every one of you in my life and in my heart.

Lastly, I need to send a huge thank you to my partner, Evan. You have always been there for me and I will forever be grateful. Thank you for coming to the lab with me on the weekends while I made a "5-minute overnight" or "just need to take out a few plates". Thank you for allowing me to practice every presentation in front of you, even though you had no idea of what I am talking about.

DEDICATION

I dedicate this to my husband, Evan Maydaniuk.

TABLE OF CONTENTS

ABSTRACT ***2***

ACKNOWLEDGEMENTS ***3***

DEDICATION ***5***

TABLE OF CONTENTS ***6***

PERMISSIONS ***10***

AUTHOR CONTRIBUTIONS ***11***

LIST OF TABLES ***12***

LIST OF FIGURES ***13***

LIST OF ABBREVIATIONS ***16***

CHAPTER 1: LITERATURE REVIEW ***19***

1.1 *Burkholderia cenocepacia* and cystic fibrosis **19**

1.1.1 The genus Burkholderia 19

1.1.2 Cystic fibrosis and bacterial pathogens 20

1.1.3 Antibiotic resistance in Burkholderia species 23

1.2 Auranofin analogs as antimicrobials **26**

1.2.1 Repurposing auranofin 26

1.2.3 Auranofin analogs 29

1.3 Thioredoxin and glutathione system **30**

1.3.1 Thioredoxin system 30

1.3.2 Glutathione system 32

1.4 Next generation sequencing and transposon mutagenesis to find mechanism of action 36

1.4.1 Global effects of antibiotics beyond the target 36

1.4.2 Next generation sequencing 37

1.4.3 Transposon sequencing to find mechanism of action 40

1.5 Rationale and Hypothesis 44

1.6 Objectives 44

CHAPTER 2: MATERIAL AND METHODS 46

2.1 Primers, plasmids, and strains used 46

2.2 Synthesis of Auranofin and Auranofin Analogs 56

2.3 Auranofin Analogs and Antibiotic Stock Solutions 58

2.4 Antimicrobial Susceptibility Testing and Multistep Resistance to Active Analogs 58

2.5 Time Kill Assays 59

2.6 Time Kill of Persister Cells 60

2.7 Persister Frequency Assay 60

2.8 *C. elegans* Survival 61

2.9 *Galleria* Toxicity 61

2.10 CRISPRi Mutant Construction 62

2.11 Thioredoxin Reductase Purification and Inhibition Assay 62

2.12 NPN Permeability Assay 63

2.13 Glutathione Reductase Purification and Inhibition Assay 64

2.14 ROS Detection **64**

2.15 Microscopy **65**

2.16 Barcoded Transposon Mutant Pool Exposure, Library Preparation, and Sequencing **66**

2.17 Fitness Calculation for BarSeq **67**

2.18 BioCyc Pathway Perturbation Score and Pathway Enrichment **68**

2.19 Unmarked Gene Deletions **68**

2.20 Growth Detection of Glutathione Mutants **69**

2.21 ATP Detection of Exponential Phase Cells Exposed to MS-40 and MS-40S **69**

CHAPTER 3: RESULTS ***71***

3.1 Analogs of Auranofin have lower MICs than Auranofin **71**

3.2 MS-40 and MS-40S have Broad Bactericidal Activity from **77**

3.3 MS-40 and MS-40S do not Select for Multistep Resistant Mutants **79**

3.4 MS-40 and MS-40S are Bactericidal against Both Replicating and Non-Replicating Cells by Time Kills **81**

3.5 MS-40 and MS-40S Kill and Inhibit the Formation of Persister Cells from Time Kills and Persister Frequency Assays **83**

3.6 MS-40 and MS-40S are non-toxic in *C. elegans* and *G. mellonella* Model Toxicity Assay's **87**

3.7 Auranofin may be Inactive in *Burkholderia cenocepacia* Due to High Efflux and not the Presence of Glutathione Reductase **89**

3.8 MS-40 and MS-40S Cause an Increase in Reactive Oxygen Species (ROS) **106**

3.9 BarSeq Analysis of Cells Exposed to MS-40, MS-40S, and other ROS Inducers 108

3.10 BioCyc Analysis Identifies Glutathione and Purine Biosynthesis in the MOA of MS-40 and MS-40S 114

3.11 Reactive Oxygen Species Related Genes and their Fitness Values in BarSeq 120

3.12 Glutathione biosynthetic pathway is involved in protection against MS-40 and MS-40S 123

3.13 Disrupting Purine Metabolism Leads to Decreased Susceptibility to MS-40 and MS-40S 128

CHAPTER 4: DISCUSSION 131

4.1 Identification of MS-40 and MS-40S and their activity 131

4.2 Mechanism of Action of MS-40 and MS-40S 133

CHAPTER 5: CONCLUSION AND FUTURE DIRECTIONS 139

CHAPTER 6: APPENDIX 140

REFERENCES 156

PERMISSIONS

Figures, tables and passages within this thesis have been adapted from published works in academic journals that I have authored.

Maydaniuk, D.; Wu, B.; Truong, D.; Liyanage, S.H.; Hogan, A.M.; Yap, Z.L.; Yan, M.; Cardona, S.T. New Auranofin Analogs with Antibacterial Properties against Burkholderia Clinical Isolates. Antibiotics 2021, 10, 1443. https:// doi.org/10.3390/antibiotics10121443

AUTHOR CONTRIBUTIONS

Multiple authors contributed to the work described in Chapters 3. Bin Wu, Dang Truong, and Sajani H. Liyanage synthesized auranofin and auranofin analogs. Brielle Martens performed the ROS detection of MS-40 and MS-40S, as well as ATP detection assays. Sarah Iqbal performed the CRISPRi mutant MICs with MS-40 and MS-40S and also ROS detection of purine CRISPRi mutants.

While these individuals performed the experiments, they worked under my supervision, and I was responsible for the experimental designs, data analysis, and interpretation of the results.

LIST OF TABLES

Table 1. Primers used in this study. 46

Table 2. Plasmids used in this study 53

Table 3. Strains and mutants used in this study. 54

Table 4. Broth microdilution minimum inhibitory concentrations (MICs) of group one auranofin analogs against a panel of *Burkholderia cepacia* complex (Bcc) species . 73

Table 5. Broth microdilution minimum inhibitory concentrations (MICs) of group two auranofin analogs against a panel of *Burkholderia cepacia* complex (Bcc), *B. mallei* and *B. pseudomallei* . 76

Table 6. Broth microdilution minimum inhibitory concentrations (MICs) of MS-40 and MS-40S compared to clinical antibiotics used to treat CF patients. 76

Table 7. MS-40 and MS-40S are bactericidal against other bacteria that infect CF patients from broth microdilution assay. 78

Table 8. Percent survival of *C. elegans* exposed to MS-40, MS-40S, and clinical antibiotics by a *C. elegans* toxicity assay. 88

Table 9. Percent survival of *Galleria mellonella* larvae exposed to doxycycline (DOX) MS-40, and MS-40S by a *Galleria* toxicity assay. 88

Table 10. Inhibitory Concentrations of ROS inducers, with known mechanism of action, used in BarSeq. 109

Table 11. Minimum inhibitory concentration and minimum bactericidal concentration of *gshA1B* CRISPRi mutant against bactericidal antibiotics using broth microdilution assays. 127

LIST OF FIGURES

Figure 1. Structure of auranofin and its mechanism of action. 28

Figure 2. Thioredoxin system in *B. cenocepacia* K56-2. 32

Figure 3. Glutathione system in *B. cenocepacia* K56-2. 35

Figure 4. BarSeq to find antimicrobial's mechanism of action. 42

Figure 5. Chemical structure of auranofin and auranofin analogs. 72

Figure 6. Mutational resistance is not generated to MS-40 and MS-40S from spontaneous resistance assay. 80

Figure 7. Exponential and stationary time kills of *Burkholderia cenocepacia* K56-2. 82

Figure 8. MS-40 and MS-40S kills and inhibits the formation of persister cells from persister time kills and persister frequency assays. 85

Figure 9. Expression Trial of pET-24b-TrxB. 91

Figure 10. Purification of TrxB. 92

Figure 11. Size exclusion chromatography of TrxB. 93

Figure 12. Size exclusion chromatography of TrxB on an acrylamide gel. 94

Figure 13. Auranofin inhibits TrxB *in vitro* but not *in vivo* from TrxB inhibition assays and enhanced susceptibility assays. 96

Figure 14. Expression Trial of pET-22-GOR. 99

Figure 14. Purification of GOR. 100

Figure 15. Size exclusion chromatography of GOR. 101

Figure 16. Size exclusion chromatography of GOR on an acrylamide gel. 102

Figure 17. Auranofin, MS-40, nor MS-40S inhibit GOR and auranofin may be inactive due to high efflux from CRISPRi susceptibility assays. 105

Figure 18. ROS Detection of *B. cenocepacia* K56-2 exposed to MS-40 and MS-40S. 107

Figure 19. Mutants with significant altered fitness scores for each compound used in BarSeq. 112

Figure 20. Comparison of BarSeq data of MS-40 and MS-40S with the benchmarking compounds. 113

Figure 21. BioCyc pathway enrichment with BarSeq data with positive fitness. 116

Figure 22. BioCyc pathway enrichment with BarSeq data with negative fitness 117

Figure 23. BioCyc pathway perturbation score with BarSeq data with positive fitness. 118

Figure 24. BioCyc pathway perturbation score with BarSeq data with negative fitness. 119

Figure 25. Mutant fitness profile for ROS related mutants in BarSeq. 122

Figure 26. Glutathione system may be involved in the MOA of MS-40 and MS-40S. 125

Figure 27. Disrupting purine biosynthesis leads to decreased susceptibility to MS-40 and MS-40S. 130

Figure A1. ^{1}H NMR spectrum of compound WB-19-HL4170 (MS-40S) in $CDCl_3$. 140

Figure A2. ^{13}C NMR spectrum of compound WB-19-HL4170 (MS-40S) in $CDCl_3$. 141

Figure A3. ^{31}P NMR spectrum of compound WB-19-HL4170 (MS-40S) in $CDCl_3$. 142

Figure A4. ^{1}H NMR spectrum of compound WB-19-HL4171 in $CDCl_3$. 143

Figure A5. ^{13}C NMR spectrum of compound WB-19-HL4171 in $CDCl_3$. 144

Figure A6. ^{31}P NMR spectrum of compound WB-19-HL4171 in $CDCl_3$. 145

Figure A7. ^{1}H NMR spectrum of compound WB-19-HL4172 in $CDCl_3$. 146

Figure A8. ^{13}C NMR spectrum of compound WB-19-HL4172 in $CDCl_3$. 147

Figure A9. ^{31}P NMR spectrum of compound WB-19-HL4172 in $CDCl_3$. 148

Figure A10. ^{1}H NMR spectrum of compound WB-19-HL4181 in $CDCl_3$. 149

Figure A11. ^{13}C NMR spectrum of compound WB-19-HL4181 in $CDCl_3$. 150

Figure A12. ^{31}P NMR spectrum of compound WB-19-HL4181 in $CDCl_3$. 151

Figure A13. ^{1}H NMR spectrum of compound WB-19-HL4121a in CD_2Cl_2. 152

Figure A14. ^{31}P NMR spectrum of compound WB-19-HL4121a in CD_2Cl_2. 153

Figure A15. Susceptibility tests of CRISPRi mutants with MS-40 and MS-40S. 154

Figure A16. ROS detection of glutathione related mutants. 155

LIST OF ABBREVIATIONS

ABC	ATP-binding cassette
AF	Auranofin
ATP	Adenosine triphosphate
BarSeq	Barcode sequencing
Bcc	*Burkholderia cepacia* complex
CAMHB	Cation adjusted Mueller Hinton broth
CAZ	Ceftazidime
CF	Cystic fibrosis
CIP	Ciprofloxacin
CRISPRi	Clustered regularly interspaced short palindromic repeats interference
CZA	Ceftazidime/avibactam
CFTR	Cystic fibrosis transmembrane conductance regulator
DMSO	Dimethyl sulfoxide
DNA	Deoxyribonucleic acid
DOX	Doxycycline
GOR	Glutathione reductase
Grx	Glutaredoxin
GSH	Reduced glutathione
GSSG	Oxidized glutathione
HDTM	High density transposon mutant
H_2O_2	Hydrogen peroxide

ICx	Inhibitory concentration X%
IPTG	Isopropyl β-D-1-thiogalactopyranoside
LB	Lysogeny broth
LPS	Lipopolysaccharide
M9	M9 minimal media
MDR	Multi-drug resistant
MEM	Meropenem
MIC	Minimum inhibitory concentration
MBC	Minimum bactericidal concentration
MFS	Major facilitator superfamily
MOA	Mechanism of action
NADPH	Nicotinamide adenine dinucleotide phosphate (reduced)
NBD	Nuclear binding domain
NGM	Nematode growth media
NGS	Next generation sequencing
PBS	Phosphate buffered saline
PCR	Polymerase chain reaction
Rha	L-rhamnose
RND	Resistance-nodulation division
ROS	Reactive oxygen species
RNS	Reactive nitrogen species
SCV	Small colony variant
TET	Tetracycline

TnSeq	Transposon sequencing
TOB	Tobramycin
TrxR	Thioredoxin reductase
WT	Wild type

CHAPTER 1: LITERATURE REVIEW

1.1 *Burkholderia cenocepacia* and cystic fibrosis

1.1.1 The genus Burkholderia

The first identification of the *Burkholderia* genus was in 1950 by W. H. Burkholder, and was found to be the causative agent of soft onion rot (Burkholder 1950; Mahenthiralingam et al. 2005). The genus *Burkholderia* has grown ever since to now containing over 120 species (https://www.bacterio.net/genus/burkholderia). *Burkholderia* was initially classified as *Pseudomonas cepacia* but it wasn't until 1992 that the genus *Burkholderia* was named and seven species were included in it that were originally named *Pseudomonas* (Yabuuchi et al. 1992; Coenye et al. 2001), which moved these species from the phylum γ-proteobacteria to β-proteobacteria. These species were *Burkholderia cepacia*, *Burkholderia mallei*, *Burkholderia pseudomallei*, *Burkholderia caryophylli*, *Burkholderia gladioli*, *Burkholderia pickettii*, and *Burkholderia solanacearum* (Yabuuchi et al. 1992). However, two of these seven species were transferred to the genus *Ralstonia*, these were *B. solanacearum* and *B. pickettii* (Yabuuchi et al. 1992).

In 1997 *B. cepacia*, which was considered one species, was split into several genomovars, which represent species that are phenotypically similar, but genotypically distinct (Vandamme et al. 1997). These species are now termed the *Burkholderia cepacia* complex (Bcc). Now, the Bcc contains over 20 species and all are opportunistic pathogens in immunocompromised patients (Eberl and Vandamme 2016), with *Burkholderia cenocepacia* and *Burkholderia multivorans* being the most common and causes the most serious lung infections in patients with the genetic disease

cystic fibrosis (LiPuma 2010). Advancement in DNA sequencing further divided the *Burkholderia* genus when the genus was split into two genera: first was *Burkholderia*, which contain clinically relevant human and plant pathogens, and second was *Paraburkholderia*, which consist of other environmental species (Sawana et al. 2014). However, this division is not accepted by all individuals in the field of *Burkholderia* research.

Burkholderia species can survive in many different environmental niches, such as soil, the rhizosphere, and water (Bazzini et al. 2011; Eberl and Vandamme 2016). In the soil, *Burkholderia* are outcompeted in alkaline soils but are fierce competitors in acidic soils due to the intrinsic acid tolerance of these species (Stopnisek et al. 2014; Eberl and Vandamme 2016). There is also a various degree of *Burkholderia* and plant dependence. *Burkholderia* can exist as free living organisms in the rhizosphere, nodulating legumes, and also obligate lead symbionts (Eberl and Vandamme 2016). *Burkholderia* have been found in a endophytic lifestyle in the roots, shoots, leaves, and seeds of various plant species such as sugarcane, rice, and canola (Pal et al. 2022). *Burkholderia* may even be obligate symbionts of some insect species, including stinkbugs, bean bugs, and some species of beetles (Kikuchi and Yumoto 2013; Kikuchi and Fukatsu 2014; Flórez et al. 2017; Flórez and Kaltenpoth 2017). The most studied is the association of *Burkholderia* with stinkbugs, in which *Burkholderia* species provide a nutritional benefit (Kaltenpoth and Flórez 2020).

1.1.2 Cystic fibrosis and bacterial pathogens

Cystic fibrosis (CF) is an autosomal recessive disease that affects approximately one in 3,500 children in the United States (Elborn 2016; Corriveau et al. 2018). The disease is caused by

a mutation in the cystic fibrosis transmembrane conductance regulator gene (*CFTR*) (Elborn 2016; Rafeeq and Murad 2017), which causes a build-up of mucus in the lungs and airways, leading to a less active innate immune system and serves as a breeding ground for many pathogenic bacteria (Elborn 2016; Bhagirath et al. 2016). The CFTR protein is a member of the ATP-binding cassette (ABC) transporter family and is responsible for the transport of chloride ions and bicarbonate ions outside of the cell (Infield et al. 2021) and sits in the membrane of epithelial cells and is further modified by glycoproteins (Cheng et al. 1990). This protein contains approximately 1480 amino acids and has 12 membrane helices (Bahia et al. 2021; Infield et al. 2021). Additionally, there are two nuclear binding domains (NBD) responsible for the binding and hydrolysis of ATP for active import/export (Infield et al. 2021). There are over 2,000 mutations identified in the CFTR gene, however, only 127 of these are able to cause disease (Sosnay et al. 2013). The most common of these mutations, ΔF508, which was found in 70% of alleles in one study (Sosnay et al. 2013), and occurs in the NBD-1 (Chong et al. 2015). Dysfunction of this protein is the primary cause of cystic fibrosis and leads to a build-up of sticky mucus in the lungs (Ratjen et al. 2015). It is also thought that the increase in acidity of the airway surface liquid, due to the lack of bicarbonate transport by mutated CFTR, can also lead to disease (Malhotra et al. 2019). This mucus blocks the activity of the mucociliary elevator in the lungs, which normally sweeps out any bacteria that land in this area, preventing infection (Ratjen et al. 2015).

Patients with CF are commonly infected by multiple species of bacteria, and interestingly, as the patient ages the microbial diversity decrease (Malhotra et al. 2019). One of the most common bacteria to infect CF patients is the highly drug resistant pathogen, *Pseudomonas aeruginosa* (LiPuma 2010; Pang et al. 2019). The prevalence of infection varies by age, with adults having more *P. aeruginosa* infections than children (LiPuma 2010). In one study from 2021, they isolated

721 multi-drug resistant (MDR) *P. aeruginosa* clinical isolates, 69% of which were resistant to the three main groups of antibiotics: aminoglycosides, β-lactams, and fluoroquinolone (Okoliegbe et al. 2021). Whereas, 22% of the clinical isolates were resistant to two of the mentioned groups (Okoliegbe et al. 2021). In another study, they found that 22% of *P. aeruginosa* isolates were hypermutable with a 48-fold increase in mutation frequencies compared to wild type (Rees et al. 2019). These hypermutable strains were shown to be associated with a poorer patient outcome (Ferroni et al. 2009), and can more quickly adapt to antibiotic exposure (Oliver et al. 2000; Oliver 2010).

Another common species that infect those with CF is *Staphylococcus aureus* (LiPuma 2010). This bacterium is usually acquired early in life (Malhotra et al. 2019) and can be resistant to many different antibiotics, such as aminoglycosides, β-lactams, and glycopeptides (Bernardy et al. 2020). Previously, many young patients with CF died from *S. aureus* infections, but now they are manageable with antibiotics (Kahl 2010). *S. aureus* is the most common pathogen in CF patients early in life, then as the patient ages, the most common pathogen becomes *P. aeruginosa*, however, 40% of adults remain colonized by *S. aureus* (Kahl 2010). This bacterium can form small colony variants (SCV), and it has been found that 17% of CF patients infected with *S. aureus* have *S. aureus* containing SCV (Besier et al. 2007). Interestingly, SCV *S. aureus* is thought to be better adapted to the CF lung (Goerke and Wolz 2010; Kahl 2010). These SCV's have a slower growth rate and are more resistant to antibiotics (Goerke and Wolz 2010), allowing them to persist in the lung of CF patients.

Lastly, although not common, accounting for 3-4% of all CF infections, is the *Burkholderia cepacia* complex (Bcc). Similar to *P. aeruginosa*, Bcc infections are also acquired later in life (Malhotra et al. 2019). The two most common Bcc species that cause infections are *B. multivorans*

and *B. cenocepacia*, with *B. cenocepacia* being associated with one of the worst clinical outcomes of all CF pathogens (Scoffone et al. 2017). *Burkholderia cenocepacia* is a MDR bacterium in the *Burkholderia cepacia* complex (Bcc) (Eberl and Vandamme 2016) and a fearsome pathogen for people with CF (Scoffone et al. 2017). *B. cenocepacia* infects the lungs of these patients, causing a severe drop in lung function progressing to a life-threatening systemic infection called *cepacia* syndrome which consists of a necrotizing pneumoniae and sepsis (Scoffone et al. 2017). *B. cenocepacia* infections are difficult to treat and hard to eliminate from respiratory tissues. The challenge in combating *B. cenocepacia* infections, as well as other Gram-negative bacteria, is the outer membrane decreases the permeability of the bacterial cell, reducing the amount of antibiotic available inside the cell (Scoffone et al. 2017). Patients infected with *B. cenocepacia* often have a poorer outcome post-operation making them ineligible for lung transplants (De Soyza et al. 2010), which is a life-extending therapy in individuals with CF (Dupont 2017).

In the lungs, *B. cenocepacia* can survive intracellularly, such as in macrophages (Rosales-Reyes et al. 2018), effectively hiding from the immune system and establishing a chronic infection. Macrophages use free radicals to produce reactive oxygen species (ROS) to fight invading bacteria and other pathogens entering the body (Rahal et al. 2014). An important trait for a bacterium to have for surviving intracellularly in macrophages is to have a system able to combat ROS. *B. cenocepacia* has multiple enzymes to scavenge ROS: thioredoxin reductase (TrxB), glutathione reductase (GOR), the glutathione system, and various superoxide dismutases and catalases for combating host derived ROS (Valvano and Lefebre 2001; Peeters et al. 2010).

1.1.3 Antibiotic resistance in Burkholderia species

There are four main ways bacteria may be inherently resistant to or acquire resistance to antibiotics: decreased uptake by reduced permeability, an increase in efflux pump expression, mutations in the antibiotic target, and enzymatic alteration/inactivation of the antibiotic itself (Munita and Arias 2016; Scoffone et al. 2017). *Burkholderia* species are highly resistant to many of the available antibiotics (Leitao et al. 2008) and have acquired many of the aforementioned mechanisms of resistance. Currently, there is no set treatment for CF patients infected with these bacteria, thus new antibiotics with novel mechanisms of action are urgently needed. One group found that all their Bcc isolates were resistant to tobramycin, most were resistant to ceftazidime, and all were susceptible to meropenem (Narayanaswamy et al. 2019). Another study tested 50 clinical isolates each of *B. cenocepacia* and *B. multivorans* against ceftazidime, meropenem, minocycline, levofloxacin, chloramphenicol, ciprofloxacin, trimethoprim-sulfamethoxazole, and piperacillin-tazobactam (Huse et al. 2021). They found low susceptibility of to all antibiotics tested with their clinical isolates (Huse et al. 2021).

Many of the currently used antibiotics have cellular targets and thus, must pass through one or two membranes in Gram-positives or Gram-negatives, respectively. The membrane of *Burkholderia* species is 10-fold less permeable than *Escherichia coli*, due to the levels of general porins (Parr et al. 1987; Rhodes and Schweizer 2016), making it extremely difficult for antibiotics to enter. Additionally, it was found in 1986, that the membrane of, at the time *Pseudomonas cepacia*, was arranged in a way to protect the cation-binding sites, giving resistance to cationic antimicrobials, such as polymyxin and aminoglycosides (Moore and Hancock 1986). It is now known that the lipopolysaccharide (LPS) of *Burkholderia* species is constitutively modified with a 4-amino-4-deoxy-L-arabinose moiety, giving the membrane a positive charge, and thus, repels cationic antimicrobials (Loutet 2011; Rhodes and Schweizer 2016).

Not only must antibiotics pass through the membrane(s), they also must stay in the cell without being effluxed. When the complete genome sequence of *B. cenocepacia* strain J2315 was made available, it was found that this strain encodes 16 efflux systems of the resistance-nodulation division (RND) family (Holden et al. 2009; Podnecky et al. 2015). Specifically, RND-4 was found to give resistance to aztreonam, chloramphenicol, gentamicin, tobramycin, nalidixic acid, ciprofloxacin, levofloxacin, and norfloxacin, by testing the MIC of deletion mutants compared to wild type (Buroni et al. 2009). Additionally, the gene *bcrA* encodes an efflux pump belonging to the major facilitator superfamily (MFS) which gives resistance to tetracycline and nalidixic acid (Wigfield et al. 2002). It was found that mutations in *ampD* lead to increased resistance to β-lactams, such as ceftazidime and cefotaxime (Hwang and Kim 2015). This phenotype can be attributed to increased RNA levels of *ampC* and *penB*, two β-lactamases (Hwang and Kim 2015). Additionally, levofloxacin is a fluoroquinolone that inhibits the essential process DNA synthesis by binding to and inactivating DNA gyrase and topoisomerase (Fàbrega et al. 2009). Upon sequence analysis of levofloxacin resistant Bcc clinical isolates, single base mutations in the *gyrA* gene that encodes for DNA gyrase, causing missense mutations at codon positions 81, 83, and 87, preventing levofloxacin from binding its target (Tseng et al. 2014).

Despite the high level of antibiotic resistance, a few groups have been able to identify new ways to treat Bcc infections. Ceftazidime-avibactam is the last resort treatment for Bcc infections, however, there are a few studies showing Bcc clinical isolates being resistant to this combination (Van Dalem et al. 2018; Massip et al. 2019). Thankfully, one group found that switching ceftazidime with piperacillin, creating the novel combination piperacillin-avibactam, makes a potent combination to treat Bcc infections (Zeiser et al. 2019). Additionally, another antibiotic combination that has been shown to have efficacy against Bcc clinical isolates is moxifloxacin-

ceftazidime (El-Halfawy et al. 2017). Alone, moxifloxacin and ceftazidime had an MIC of 8 and 128 μg/mL, respectively, for *B. cenocepacia* K56-2, but in combination, the MIC dropped to 2 μg/mL showing a synergistic interaction (El-Halfawy et al. 2017). Another group identified a natural polysaccharide, poly-N-acetyl-glucosamine (PAAG) that acts in synergy with meropenem and tobramycin (Narayanaswamy et al. 2017). At low concentrations of PAAG, at 8 μg/mL, the MIC's of meropenem and tobramycin had decreased between 2- and 16-fold in all Bcc strains tested (Narayanaswamy et al. 2017). There have been new antibiotic combinations that have been shown to be effective against the Bcc, as mentioned above, but very few antimicrobials have been developed for Bcc infections.

1.2 Auranofin analogs as antimicrobials

1.2.1 Repurposing auranofin

One method to find new antibiotics is to look at current or outdated medications and repurpose them as antibiotics. This is the case of auranofin, a sugar-gold compound originally used to treat rheumatoid arthritis and is approved to be used in humans (Kean et al. 1997). Auranofin was administered to individuals with rheumatoid arthritis to decrease swollen/tender joints and stiffness (Kean et al. 1997), but fell out of practice, although the side effects of auranofin were minor, other less toxic compounds were developed (Case 2001). Auranofin has three key structural features contributing to the action of the drug, a thioglucose, a gold atom, and triethylphosphine (PEt_3) (Figure 1). The thioglucose reduces the toxicity of the compound, the gold atom is the active

component which binds and inactivates the target, and finally, the triethylphosphine (PEt_3), aids in transport of the gold across the cellular membrane (Sutton et al. 1972; Kean et al. 1997).

In *Mycobacterium tuberculosis* and *Staphylococcus aureus*, auranofin was shown to have antibiotic activity by inhibiting thioredoxin reductase (TrxR), an enzyme involved in redox reactions and protection from reactive oxygen species (ROS) (Harbut et al. 2015). Auranofin was also shown to be active against *Helicobacter pylori*, also inhibiting TrxR (Epstein et al. 2019). It is thought that the gold of auranofin, upon entering the cell, unbinds from the glucose moiety, and the gold is available to form a covalent bond with TrxR (Figure 1). Once bound, the enzyme cannot form a disulfide bond, which is critical for the function of the enzyme. Auranofin is thought to be inactive in bacteria containing a secondary antioxidant mechanism to compensate for the loss of TrxR and the rise of ROS, such as glutathione reductase (GOR) (Lu and Holmgren 2014). *H. pylori* does not contain the GOR enzyme (Wang et al. 2006), maybe allowing auranofin to be effective. One group suggests TrxR is not the sole target of auranofin (Thangamani et al. 2016). They demonstrate that auranofin can lead to other effects in the cell, such as inhibition of DNA, protein, and cell wall synthesis, however, they had no direct evidence of auranofin binding/inhibiting other thiol-containing proteins (Thangamani et al. 2016). Nevertheless, the notion that auranofin can bind other thiol-containing proteins is plausible.

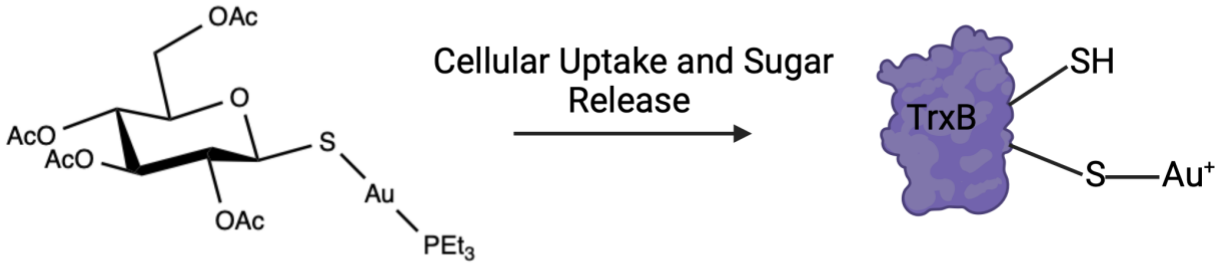

Figure 1. Structure of auranofin and its mechanism of action.

Structure of auranofin and its mechanism of action. Structure of auranofin was generated using ChemDraw 16.0. Mechanism of action of auranofin image was generated using BioRender.

1.2.3 Auranofin analogs

Auranofin does not have antimicrobial activity in many Gram-negative species such as *Klebsiella pneumoniae, Pseudomonas aeruginosa,* and *Acinetobacter baumannii* (Wu et al. 2019; Liu et al. 2022). This may be due to reduced permeability of the Gram-negative membrane, or as mentioned, because many Gram-negatives contain the glutathione system in addition to the thioredoxin system (Smirnova and Oktyabrsky 2005). Thus, to create novel antimicrobials for hard to treat Gram-negatives, auranofin analogs were made in a structure activity relationship (SAR) study (Wu et al. 2019).

The first group of auranofin analogs in this SAR study modified the thiol sugar chemical structure (Wu et al. 2019). These changes did not increase the activity of these compounds towards Gram-negatives, however, a slightly decrease in cytotoxicity was observed (Wu et al. 2019). The group two analogs involved the replacement of the glucose moiety with aromatics or aliphatic structures (Wu et al. 2019). The aromatic analogs still did not show activity against Gram-negatives, however, when they replaced the glucose moiety with mercaptoethanol, the minimum inhibitory concentrations (MICs) dropped 4-, 9-, and 18-fold for *A. baumannii*, *P. aeruginosa*, and *K. pneumoniae*, respectively (Wu et al. 2019). Finally, group three analogs had modifications to the triethylphosphine and they found that replacing it with trimethylphosphine increased the activity (Wu et al. 2019). By combining these two modifications together, a novel compound that had mercaptoethanol and trimethylphosphine was produced, which became MS-40 (Wu et al. 2019). This compound had the lowest MIC and was less toxic than auranofin and was a better inhibitor of thioredoxin reductase (Wu et al. 2019), a novel antimicrobial target.

1.3 Thioredoxin and glutathione system

1.3.1 Thioredoxin system

The thioredoxin system contains the proteins thioredoxin reductase (TrxR), thioredoxin (Trx), as well as NADPH as a source of electron and represents one of the major antioxidant systems in the cell, along with the glutathione system and catalases (Lu and Holmgren 2014). Most Gram-negatives contain thioredoxin reductase and two thioredoxins (Lu and Holmgren 2014). Originally described in *E. coli*, thioredoxin reductase is in the enzyme family pyridine-nucleotide-disulfide oxidoreductase, along with glutathione reductase, and contain sites for NADPH and FAD binding (Lu and Holmgren 2014). Additionally, TrxR contains an NADPH binding domain harbouring the enzyme's active site (Lu and Holmgren 2014) and the *E. coli* structure was solved in 1994 (Waksman et al. 1994). Thioredoxin and thioredoxin reductase have a single -CXXC- motif in their active site for redox reactions (Serata et al. 2012; Lu and Holmgren 2014; Liao et al. 2017). The thioredoxin protein is an electron donor for ribonucleotide reductase, which creates deoxyribonucleotides from ribonucleotides (Carmel-Harel and Storz 2000; Sengupta and Holmgren 2014). This then oxidized thioredoxin is reduced by thioredoxin reductase with electrons from NADPH (Carmel-Harel and Storz 2000; Sengupta and Holmgren 2014). The putative thioredoxin system (Lu and Holmgren 2014) of *B. cenocepacia* based on sequence similarity to *Escherichia coli* can be found in Figure 2.

Thioredoxin reductase is an essential protein in aerobic conditions (Serata et al. 2012; Gislason et al. 2017), making it potential target for antimicrobials. However, the thioredoxin system is also in eukaryotes, thus, compounds that bind thioredoxin or thioredoxin reductase may

have cytotoxic effects if they can also permeate into eukaryotic cells. Additionally, ebselen, a drug being repurposed as a potential antimicrobial (Thangamani et al. 2015), also inhibits prokaryotic and eukaryotic thioredoxin reductase (Lu et al. 2013). Thus, even though auranofin and ebselen have antimicrobial properties, their cytotoxicity needs to be alleviated by further chemical modifications before further development as antibiotics.

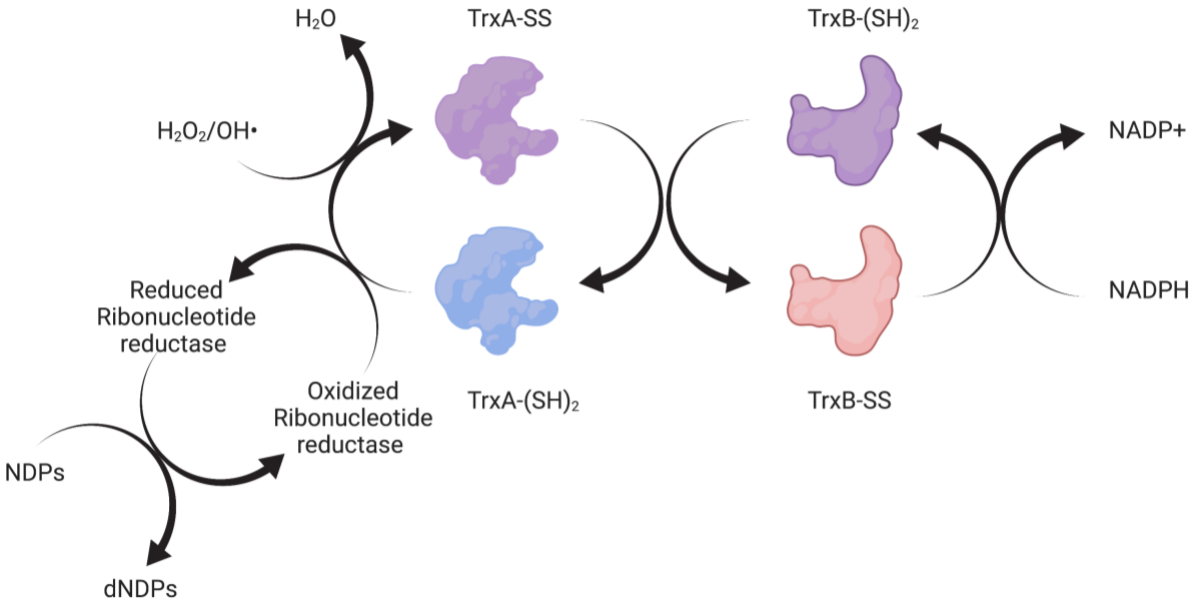

Figure 2. Thioredoxin system in *B. cenocepacia* K56-2.

Electrons from NADPH are used to reduce thioredoxin reductase (TrxB) which can then reduce thioredoxin (TrxA). Thioredoxin can give electrons to ROS, H_2O_2 or OH radical, or to oxidized ribonucleotide reductase. Ribonucleotide reductase role is to convert nucleoside diphosphate (NDP) to deoxynucleoside diphosphate (dNDP). Model based on sequence similarity to *E. coli*.

1.3.2 Glutathione system

Biosynthesis of glutathione, a tripeptide, is dependent on the enzymes γ-glutamylcysteine synthetase (GshA) and glutathione synthetase (GshB) and involves the amino acids glutamate, cysteine, and glycine, with both steps in the synthesis requiring energy from ATP (Carmel-Harel and Storz 2000; Smirnova and Oktyabrsky 2005; Couto et al. 2016). Cysteine, in the cell, is in the lowest abundance compared to glutamate and glycine, and thus, is the rate limiting step in glutathione biosynthesis (Loewen 1979; Smirnova and Oktyabrsky 2005; Couto et al. 2016). Glutathione can also be a reservoir of cysteine in bacteria (Couto et al. 2016). It was found that

deleting *gshA* and *gshB* in *E. coli* had wild type growth, but the cell had no intracellular glutathione (Apontoweil and Berends 1975). Instead of synthesis, bacteria can also import glutathione using an ABC transporter, and Gram-positives solely rely on the import of glutathione as they lack the necessary genes to synthesize it (Couto et al. 2016). Typically, the cellular concentration of reduced glutathione is between 1 and 10 mM, with a reduced to oxidized ratio between 30:1 to 100:1 (Couto et al. 2016).

In its reduced form, glutathione (GSH) can detoxify reactive oxygen species (ROS) and reactive nitrogen species (RNS) by reducing ROS/RNS and itself becoming oxidized (GSSG), forming a disulfide bond between two molecules of glutathione (Carmel-Harel and Storz 2000; Couto et al. 2016). Organisms that use glutathione to detoxify ROS/RNS need a way to recycle oxidized glutathione to its reduced form. This is accomplished by the enzyme glutathione reductase (Carmel-Harel and Storz 2000; Couto et al. 2016). This enzyme uses electrons from NADPH to accomplish this reaction and has a domain for NADPH binding (Smirnova and Oktyabrsky 2005; Couto et al. 2016). In its active site, it contains two catalytically active cysteine amino acids for redox reactions (Couto et al. 2016). Deleting *gor* in *E. coli* had wild type growth levels and still had wild type levels of GSH and GSSG suggesting there is a backup mechanism to reduce GSSG (Tuggle and Fuchs 1985). The putative glutathione system (Smirnova and Oktyabrsky 2005) of *B. cenocepacia* based on sequence similarity to *Escherichia coli* can be found in Figure 3.

In addition, one type of post-translational modification is gluthionylation (Dalle-Donne et al. 2009). Gluthionylation of thiols in proteins leads to changes in enzyme activity, thus, these disulfides may play a role in transmission of cellular signals (Dalle-Donne et al. 2009), and can

alter the activities of enzymes involved in glycolysis and gluconeogenesis, as well as adenylate cyclases and protein kinases (Dalle-Donne et al. 2009)

Reduction of disulfides in the cell is catalyzed by glutaredoxins, which acquire electrons from GSH (Ogata et al. 2021). They also have a role in redox regulation of transcription factors, such as OxyR (Zheng et al. 1998), a well-known regulator of the ROS regulon (Imlay 2015), and involved in transduction of intracellular regulatory signals (Smirnova and Oktyabrsky 2005). Glutaredoxins can also provide electron equivalents for ribonucleotide reductase, creating deoxyribonucleotides, similar to thioredoxin (Sengupta and Holmgren 2014). *E. coli* contains three glutaredoxins, Grx1, Grx2, and Grx3, and the active site of Grx1 contains a -CXXC- motif (Aslund et al. 1994; Smirnova and Oktyabrsky 2005), similar to the thioredoxin system. Deleting each of the glutaredoxins or all three together, *E. coli* can still grow (Potamitou et al. 2002), indicating that they are not essential.

It is known that auranofin and its analogs inhibit the function of the enzyme thioredoxin reductase. It is not known if the compounds can also inhibit other proteins with active cysteine amino acids, such as glutathione reductase. Also, how the glutathione system affects the susceptibility of auranofin and auranofin analogs is unknown.

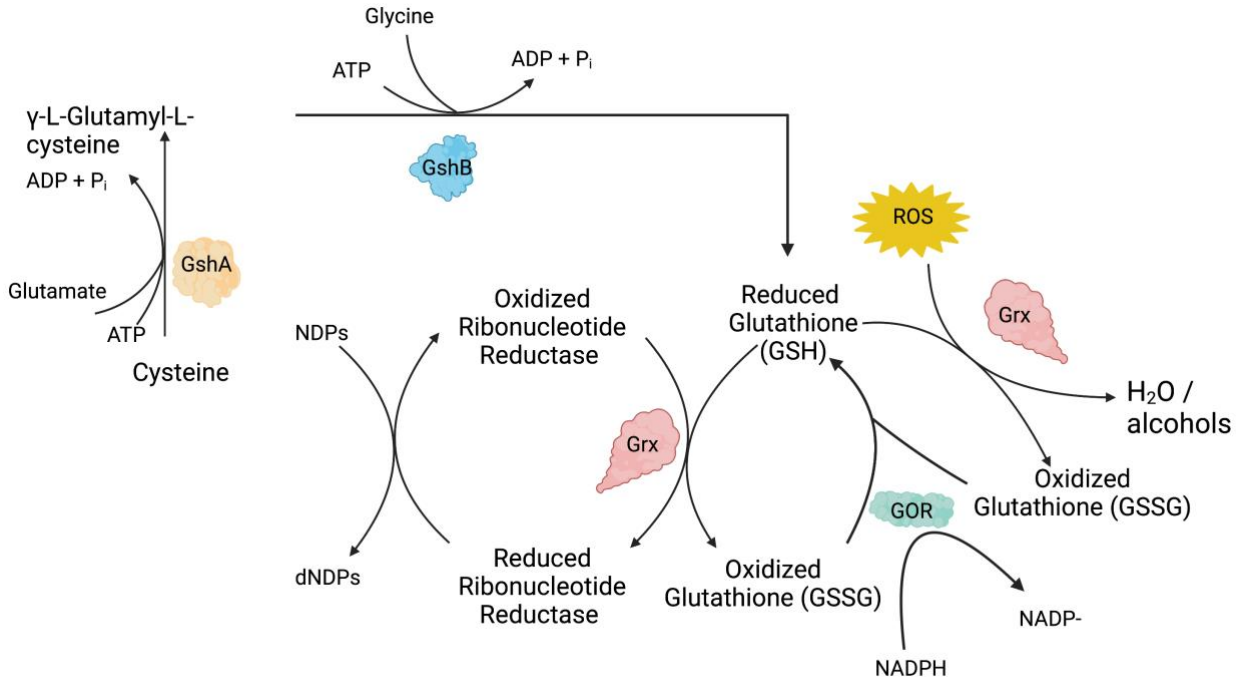

Figure 3. Glutathione system in *B. cenocepacia* K56-2.

Glutathione is synthesized from the amino acids: cysteine, glutamate, and glycine catalyzed from the enzymes GshA and GshB. Reduced glutathione (GSH) can be used to convert ROS to water and other alcohols from the action of glutaredoxins (Grx). GSH can also be used as a redox equivalent for ribonucleotide reductase, through Grx, to convert nucleoside diphosphate (NDP) to deoxynucleoside diphosphate (dNDP). Oxidized glutathione (GSSG) is then reduced back to GSH through glutathione reductase, GOR, using electrons from NADPH. Model based on sequence similarity to *E. coli*.

1.4 Next generation sequencing and transposon mutagenesis to find mechanism of action

1.4.1 Global effects of antibiotics beyond the target

Despite most antibiotics being used since the golden era of antibiotic discovery, researchers are still learning about their mechanism of action (MOA). First, auranofin has been shown inhibit thioredoxin reductase as its primary target (Harbut et al. 2015), but another group showed that auranofin can also inhibit DNA, RNA, protein, cell wall and lipid synthesis (Thangamani et al. 2016). This suggests that there is more to the MOA of auranofin than only inhibiting thioredoxin reductase. It may be that auranofin has other targets in the cell or there are various downstream affects from inhibition of thioredoxin reductase.

Ciprofloxacin, a fluoroquinolone, has been in use to treat bacterial infections since the 1980's and target DNA gyrase (*gyrA* and *gyrB*) and topoisomerase IV (*parC* and *parE*) (Ezelarab et al. 2018; Rehman et al. 2019). Both enzymes relieve supercoiling by breaking the DNA backbone and re-ligation, which serves an essential function for replication, separating daughter chromosomes, and transcription initiation (Ezelarab et al. 2018; Rehman et al. 2019). Fluoroquinolones, prevent the re-ligation of the DNA, causing a double strand break and, ultimately, cell death (Ezelarab et al. 2018; Rehman et al. 2019). Geisinger et al., studied the MOA of ciprofloxacin via next generation sequencing (NGS), in which they were able to confirm elements involved in the mechanism, such as *gyrA* and *parC* (Geisinger et al. 2019). The authors also identified that mutants in translation, lipid metabolism, envelope biosynthesis, and amino acid synthesis had altered sensitivity, indicating novel responses upon exposure to this antimicrobial beyond just the antibiotics target (Geisinger et al. 2019). This highlights that looking at the global

effects of antibiotic exposure can lead to identifying new cellular processes that affect antibiotic killing.

Triclosan, a broad-spectrum antibiotic that targets FabI, a protein involved in type II fatty acid synthesis, was exposed to a transposon mutant library, with an outward facing *tac* promoter in *E. coli* to determine its full mechanism of action, as it is not well understood (Yasir et al. 2020). Their experiments confirmed FabI as an element in the MOA, as multiple transposons upstream of the FabI gene were identified only in the inducible conditions with IPTG (Yasir et al. 2020). The authors were also able to identify other pathways in the cell that triclosan was affecting, such as the stress response (*soxR* and *marR*), purine biosynthesis (*purL* and *purH*), phospholipid recycling (*mlaBCDEF*), among others (Yasir et al. 2020). The power of next generation sequence allowed the identification of a genomic wide view of the full mechanism of action of triclosan.

1.4.2 Next generation sequencing

The beginning of next generation sequencing (NGS) began with the development of Sanger sequencing in 1977, which is known as the "1st generation" (Rothberg and Leamon 2008; Shendure and Ji 2008; Slatko et al. 2018). Sanger was developed through the idea of dideoxy synthesis that allows for termination after the dideoxy nucleotide, which is fluorescently tagged and added to the growing chain (Sanger and Coulson 1975; Sanger et al. 1977; Slatko et al. 2018). This technique is still used today to sequence 600-1000 base pairs with high accuracy (Shendure and Ji 2008; Slatko et al. 2018), however, it is not applicable for high throughput methods for two main reasons. First, it relied on the formation of multiple vectors that contain random short DNA fragments, thus called shot-gun sequencing, that are transformed into *E. coli* to obtain copies of the DNA fragment (Rothberg and Leamon 2008). Additionally, this approach requires physical separation of the

fragments that contain the dideoxy nucleotides that are fluorescently labelled to determine the order of the nucleotides (Rothberg and Leamon 2008; Slatko et al. 2018). These two limitations prevent the use of Sanger sequencing for various high throughput techniques, and thus, new sequencing platforms were developed to fit this purpose, called the "2nd generation" (Shendure and Ji 2008; Metzker 2010; Slatko et al. 2018).

The primary 2nd generation method was 454 pyrosequencing, which relied on the chemical reaction of pyrophosphate, which is released when a nucleotide is added to the growing DNA chain (Ronaghi et al. 1996; Rothberg and Leamon 2008; Shendure and Ji 2008). The pyrophosphate is converted to light via sulfurylase, yielding ATP from pyrophosphate, and luciferase creates light from ATP (Rothberg and Leamon 2008; Slatko et al. 2018). This eliminated the need to physically separate the synthesized DNA strands via electrophoresis, allowing the reduction of the reaction volume down to the limit of light detection, reducing the quantity of reagents used. These new methods sequence by synthesis and in the preparation of the template uses amplification to generate clusters of "clones" of DNA separated on a solid surface, eliminating the process of using various vectors containing short fragments and the transformation into *E. coli* to amplify these pieces (Rothberg and Leamon 2008). Additionally, the production of light allowed for separate samples to be sequenced at once, allowing NGS to be massively parallel, unlike Sanger (Rothberg and Leamon 2008; Shendure and Ji 2008). The mentioned advancements made this generation of techniques useable for high throughput methods by vastly decreasing the cost and library preparation and increasing the technologies for template amplification and sequencing itself (Rothberg and Leamon 2008).

Library preparation starts by randomly fragmentizing the DNA sample, or creating amplicons via PCR, in which adapters are added to the DNA that are complementary to the

sequencing primers (Shendure and Ji 2008; Qin 2019). These pieces are then used to generate spatial clusters of clones on a solid surface, by emulsion or bridge PCR, for example, containing 1000s of identical fragments (Shendure and Ji 2008; Metzker 2010). The groups of DNA are attached to a flow cell, in which media with fresh reagents are added, bringing new nucleotides as well as removing by-products (Rothberg and Leamon 2008), with each flow cell being able to contain millions of groups within eight separate lanes (Shendure and Ji 2008; Metzker 2010). These are detected by the presence of light or fluorescence as each nucleotide is added to the growing chain, allowing to determine the order of nucleotides (Rothberg and Leamon 2008; Shendure and Ji 2008; Slatko et al. 2018). The addition of nucleotide indices/barcodes on the DNA made it possible to sequence multiple conditions on the same lane, then can separate each or "de-multiplex" by the identity of the index (Qin 2019), increasing the number of samples that can be processed in parallel.

NGS can be used for various purposes, such as identifying human pathogens via whole genome sequencing, surveillance of antibiotic resistance, and epidemiology and infection control (Behjati and Tarpey 2013; Cao et al. 2017; Qin 2019; Lepuschitz et al. 2020), as a few examples. Despite its widespread usage, NGS has its limitations. It can only do short reads of DNA, usually between 50-300 base pairs for Illumina and ion torrent systems (Shendure and Ji 2008; Slatko et al. 2018). It is also more prone to error than Sanger, which has greater than 99.9% accuracy, making it more useful for checking for specific mutations up to 1000 bases (Shendure and Ji 2008; Slatko et al. 2018). Despite its limitations, NGS is a powerful tool, a huge advancement in research, and as techniques and ideas develop, it may be possible that newer sequencing systems can create longer reads with higher accuracies.

1.4.3 Transposon sequencing to find mechanism of action

Transposon sequencing (TnSeq) involves creating a library in the bacteria of interest, in which each gene in the genome is disrupted via a transposon (Goodman et al. 2009; Gawronski et al. 2009; Opijnen et al. 2009; Gallagher et al. 2011; Kwon et al. 2016). The collective mutants are then pooled and can be grown in the presence of an antibiotic, often sub-lethal concentrations, as well as with a non-exposure control (Vitale et al. 2020; Lazarus et al. 2021). Sequencing of the transposon-genome junction will identify the relative amount of each individual mutant, revealing the fitness of each (Opijnen et al. 2009; Kwon et al. 2016), with positive fitness (increased resistance) and negative fitness (increased susceptibility) correlating to more and less abundance, respectively (Geisinger et al. 2020). This will characterize the genetic network associated with the antibiotic response, as well as indicating putative binding factors, due to a process called hypersensitivity, in which as the target decreases, less of the drug is needed to kill the cell (Cardona et al. 2015). Following up from the TnSeq experiment and after analysis, deletions are often made to validate the results and confirm hypersensitivity (Rajagopal et al. 2016; Hogan et al. 2018; Sonnabend et al. 2020). For example, the target of a novel antimicrobial, C109, was identified through TnSeq in *Burkholderia cenocepacia* and determined to be FtsZ, an essential protein in cell division (Hogan et al. 2018). This was then validated via the creation of a genetic knockdown, which showed hypersensitivity to C109, as well as enzymatic assays on purified FtsZ to confirm C109 inhibits the function of the enzyme (Hogan et al. 2018).

A further adaption of this approach was made via the addition of 20 nucleotides in the transposon that is unique for each insertion (Smith et al. 2009; Wetmore et al. 2015). This method, randomly-barcode transposon sequencing, or BarSeq, has easier identification of individual

mutants because only the barcode itself will need to be sequenced, decreasing the time for library preparation as well as the cost (Melnyk et al. 2015; Wetmore et al. 2015; Kwon et al. 2016). This relies on additional preliminary experiments, such as creating the transposons with the unique 20 nucleotides, making the mutant library, and one round of NGS to link each unique identifier to a specific gene disruption, before the use in mechanism of action studies (Wetmore et al. 2015).

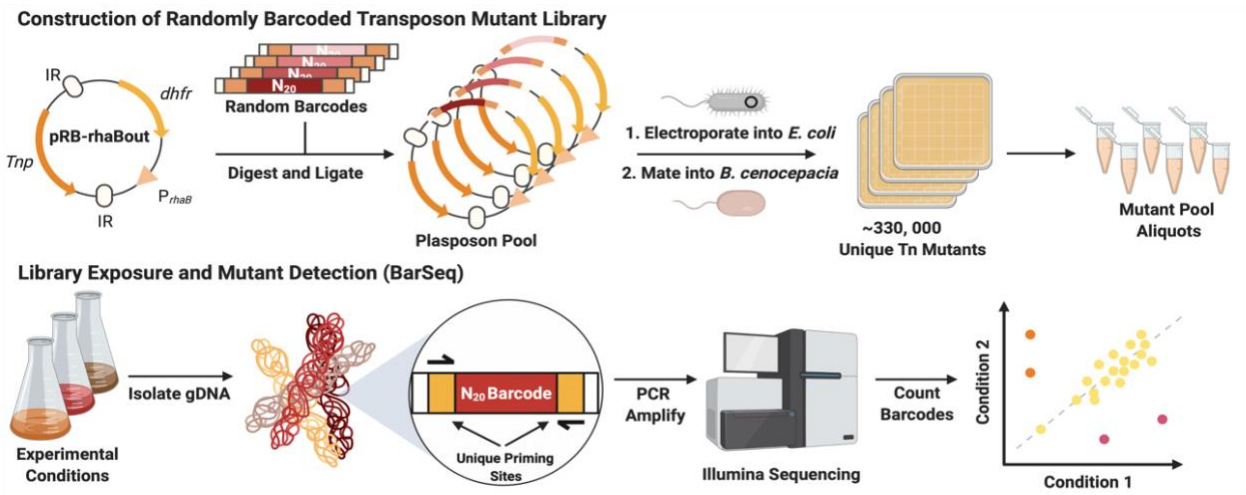

Figure 4. BarSeq to find antimicrobial's mechanism of action.

Image was generated from BioRender, showing the construction of the randomly barcoded transposon mutant library and its usage. Image modified from (Hogan et al. 2023).

Two major limitations exist with the TnSeq technique. First, it requires extensive preparation in building the transposon mutants in the bacterium of choice, especially for BarSeq, and thus, it not as easily adaptable as the others, as briefly explained above. Second, because this relies on disruptions, it cannot include information about essential genes. These encode functions for growth and survival, and thus, disrupting this will lead to an unviable cell (Kwon et al. 2016; Gislason et al. 2017; Sonnabend et al. 2020). Essential genes and their products are often the target of antimicrobials (Amini and Tavazoie 2011; Fields et al. 2016), and thus, are of importance. Despite the limitation of excluding these critical elements, TnSeq leads to a non-essential genome wide view, capable of creating immense genetic networks and phenotypic signatures (Santiago et al. 2018; Geisinger et al. 2020). Geisinger et al., (Geisinger et al. 2020) exposed an *Acinetobacter baumannii* transposon mutant library to 19 different compounds with various cellular mechanisms to create drug susceptibility signatures, in which they could identify relationships between gene functions based on the role of each in various MOAs (Geisinger et al. 2020). In this TnSeq, not only were they able to identify elements involved with susceptibility, they also were able to characterize a hypothetical protein based on how it clustered with others with similar functions and identified AdvA, which is involved in cell division, could be a novel antimicrobial target (Geisinger et al. 2020).

One possibility of including essential genes in the library is by adding an outward facing inducible promoter in the transposon that can control expression if inserted upstream and in the correct orientation (Wang et al. 2011; Yasir et al. 2020; Coward et al. 2020). However, this increases the complexity of the data analysis.

Despite these limitations, BarSeq is a powerful method that can be used to determine the mechanism of action, and the overall global response, of an antimicrobial.

1.5 Rationale and Hypothesis

There is no recommended treatment for people with CF infected with *Burkholderia* species because of the high rate of antibiotic resistance. Thus, new antimicrobials are needed to treat these infections. Auranofin has been shown to have antimicrobial properties with a novel mechanism of action by inhibiting the essential enzyme thioredoxin reductase (Harbut et al. 2015; Thangamani et al. 2016), which is part of the thioredoxin system, one of the dominant antioxidant system. Auranofin has no bactericidal activity in Gram-negatives and this is thought to be due to one of two reasons: lack of uptake of auranofin or the presence of the additional glutathione system, which involves glutathione reductase, a structurally and functionally similar protein to thioredoxin reductase. In order for the auranofin analogs to be active, I hypothesize the compounds would have a slightly different mechanism of action and need to inhibit both thioredoxin reductase and glutathione reductase. If it inhibited thioredoxin reductase only, the bacterium would have another mechanism to combat the rise of reactive oxygen species, preventing cell death. It will therefore be necessary to determine the full mechanism of action of any potent bactericidal auranofin analogs.

I hypothesize auranofin analogs will have greater bactericidal activity, compared to auranofin, against *B. cenocepacia* K56-2 and other CF pathogens and that the mechanism of action of these antimicrobials can be determined using randomly barcoded transposon sequencing (BarSeq).

1.6 Objectives

The objectives of this work were as follows:

1. Identify auranofin analogs with potent bactericidal activity and determine the efficacy of these auranofin analogs towards the Bcc and, and more specifically, *B. cenocepacia* K56-2; and
2. Use a barcoded transposon mutant library to identify genetic elements involved with the mechanism of action of the auranofin analogs.

CHAPTER 2: MATERIAL AND METHODS

2.1 Primers, plasmids, and strains used

Table 1. Primers used in this study.

Primer Number	Sequence (5'-3')	Notes
848	CCGCCAGGCAAATTCTGTTT	Reverse primer for colony PCR, all gRNAs
1092	ACTAGTATTATACCTAGGACTGAGCTAGC	Reverse primer, all gRNAs
1409	GGCTTATGTCAACTGGGTTCG	Forward primer for general colony PCR of sgRNA plasmids
2163	CAAGCAGAAGACGGCATACGAGAT GCTTACGGACGTCTCGTGG GCTCGGAGATGTGTATAAGAGA CAGGTCGACCTGCAGCGTACG	BarSeq primer with i7 adapter; UDP0089
2164	CAAGCAGAAGACGGCATAC GAGATCGCTTGAAGTGTCTCGT GGGCTCGGAGATGTGTATAAGAG ACAGGTCGACCTGCAGCGTACG	BarSeq primer with i5 adapter; UDP0089
2171	AATGATACGGCGACCACCG AGATCTACACCGTGTATCTTT CGTCGGCAGCGTCAGATGTGTATA AGAGACAGGATGTCCACGAGGTCTCT	BarSeq primer with i7 adapter; UDP0090
2172	AATGATACGGCGACCACCGA GATCTACACGAACCATGAATCGT CGGCAGCGTCAGATGTGTATAA GAGACAGGATGTCCACGAGGTCTCT	BarSeq primer with i5 adapter; UDP0090
2224	CAAGCAGAAGACGGCATACGA GATGTTCCGCAGGGTCTCGTGGGC TCGGAGATGTGTATAAGAG ACAGGTCGACCTGCAGCGTACG	BarSeq primer with i7 adapter; UDP0073
2225	AATGATACGGCGACCACCGAGAT CTACACATCATAGGCTTCGTCGGCAG CGTCAGATGTGTATAAGAG ACAGGATGTCCACGAGGTCTCT	BarSeq primer with i5 adapter; UDP0073
2226	CAAGCAGAAGACGGCATACGAG ATACCTTATGAAGTCTCGTGGGCTC GGAGATGTGTATAAGAGA CAGGTCGACCTGCAGCGTACG	BarSeq primer with i7 adapter; UDP0074
2227	AATGATACGGCGACCACCGAGAT CTACACTGTTAGAAGGTCGTCGGCA	BarSeq primer with i5 adapter; UDP0074

	GCGTCAGATGTGTATAAGAG ACAGGATGTCCACGAGGTCTCT	
2228	CAAGCAGAAGACGGCATACGA GATCGCTGCAGAGGTCTCGTGGGC TCGGAGATGTGTATAAGAGA CAGGTCGACCTGCAGCGTACG	BarSeq primer with i7 adapter; UDP0075
2229	AATGATACGGCGACCACCGAG ATCTACACGATGGATGTATCGTC GGCAGCGTCAGATGTGTATAAG AGACAGGATGTCCACGAGGTCTCT	BarSeq primer with i5 adapter; UDP0075
2230	CAAGCAGAAGACGGCATACG AGATGTAGAGTCAGGTCTCGT GGGCTCGGAGATGTGTATAAGA GACAGGTCGACCTGCAGCGTACG	BarSeq primer with i7 adapter; UDP0076
2231	AATGATACGGCGACCACCGA GATCTACACACGGCCGTCATC GTCGGCAGCGTCAGATGTGTATAA GAGACAGGATGTCCACGAGGTCTCT	BarSeq primer with i5 adapter; UDP0076
2232	CAAGCAGAAGACGGCATAC GAGATGGATACCAGAGTCTCGT GGGCTCGGAGATGTGTATAAGA GACAGGTCGACCTGCAGCGTACG	BarSeq primer with i7 adapter; UDP0077
2233	AATGATACGGCGACCACCG AGATCTACACCGTTGCTTACTC GTCGGCAGCGTCAGATGTGTATA AGAGACAGGATGTCCACGAGGTCTCT	BarSeq primer with i5 adapter; UDP0077
2234	CAAGCAGAAGACGGCAT ACGAGATCGCACTAATGGTC TCGTGGGCTCGGAGATGTGTATA AGAGACAGGTCGACCTGCAGCGTACG	BarSeq primer with i7 adapter; UDP0078
2235	AATGATACGGCGACCACC GAGATCTACACTGACTACATAT CGTCGGCAGCGTCAGATGTGTATA AGAGACAGGATGTCCACGAGGTCTCT	BarSeq primer with i5 adapter; UDP0078
2236	CAAGCAGAAGACGGCATAC GAGATTCCTGACCGTGTCTC GTGGGCTCGGAGATGTGTATAAG AGACAGGTCGACCTGCAGCGTACG	BarSeq primer with i7 adapter; UDP0079
2237	AATGATACGGCGACCACCG AGATCTACACCGGCCTCGTTTC GTCGGCAGCGTCAGATGTGTATAA GAGACAGGATGTCCACGAGGTCTCT	BarSeq primer with i5 adapter; UDP0079
2238	CAAGCAGAAGACGGCATAC GAGATCTGGCTTGCCGTCTC GTGGGCTCGGAGATGTGTATAAGA GACAGGTCGACCTGCAGCGTACG	BarSeq primer with i7 adapter; UDP0080

2239	AATGATACGGCGACCACCGA GATCTACACCAAGCATCCGTCG TCGGCAGCGTCAGATGTGTATAAG AGACAGGATGTCCACGAGGTCTCT	BarSeq primer with i5 adapter; UDP0080
2240	CAAGCAGAAGACGGCATA CGAGATACCAGCGACAGTCTC GTGGGCTCGGAGATGTGTATAAG AGACAGGTCGACCTGCAGCGTACG	BarSeq primer with i7 adapter; UDP0081
2241	AATGATACGGCGACCACCGAG ATCTACACTCGTCTGACTTCGT CGGCAGCGTCAGATGTGTATAAG AGACAGGATGTCCACGAGGTCTCT	BarSeq primer with i5 adapter; UDP0081
2242	CAAGCAGAAGACGGCATACG AGATTTGTAACGGTGTCTCGTGG GCTCGGAGATGTGTATAAGA GACAGGTCGACCTGCAGCGTACG	BarSeq primer with i7 adapter; UDP0082
2243	AATGATACGGCGACCACCGAG ATCTACACCTCATAGCGATCGTCGG CAGCGTCAGATGTGTATAAGA GACAGGATGTCCACGAGGTCTCT	BarSeq primer with i5 adapter; UDP0082
2244	CAAGCAGAAGACGGCATACGA GATGTAAGGCATAGTCTCGTGGGC TCGGAGATGTGTATAAGAGA CAGGTCGACCTGCAGCGTACG	BarSeq primer with i7 adapter; UDP0083
2245	AATGATACGGCGACCACCGAG ATCTACACAGACACATTATCGTCG GCAGCGTCAGATGTGTATAAGA GACAGGATGTCCACGAGGTCTCT	BarSeq primer with i5 adapter; UDP0083
2246	CAAGCAGAAGACGGCATACGA GATGTCCACTTGTGTCTCGTGGGC TCGGAGATGTGTATAAGAGA CAGGTCGACCTGCAGCGTACG	BarSeq primer with i7 adapter; UDP0084
2247	AATGATACGGCGACCACCGAGA TCTACACGCGCGATGTTTCGTCGG CAGCGTCAGATGTGTATAAGA GACAGGATGTCCACGAGGTCTCT	BarSeq primer with i5 adapter; UDP0084
2248	CAAGCAGAAGACGGCATACG AGATTTAGGTACCAGTCTCGTGG GCTCGGAGATGTGTATAAGA GACAGGTCGACCTGCAGCGTACG	BarSeq primer with i7 adapter; UDP0085
2249	AATGATACGGCGACCACCGA GATCTACACCATGAGTACTTCGT CGGCAGCGTCAGATGTGTATAA GAGACAGGATGTCCACGAGGTCTCT	BarSeq primer with i5 adapter; UDP0085
2250	CAAGCAGAAGACGGCATACGA GATGGAATTCCAAGTCTCGTGGGC	BarSeq primer with i7 adapter; UDP0086

	TCGGAGATGTGTATAAGAG ACAGGTCGACCTGCAGCGTACG	
2251	AATGATACGGCGACCACCGAGA TCTACACACGTCAATACTCGTCGG CAGCGTCAGATGTGTATAAGA GACAGGATGTCCACGAGGTCTCT	BarSeq primer with i5 adapter; UDP0086
2252	CAAGCAGAAGACGGCATACGA GATCATGTAGAGGGTCTCGTGGG CTCGGAGATGTGTATAAGAG ACAGGTCGACCTGCAGCGTACG	BarSeq primer with i7 adapter; UDP0087
2253	AATGATACGGCGACCACCGAG ATCTACACGATACCTCCTTCGTCG GCAGCGTCAGATGTGTATAAG AGACAGGATGTCCACGAGGTCTCT	BarSeq primer with i5 adapter; UDP0087
2254	CAAGCAGAAGACGGCATACGA GATTACACGCTCCGTCTCGTGGG CTCGGAGATGTGTATAAGAG ACAGGTCGACCTGCAGCGTACG	BarSeq primer with i7 adapter; UDP0088
2255	AATGATACGGCGACCACCGA GATCTACACATCCGTAAGTTCG TCGGCAGCGTCAGATGTGTATAA GAGACAGGATGTCCACGAGGTCTCT	BarSeq primer with i5 adapter; UDP0088
2303	GCATTGGGATCCCATGTCCACGCCCAAACACG	Forward primer for *trxB* amplification into pET-24b
2304	TGCGTAAAGCTTCAGGCTTTCGAGGTAGCGC	Reverse primer for *trxB* amplification into pET-24b
2315	CCCGCGAAATTAATACGACT	Colony PCR primer for pET-24+ insertions
2316	GTTAGCAGCCGGATCTCA	Colony PCR primer for pET-24+ insertions
2827	AGCTTCGAGTTTATCGCCCAGTTTTA GAGCTAGAAATAGCAAGTTAAAATAAGGC	iPCR primer sgRNA to create CRISPRi mutant targeting *ahpC* (K562_ RS08590)
2839	TGCCTGCGGTGTGGTTGAACGTTTTA GAGCTAGAAATAGCAAGTTAAAATAAGGC	iPCR primer sgRNA to create CRISPRi mutant targeting *katG* (K562_ RS15960)
2874	GCTGGAAAAGATGGCACTGC	Colony PCR primer for gor deletion
2875	ATTATCTAGAGACGCAGCTCATCAATCGCC	Forward primer for amplifying upstream region for grxC deletion
2876	ATTAAAGCTTCTGCATGCAATACGGACACAC	Reverse primer for amplifying upstream region for grxC deletion

2877	ATTAAAGCTTCCTCGTGCCGCTTCTGC	Forward primer for amplifying downstream region for grxC deletion
2878	ATTACCCGGGGAAAATGCCGGCCTGCTTC	Reverse primer for amplifying downstream region for grxC deletion
2879	CGTCCGGAATGTTGCGAATG	Colony PCR primer for *grxC* deletion
2880	CCAATTACACGAACCTGGCC	Colony PCR primer for *grxC* deletion
2881	ATTATCTAGACGCATCTCGCCCAGGG	Forward primer for amplifying upstream region for *grxD* deletion
2882	ATTAAAGCTTGCTTGATACGTTGTTGGGTGTC	Reverse primer for amplifying upstream region for *grxD* deletion
2883	ATTAAAGCTTCTCGGACATCATGATGGAGATGT	Forward primer for amplifying downstream region for *grxD* deletion
2884	ATTACCCGGGCGATCACCATGCCATCGG	Reverse primer for amplifying downstream region for *grxD* deletion
2885	GCAACCCGCCGTACATCG	Colony PCR primer for *grxD* deletion
2886	CGAGGTTGAACGGCGTTTC	Colony PCR primer for *grxD* deletion
2887	ATTATCTAGAGCTGATCACGCTGGTCTACA	Forward primer for amplifying upstream region for *gshA1* deletion
2888	ATTAAAGCTTGGAACCATGAATCACTCGCGAG	Reverse primer for amplifying upstream region for *gshA1* deletion
2889	ATTAAAGCTTCGATCGAACTGGAAAAGACCG	Forward primer for amplifying downstream region for *gshA1* deletion
2890	ATTACCCGGGCGTCACGTACTCCATGTCGAAC	Reverse primer for amplifying downstream region for *gshA1* deletion
2891	CGTATTCGCGGTCAAGGAC	Colony PCR primer for *gshA1* deletion
2892	CTTGTTGAACACGCGTGC	Colony PCR primer for *gshA1* deletion
2893	ATTATCTAGAGTGCAGGAAGGCGTCTACAC	Forward primer for amplifying upstream region for *gshB* deletion

2894	ATTAAAGCTTGAATGTCCATGCGGGTCCTG	Reverse primer for amplifying upstream region for *gshB* deletion
2895	ATTAAAGCTTGAGATCATGGAGCAGACGGG	Forward primer for amplifying downstream region for *gshB* deletion
2896	ATTACCCGGGGGATCCCGGCCATGTCAGAT	Reverse primer for amplifying downstream region for *gshB* deletion
2897	CGATACAGTCCCGCAGC	Colony PCR primer for *gshB* deletion
2898	GAGATCGGCCGCATGAC	Colony PCR primer for *gshB* deletion
2899	ATTATCTAGAGTGCCGGCGTGACGTG	Forward primer for amplifying upstream region for *gshA2* deletion
2900	ATTAAAGCTTCATGGTGTTCGACATGGAGAC	Reverse primer for amplifying upstream region for *gshA2* deletion
2901	ATTAAAGCTTCCTATACGCTGAACCGCTTCA	Forward primer for amplifying downstream region for *gshA2* deletion
2902	ATTACCCGGGGAAGACGATGAAACACGCG	Reverse primer for amplifying downstream region for *gshA2* deletion
2903	GCTCGCCAGCCAGAAG	Colony PCR primer for *gshA2* deletion
2904	GCATCGTTTCCGCCCG	Colony PCR primer for *gshA2* deletion
2874	GCTGGAAAAGATGGCACTGC	Colony PCR primer for *gor* deletion
2926	CGTGTCAAACGGCCGTCAGCGTTTTA GAGCTAGAAATAGCAAGTTAAAATAAGGC	iPCR primer sgRNA to create CRISPRi mutant targeting *sodC* (K562_ RS05960)
2934	ATCGACGTCAGTCCAGCCCAGTTTTAGAGC TAGAAATAGCAAGTTAAAATAAGGC	iPCR primer to create CRISPRi mutant targeting *purL* (K562_ RS08740)
2952	GGGAATTCCGGCCAACGGGC GTTTTAGAGCTAGAAA TAGCAAGTTAAAATAAGGC	iPCR primer sgRNA to create CRISPRi mutant targeting *purM* (K562_RS15775)
2956	ATTTCCGTTTCCGACAAGA CGTTTTAGAGCTAGAAA TAGCAAGTTAAAATAAGGC	iPCR primer sgRNA to create CRISPRi mutant targeting *purH* (K562_RS16140)

2962	CCACTCCGAAGAGATCGTCT GTTTTAGAGCTAGAAA TAGCAAGTTAAAATAAGGC	iPCR primer sgRNA to create CRISPRi mutant targeting hypoxanthine-guanine phoshoribosyltransferase (K562_RS16640)
2964	TTCACTTCGAACCATTCCC GGTTTTAGAGCTAGAAA TAGCAAGTTAAAATAAGGC	iPCR primer sgRNA to create CRISPRi mutant targeting dyp-type peroxidase (K562_RS21385)
2967	AGGTGTTATCTCCCAATCCCG TTTTAGAGCTAGAAATA GCAAGTTAAAATAAGGC	iPCR primer sgRNA to create CRISPRi mutant targeting *purF* (K562_RS22230)
2974	TAGGATTCATCTCAACCCTT GTTTTAGAGCTAGAAAT AGCAAGTTAAAATAAGGC	iPCR primer sgRNA to create CRISPRi mutant targeting *nadR* (K562_RS27675)
3002	ATTACATATGATGGA TTTCGACTACGACCTGTTC	Forward primer for GOR insertion into pET-22+
3006	GACACGATCGGCATTCATC	Colony PCR for GOR insertion into pET-22+
3008	CGCGTAACCACCACACCC	Colony PCR for GOR insertion into pET-22+
3122	GAACGTCGTGGGTGAAATCGC	Colony PCR primer for *gor* deletion
3123	ATTATCTAGAGGCATGCTCGAGAAGAAGGAC	Forward primer for amplifying upstream region for *gor* deletion
3124	ATTAAAGCTTGGTCGTAGTCGAAATCCATCGC	Reverse primer for amplifying upstream region for *gor* deletion
3125	ATTAAAGCTTCCGATATCGACGCGGAAGA	Forward primer for amplifying downstream region for *gor* deletion
3126	ATTACCCGGGGGGGCACACGCACGC	Reverse primer for amplifying downstream region for *gor* deletion
3136	CACCTCGTTACCGCGTTGAAG TTTTAGAGCTAGAAATAGCAAGTTAAAATAAGGC	iPCR primer sgRNA to create CRISPRi mutant targeting *gshA1* and *gshB* (K562_RS03750 and K562_RS03755)
3385	TCGTACAAGCTTCTTCTGCCGCATCGTTACG	Reverse primer for GOR insertion into pET-22+

Table 2. Plasmids used in this study

Plasmids	Features	Source
pDAI-SceI-*sacB*	pDAI-SceI expressing *sacB*	(Hamad et al. 2010; Aubert et al. 2014)
pGPI-SceI	ori_{R6K} Tmp^r mob^+ carries I-SceI cut site	(Flannagan et al. 2008)
pSCB2-sgRNA	Template for pgRNA created by inverse PCR; derived from pSCrhaB2-sgRNA by inverse PCR to remove *rhaS*, *rhaR*, and P*rhaB*	(Hogan et al. 2019)
pgRNA-non-target	Derived from pSCB2-sgRNA; random 20 nt sequence added as gRNA binding region by inverse PCR	(Hogan et al. 2019)
pGPI-SceI-*gor*	pGPI-SceI with a fusion of approximately 350 bp regions immediately upstream and downstream of *gor* cloned into *Xba*I and *Xma*I sites. Enables deletion of *gor* gene.	This study
pGPI-SceI-*gshA1*	pGPI-SceI with a fusion of approximately 350 bp regions immediately upstream and downstream of *gshA1* cloned into *Xba*I and *Xma*I sites. Enables deletion of *gshA1* gene.	This study
pGPI-SceI-*gshA2*	pGPI-SceI with a fusion of approximately 350 bp regions immediately upstream and downstream of *gshA2* cloned into *Xba*I and *Xma*I sites. Enables deletion of *gshA2* gene.	This study
pGPI-SceI-*gshB*	pGPI-SceI with a fusion of approximately 350 bp regions immediately upstream and downstream of *gshB* cloned into *Xba*I and *Xma*I sites. Enables deletion of *gshB* gene.	This study
pGPI-SceI-*grxC*	pGPI-SceI with a fusion of approximately 350 bp regions immediately upstream and downstream of *grxC* cloned into *Xba*I and *Xma*I sites. Enables deletion of *grxC* gene.	This study
pGPI-SceI-*grxD*	pGPI-SceI with a fusion of approximately 350 bp regions immediately upstream and downstream of *grxD* cloned into *Xba*I and *Xma*I sites. Enables deletion of *grxD* gene.	This study
pgRNA-*trxB*	pSCB2-sgRNA expressing sgRNA targeting *trxB*	This study
pgRNA-*rodA*	pSCB2-sgRNA expressing sgRNA targeting *rodA*	This study
pET-24-TrxB	pET-24 containing *trxB* gene from *B. cenocepacia* K56-2	This study
pET-22-GOR	pET-22 containing *gor* gene from *B. cenocepacia* K56-2	This study
pgRNA-*katG*	pSCB2-sgRNA expressing sgRNA targeting *katG*	This study
pgRNA-*sodC*	pSCB2-sgRNA expressing sgRNA targeting *sodC*	This study
pgRNA-K562_RS21385	pSCB2-sgRNA expressing sgRNA targeting K562_RS21385	This study
pgRNA-*purL*	pSCB2-sgRNA expressing sgRNA targeting *purL*	This study

pgRNA-*purM*	pSCB2-sgRNA expressing sgRNA targeting *purM*	This study
pgRNA-*purH*	pSCB2-sgRNA expressing sgRNA targeting *purH*	This study
pgRNA-K562_RS16640	pSCB2-sgRNA expressing sgRNA targeting K562_RS16640	This study
pgRNA-*purF*	pSCB2-sgRNA expressing sgRNA targeting *purF*	This study
pgRNA-*nadR*	pSCB2-sgRNA expressing sgRNA targeting *nadR*	This study
pgRNA-*gshA1gshB*	pSCB2-sgRNA expressing sgRNA targeting *gshA1 gshB* operon	This study

Table 3. Strains and mutants used in this study.

Strain	**Features**	**Source**
B. cenocepacia K56-2	ET12 lineage CF clinical isolate from Toronto	(Darling et al. 1998)
B. lata BCC6	Isolated from mirror defogger	C. Deschênes
B. contaminans MF16	Clinical Isolate	(Nunvar et al. 2016)
B. contaminans FFH-2050MA	Clinical Isolate	Hospital de Niños Ricardo Gutierrez, Buenos Aires, Argentina
B. dolosa CEP021	Clinical isolate	D. Speert
B. multivorans ATCC 17616	Environmental Isolate	Dr. Tiedge
B. cenocepacia 140485	Clinical Isolate	National Microbiology Laboratory
B. ubonensis LMG 20358	Surface soil isolate	(Yabuuchi et al. 2000; Schmidt et al. 2009)
B. contaminans FFH-4004	Clinical isolate	CF Isolate from Argentina
B. mallei China 5 (NBL 4)	Animal Isolate	BEI Resources
B. mallei Ivan (NCTC 10230)	Animal Isolate	BEI Resources
B. mallei China 7 (NBL 7)	Clinical Isolate	BEI Resources
B. pseudomallei 1710b	Clinical Isolate	BEI Resources
B. pseudomallei MSHR465a	Clinical Isolate	BEI Resources
B. pseudomallei HBPUB10134a	Clinical Isolate	BEI Resources
B. pseudomallei MSHR305	Clinical Isolate	BEI Resources
Stenotrophomonas maltophilia DH57	Clinical isolate	ATCC
Stenotrophomonas maltophilia K279a	Clinical isolate	ATCC
Pseudomonas. aeruginosa PA01	Reference strain	A. Kumar
Pseudomonas aeruginosa PA7	Multi-drug resistant, non-respiratory isolate	A. Kumar, (Roy et al. 2010)

Escherichia coli 120955	Extended spectrum beta-lactamase-producing clinical isolate	G. Zhanel
Escherichia vulneris CEP511	Clinical isolate	D. Speert
Klebsiella pneumoniae 120310	Extended spectrum beta-lactamase -producing clinical isolate	G. Zhanel
Acinetobacter baumannii ATCC 17978	Reference strain	A. Kumar
Staphylococcus aureus ATCC 27700	Reference Strain	K. Lovetri
Staphylococcus aureus 107094	MRSA, clinical isolate	Paediatric Hospital of Buenos Aires, Argentina
B. cenocepacia K56-2::dCas9	Derived from K56-2; pAH-CTX1rhadCas9 integrated at *attB* site; clean deletion of plasmid accessory genes	(Hogan et al. 2019)
B. cenocepacia K56-2 ΔgshA1	Unmarked gene deletion of gshA1, K562_ RS03750	This study
B. cenocepacia K56-2 ΔgshA2	Unmarked gene deletion of gshA2, K562_ RS02270	This study
B. cenocepacia K56-2 ΔgshB	Unmarked gene deletion of gshB, K562_ RS03755	This study
B. cenocepacia K56-2 ΔgrxC	Unmarked gene deletion of grxC, K562_ RS03795	This study
B. cenocepacia K56-2 ΔgrxD	Unmarked gene deletion of grxD, K562_ RS01940	This study
B. cenocepacia K56-2 Δgor	Unmarked gene deletion of gor, K562_ RS03010	This study
B. cenocepacia K56-2::dCas9 pgRNA-*trxB*	CRISPRi mutant targeting *trxB;* K562_ RS14600	This study
B. cenocepacia K56-2::dCas9 pgRNA-*rodA*	CRISPRi mutant targeting *rodA;* K562_ RS02475	This study
B. cenocepacia K56-2::dCas9 pgRNA-non-target	Non-targeting CRISPRi mutant	(Hogan et al. 2019)
B. cenocepacia K56-2::dCas9 pgRNA-*katG*	CRISPRi mutant targeting *katG;* K562_ RS15960	This study
B. cenocepacia K56-2::dCas9 pgRNA-*sodC*	CRISPRi mutant targeting *sodC;* K562_ RS05960	This study
B. cenocepacia K56-2::dCas9 pgRNA-K562_RS21385	CRISPRi mutant targeting dyp-type peroxidase*;* K562_ RS21385	This study
B. cenocepacia K56-2::dCas9 pgRNA-*purL*	CRISPRi mutant targeting *purL;* K562_ RS08740	This study
B. cenocepacia K56-2::dCas9 pgRNA-*purM*	CRISPRi mutant targeting *purM;* K562_ RS15775	This study

B. cenocepacia K56-2::dCas9 pgRNA-*purH*	CRISPRi mutant targeting *purH;* K562_ RS16140	This study
B. cenocepacia K56-2::dCas9 pgRNA-K562_RS16640	CRISPRi mutant targeting hypoxanthine-guanine phosphoribosyltransferase*;* K562_ RS16640	This study
B. cenocepacia K56-2::dCas9 pgRNA-*purF*	CRISPRi mutant targeting *purF;* K562_ RS22230	This study
B. cenocepacia K56-2::dCas9 pgRNA-*nadR*	CRISPRi mutant targeting *nadR;* K562_ RS27675	This study
B. cenocepacia K56-2::dCas9 pgRNA-*gshA1gshB*	CRISPRi mutant targeting *gshA1 gshB* operon*;* K562-RS03750 and K562_RS03755	This study

2.2 Synthesis of Auranofin and Auranofin Analogs

Auranofin, WB-19-HL4118 (MS-40), WB-18-FI3683, WB-16-EO9899, WB-19-HG5899 and WB-19-HB2664 were synthesized following our previously published protocol (Wu et al. 2019).

WB-19-HL4170 (MS-40S). To a solution of Me_3PAuCl (150 mg, 0.486 mmol) and 1-mercapto-2-propanol (43 μL, 0.486 mmol) in MeOH (10 mL), $NaOCH_3$ was added (25 wt% in methanol, 125 μL). The solution was stirred at room temperature for 2 h. The reaction mixture was then concentrated on a rotary evaporator, diluted with dichloromethane, and poured into water followed by 3 times extraction by dichloromethane. The combined organic phase was dried over Na_2SO_4, concentrated, passed through a PTFE syringe filter (0.2 μm), and dried under vacuum to afford the product as light beige crystals (172 mg, 97%). ^{1}H NMR (500 MHz, $CDCl_3$) δ 3.70 (dqd, *J* = 9.4, 6.1, 3.4 Hz, 1H), 3.47 (s, 1H), 3.09 (dd, *J* = 12.7, 3.3 Hz, 1H), 2.82 (dd, *J* = 12.7, 9.0 Hz, 1H), 1.60 (d, *J* = 10.4 Hz, 5H), 1.24 (d, *J* = 6.1 Hz, 2H), (Appendix Figure A1). ^{13}C NMR (126 MHz, $CDCl_3$) δ 70.41, 38.47, 21.57, 16.03 (d, *J* = 35.7 Hz), (Appendix Figure A2). ^{31}P NMR (162 MHz, $CDCl_3$) δ -0.31 (Appendix Figure A3).

WB-19-HL4171, WB-19-HL4172 and WB-19-HL4181 were synthesized following the same procedure as MS-40 above.

WB-19-HL4171. Light yellow crystals (183 mg, 99%) from Me_3PAuCl (150 mg, 0.486 mmol) and 1-thioglycerol (36 μL, 0.486 mmol). ^{1}H NMR (500 MHz, $CDCl_3$) δ 3.83–3.60 (m, 4H), 3.10 (dd, *J* = 12.8, 4.4 Hz, 1H), 3.00 (dd, *J* = 12.8, 7.7 Hz, 1H), 2.93 (s, 1H, OH_α), 2.32 (s, 1H, OH_β), 1.60 (d, *J* = 10.4 Hz, 9H), (Appendix Figure A4). ^{13}C NMR (126 MHz, $CDCl_3$) δ 74.49, 65.58, 32.65, 16.13 (d, *J* = 35.8 Hz), (Appendix Figure A5). ^{31}P NMR (162 MHz, $CDCl_3$) δ -0.36, (Appendix Figure A6).

WB-19-HL4172. Light grey semi-solids (175 mg, 99%) from Me_3PAuCl (150 mg, 0.486 mmol) and 3-mercapto-1-propanol (42 μL, 0.486 mmol). ^{1}H NMR (500 MHz, $CDCl_3$) δ 3.83 (t, *J* = 5.9 Hz, 2H), 3.19 (s, 1H), 3.04 (t, *J* = 6.8 Hz, 2H), 1.92 (p, *J* = 6.6 Hz, 2H), 1.60 (d, *J* = 10.4 Hz, 9H), (Appendix Figure A7). ^{13}C NMR (126 MHz, $CDCl_3$) δ 62.30, 39.20, 25.82, 16.07 (d, *J* = 35.5 Hz), (Appendix Figure A8). ^{31}P NMR (162 MHz, $CDCl_3$) δ -0.41, (Appendix Figure A9).

WB-19-HL4181. Colorless viscous solids (113 mg, quantitative) from Me_3PAuCl (100 mg, 0.324 mmol) and cysteamine hydrochloride (37 mg, 0.324 mmol). ^{1}H NMR (500 MHz, $CDCl_3$) δ 3.01 (t, *J* = 6.3 Hz, 2H), 2.88 (t, *J* = 6.3 Hz, 2H), 1.99 (s, 2H), 1.59 (d, *J* = 10.4 Hz, 9H), (Appendix Figure A10). ^{13}C NMR (126 MHz, $CDCl_3$) δ 47.89, 32.94, 16.02 (d, *J* = 35.6 Hz), (Appendix Figure A11). ^{31}P NMR (162 MHz, $CDCl_3$) δ -0.15, (Appendix Figure A12).

WB-19-HL4121a. To a solution of 2-mercaptoethanolatotrimethylphosphine gold(I) (MS-40, 200 mg, 0.570 mmol) in 100 mL of dichloromethane, ferrocenium hexafluorophosphate (95 mg, 0.286

mmol) was added. The solution was stirred at 0 °C for 23 h. After filtration, the filtrate was concentrated and was then transferred to a 20-mL scintillation vial with a total volume of ~ 5 mL. The solution was placed in an ether vapor environment at 4 °C overnight. The yellow crystals formed were washed by diethyl ether and were further purified by preparative silica gel TLC (10:1 *v/v* dichloromethane/methanol) to give the product as a white solid (22 mg, 7.5%). ^{1}H NMR (400 MHz, CD_2Cl_2) δ 1.60 (t, J = 4.1 Hz, 1H), (Appendix Figure A13). ^{31}P NMR (162 MHz, CD_2Cl_2) δ 8.2, 143.8 (septet, J_{PF} = 710 Hz), (Appendix Figure A14).

2.3 Auranofin Analogs and Antibiotic Stock Solutions

Stock solutions of auranofin and auranofin analogs were prepared by dissolving the compounds in dimethyl sulfoxide (DMSO) at a concentration of 20 mg/mL. Antibiotics were suspended at the following concentrations: tobramycin (Alfa Aesar), 10 mg/mL in H_2O; chloramphenicol (Sigma), 20 mg/mL in ethanol; ceftazidime (Sigma), 10 mg/mL in 0.1 M NaOH; meropenem (Sigma), 10 mg/mL in DMSO; doxycycline (Sigma), 25 mg/mL in H_2O; ciprofloxacin (Sigma), 10 mg/mL in 0.1 M HCl; and avibactam (MedKoo Biosciences), 10 mg/mL in DMSO. The following selective antibiotics were used for mutant construction: trimethoprim (Sigma; 50 µg/mL for *E. coli* and 100 µg/mL for *B. cenocepacia*), gentamicin (Fisher Scientific; 50 µg/mL for *B. cenocepacia*), kanamycin (Fisher Scientific; 40 µg/mL for *E. coli*), and tetracycline (Sigma; 20 µg/mL for *E. coli* and 100 µg/mL for *B. cenocepacia*).

2.4 Antimicrobial Susceptibility Testing and Multistep Resistance to Active Analogs

The compounds were diluted from their stock solutions to 256 µg/mL in Cation-Adjusted Mueller Hinton Broth (CAMHB) for use in the experiment. Determination of the MIC was

followed by standards set by the Clinical Laboratory Standards Institute (CLSI) (Clinical and Laboratory Standards Institute CLSI 2003). The 96-well plates were filled with 50 μL of CAMHB, combined with a concentration gradient of compound to be tested. Bacterial culture was diluted to a turbidity equal to MacFarland Standard 0.5, then diluted 100-fold in CAMHB. A total of 50 μL of culture was transferred into each well. After incubation at 37˚C with no shaking for 18 h, MIC was read visually as the lowest concentration of antibiotic that prevented growth. For CRISPRi mutants, they were grown overnight in LB with 100 μg/mL trimethoprim. For the MIC's, the same method was done, just with the addition of 100 μg/mL of trimethoprim and 30.5 mM rhamnose to the CAMHB.

To determine the rate of multistep resistance mutations from serial passaging, the assay was performed as described previously (Yarlagadda et al. 2014; AbdelKhalek et al. 2018). From the MIC plate, 30 μL from the well that had bacterial growth at the highest concentration of the antimicrobial (0.5 x MIC) for each of the compounds tested, was inoculated into 2 mL of LB without compound and incubated overnight at 37˚C with shaking. These overnight cultures were then used as the culture for a second MIC test, and this was repeated 12 times for a total of 24 days of continuous growth.

2.5 Time Kill Assays

Bacterial cultures were grown overnight and either subcultured to an OD_{600} of 0.025 or left in stationary phase. If subcultured, the bacteria were grown to early exponential phase (OD_{600} of 0.13–0.18). The bacteria were exposed to the antibiotics at 1x, 2x, and 4x the MIC, as well as no antibiotic for a negative control. Each hour from time zero to six hours, a sample of each condition

was serially diluted to a dilution factor of 10^{-8}, and 5 μL of each dilution was spotted onto LB agar. Plates were incubated for 24 hours at 37˚C to determine CFU/mL.

2.6 Time Kill of Persister Cells

The generation and collection of persister cells was adapted from (Bahar et al. 2015). Briefly, persister cells were generated by subculturing an overnight culture of *B. cenocepacia* K56-2 in LB and grown until it reached early exponential phase (OD_{600} of 0.13–0.18). The culture was then exposed to 5x MIC of ciprofloxacin (CIP; MIC = 2 μg/mL) with 0x MIC as a control for three hours. For the initial time zero count, a sample was taken and diluted to a factor of 10^{-8} and 5 μL was spotted onto LB. After the initial count, ciprofloxacin was added to the corresponding culture. A sample was taken every hour for three hours for CFU/mL counts, as mentioned above. After the third hour, the remaining population, enriched in persister cells, was collected, washed, and resuspended in phosphate buffered saline (PBS), divided into five tubes, and again exposed to 5x MIC ciprofloxacin or different concentrations of MS-40S or MS-40 (2x and 4x the MIC), along with a no antibiotic condition as a control. Samples were taken every hour for an additional three hours. Plates were incubated at 37˚C for 24 hours and counted for CFU/mL.

2.7 Persister Frequency Assay

The persister frequency assay was performed as described (Ross et al. 2018). An overnight culture of *B. cenocepacia* K56-2 was subcultured to a concentration of 1×10^8 CFU/mL in 2 mL LB. Antimicrobials tested, meropenem, ceftazidime–avibactam, MS-40S, and MS-40 were added to a final concentration of 5x and 10x MIC. The cultures were exposed to the antibiotics for 24

hours at 37˚C with shaking. After 24 hours the culture was plated on LB to determine CFU/mL. Plates were incubated at 37˚C for 24 hours.

2.8 *C. elegans* Survival

Caenorhabditis elegans was used as a model organism to test the toxicity of the compounds. The survival was performed as described in (Selin et al. 2015). *C. elegans* DH26 eggs were incubated at 26˚C until they reached the L4 stage, at approximately 48 h. L4 stage worms were collected and washed with M9 media. Worms were suspended in 100 μL of M9 and transferred to the NGMII plates containing *E. coli* OP50. Approximately ten non-infected *C. elegans* OP50-fed worms, in triplicate, were exposed to a serial dilution of antibiotics to be tested in liquid killing media (LKM; 80% M9 buffer 20% liquid NGMII) in a 96-well plate. The range of concentrations used was 4-128 μg/mL for the following antimicrobials: MS-40, MS-40S, meropenem, doxycycline, and ceftazidime–avibactam, along with a no antibiotic control. Worms were counted at day 0 and incubated at 25˚C. After 24 h, worms were counted for percent survival and the $Survival_{100}$/MIC ratio was calculated. Worms that appeared straight were considered dead, and those were moving and S-shaped were counted as alive. Three experimental replicates were performed.

2.9 *Galleria* Toxicity

Galleria mellonella was also used as a model organism to study the toxicity of MS-40 and MS-40S. The experiments were performed as done in (Cruz et al. 2018; Naguib and Valvano 2018). *Galleria* larvae were stored at 16˚C in wood shavings and used within 2 weeks of receiving them. Larvae, with an approximate weight of 250 mg, were injected with 10 μL in the last, left

proleg using a Hamilton micro-syringe (Hamilton, Nevada, USA). For each compound, MS-40S, MS-40, and doxycycline were diluted in PBS, and 10, 5, 2, and 1 mg/kg were injected in 10 worms for each condition. A total of 10 worms were also injected with 10 μL of PBS for a negative control, and 10 worms were not injected. Survival was measured every 24 hours for 72 hours. Larvae were considered dead if non-motile and unresponsive to touch. Three experimental replicates were performed. Survival curves were made on GraphPad Prism 6.

2.10 CRISPRi Mutant Construction

CRISPRi mutants were made as previously described (Hogan et al. 2019). Inverse PCR was used to introduce new sgRNA targeting regions into pSCB2-sgRNA. The 5' – GTTTTAGAGCTAGAAATAGCAAGTTAAAATAAGGC – 3' primer was used with a 5' extension of the 20-nucleotide targeting sequence. This primer was used with 1092 for PCR amplification. The PCR product was used for blunt end ligation using T4 DNA ligase (NEB), T4 PNK (NEB) and *Dpn*I (NEB) in a custom ligase buffer (132 mM Tris-HCl pH 7.5, 20 mM $MgCl_2$, 2 mM ATP, 15% PEG6000 in de-ionized water). The reaction was then incubated at 37˚C for 30 minutes. The ligation mix was then transformed into *E. coli* DH5α and tri-parental mating was done to transfer the plasmid into *B. cenocepacia* K56-2::dCas9.

2.11 Thioredoxin Reductase Purification and Inhibition Assay

The thioredoxin reductase gene (locus tag; K562_RS14600) was amplified from *B. cenocepacia* K56-2 genome using primers 2303 and 2304 (Table S3). The primers contained the cut sites *BamH*I and *Hind*III to be cloned into pET-24b+, which contains a C-terminal 6x His-tag, creating pET-24b-TrxB. The plasmid was then transformed into *E. coli* BL21(DE3)-Gold. For

purification, *E. coli* containing pET-24b-TrxB was grown to an OD_{600nm} of 0.6 at 37˚C for approximately three hours with shaking. After, 1 mM IPTG was added to induce expression of *trxB*, and the cells were allowed to grow for an additional three hours at 30˚C with shaking. Cells were pelleted and resuspended in lysis buffer: 50 mM TRIS, 500 mM NaCl, 25 mM imidazole, pH 7.5, and lyzed using an Emulsiflex-C3 High Pressure Homogenizer (Avestin). Protein was then purified using a nickel affinity column (Bio-Rad). Size exclusion was performed using an AKTA - FPLC (Cytiva). The gel filtration buffer (20 mM Tris pH 7.5, 150 mM sodium chloride, and 1 mM β-ME) was used to equilibrate the column.

In vitro inhibition assay was done as described in the protocol from the Sigma kit (catalog number CS0170). Manufacture instructions were followed except for the thioredoxin reductase protein, which we substituted with our purified protein. The undiluted enzyme was diluted in 20-fold in assay buffer, then 2 µL was added to each well, thus the resulting concentration was 0.0091 units/mL Inhibition of TrxB was measured by the reaction of DTNB to TNB, catalyzed by TrxB, which is detectable at 412 nm. MS-40 and MS-40S were serially diluted in concentrations ranging from 250 nM to 3.906 nM. A_{412nm} was measured using a Synergy2 plate reader.

2.12 NPN Permeability Assay

NPN outer membrane permeability assay was done as described previously (Hogan et al. 2023). Overnight cultures of CRISPRi mutants were grown in LB, Tp100 with 30.5 mM rhamnose. Cultures were diluted to an OD of 0.025 in LB, Tp100 with 30.5 mM rhamnose and grown until an approximate OD of 1.0. Centrifugation was used to wash the cells and resuspended in 5 mM HEPES pH 7.2 with 10 mM NaN_3 (Sigma), this was then incubated at room temperature for 30 minutes. 50 µL of cells were mixed with 50 µL of HEPES buffer containing 80 µM NPN (Sigma).

A BioTek Synergy 2 plate reader with filter sets, Ex 360/40 nm and Em 420/40 nm, was used to measure fluorescence intensity. Fluorescence values were blank corrected and divided by the OD600 of each well to normalize. Fluorescent ratios were calculated based off the dCas9 non-targeting control.

2.13 Glutathione Reductase Purification and Inhibition Assay

Glutathione reductase (locus tag K562_RS03010) was amplified from *B. cenocepacia* K56-2 genome using the primers 3002 and 3385. Primers added *Nde*I and *Hind*III cut sites for cloning into pET-22, containing a C-terminal 6x His-tag, creating pET-22-GOR. This was also transformed and purified as stated with TrxB. *In vitro* inhibition assay was done as described in the protocol from the Sigma kit (catalog number GRSA). Manufacture instructions were followed except for the glutathione reductase protein, which we substituted with our purified protein. The undiluted enzyme was diluted 20-fold in assay buffer, then 2 μL was added to each well, thus the resulting concentration was 0.0052 units/mL. Activity of GOR was measured by tracking the presence of NADPH in the following reaction: $NADPH + H^+ + GSSG \rightarrow 2GSH + NADP^+$ which is catalyzed by glutathione reductase (GOR). MS-40 and MS-40S were serially diluted in concentrations ranging from 250 μM to 3.906 μM.

2.14 ROS Detection

This protocol was adapted from (Slachmuylders et al. 2018) and (Van Acker et al. 2016). An overnight culture of *B. cenocepacia* K56-2 was subcultured in 5 mL LB and grown for 3 hours, then adjusted to an OD_{600} of 0.3 in 8 mL 1x phosphate buffered saline (PBS) (pH 7.4). The dye H_2DCFDA (Sigma) at 10 μM was added to the culture and incubated at 37˚C with shaking for 45

min, protected from light. After incubation, cultures were washed at 5000 rcf for 5 min and resuspended in PBS. Cultures were combined with 4x MIC solutions of MS-40, MS-40S, and tetracycline and 1x MIC of MS-40 and MS-40S. Each condition was added to a 96-well plate, along with exponential phase cells with and without dye, and a DMSO control, all of which were added in triplicate. Empty wells were filled with LB to prevent evaporation. Fluorescence with excitation at 485 nm and emission at 535 nm were measured every 30 min for 14 hours using a BioTek Synergy 2 plate reader. One-way ANOVA and Dunnett Test were performed using R studio.

CRISPRi mutants were grown overnight in LB with 100 μg/ml trimethoprim and 30.5 mM rhamnose. The cells were subcultured in the same conditions for three hours to reach exponential phase. Once in exponential phase, H_2DCFDA dye was added and allowed to incubate for 45 minutes at 37 C. The cells were then washed twice and resuspended in PBS with Tp100 and 30.5 mM rhamnose. Non-targeting dCas9 CRISPRi mutant was used as a control. Fluorescence (λ excitation = 485 nm, λ emission 528 nm) and OD_{600nm} readings were taken every 5 minutes for 2 hours in a BioTek Synergy 2 multimode plate reader. The ratio of ROS production was calculated by calculating relative fluorescence units (RFU) / OD, this was then normalized to the rate of ROS production of the control. Autofluorescence of H_2DCFDA dye with no cells in PBS was considered in calculations. One-way ANOVA and Dunnett Test were performed using R studio.

2.15 Microscopy

B. cenocepacia K56-2 was grown in LB until stationary phase then back diluted to an approximate OD of 0.025 in LB and allowed to grow to mid-exponential phase, about 3 hours. Then the cells were exposed to the H_2DCFDA dye for 45 minutes, washed with PBS then exposed

to the antibiotics for three hours at the respective concentrations. Next, 1 mL of cells was centrifuged and washed with PBS. Cells in PBS were spotted on 1.5% agarose pads and imaged by DIC microscopy on an Axio Imager upright microscope (Carl Zeiss Microscopy GmbH). Fluorescent microscopy was also done with the Axio Imager upright microscope with λ excitation = 450-490 nm, λ emission 500-550 nm.

2.16 Barcoded Transposon Mutant Pool Exposure, Library Preparation, and Sequencing

The BarSeq exposure, library preparation, and sequencing was done as previously described (Hogan et al. 2023). The library was thawed and mixed to have equal abundance of each of the unique mutants. This pool was then inoculated at an OD_{600nm} of 0.025 in 50 mL LB with 12.2 mM rhamnose, which was then grown at 37˚C with shaking at 230 rpm. This culture was grown to early exponential phase, an OD_{600nm} of approximately 0.15. This culture was then aliquoted into 2 mL test tubes. A 2 mL tube was used as time zero and not exposed to any antibiotics. The other remaining cultures were exposed to the IC_{25} of each compound tested and grown for 8 hours, along with a 0.128 M DMSO solvent control. These cultures were grown at 37˚C with shaking at 230 rpm.

Genomic DNA was extracted using the PureLink Genomic DNA Mini Kit (Invitrogen) after compound exposure. To amplify the barcodes, we added 200 ng genomic DNA, 20 μM of primer and each product from each condition was amplified with a unique i7 and i5 index, and Q5 high-fidelity DNA polymerase with the high-GC buffer, and standard Q5 reaction buffer (NEB). To purify the 196 bp desired product, two rounds of dual size selection with Sera-Mag Select (Cytiva) magnetic beads were used with 200 μL of BarSeq PCR products. A NextSeq 500 in high-output mode (Donnelly Centre, Toronto, Canada) was performed with reagent kit v2.5 and 20%

PhiX spike. This generated 410-510 million 30 bp single end reads. Primers used can be found in Table 1.

2.17 Fitness Calculation for BarSeq

The scripts from (Wetmore et al. 2015) were used to associate each BarSeq reads with the correct barcode. These reads, in fastq format, were trimmed using the FASTX toolkit (http://hannonlab.cshl.edu/fastx_toolkit/) to contain only the 20-nucleotide barcode, with reads containing a quality score less than 20 being filtered out. NNNGTCGACCTGCAGCGTACG and AGAGACC, are artificial pre- and post-sequences, respectively, that were added to all barcodes to make them valid according to the RunBarSeq.pl script.

Next, the scripts from (Morin et al. 2018) were used to process the barcodes to compare the abundance of each mutant between conditions (https://github.com/DuttonLab/RB-TnSeq-Microbial-interactions). With log transformations, 0 values create errors, thus, a pseudocount of 0.1 was added to all barcode counts. Barcodes were removed if they 1) had fewer than 3 reads in the Time 0 condition and 2) represented intergenic insertions, or insertions in the first or last 10% of a gene. Normalization of raw mean read counts were done against 10 non-essential genes that showed no fitness effect in any condition. These were: K562_RS24650 (ABC-type amino acid transporter), K562_RS22855 (putative glycosyltransferase), K562_RS05000 (hydrolase family protein), K562_RS12100 (acyl-CoA dehydrogenase), K562_RS01045 (Raf kinase inhibitor-like protein), K562_RS06455 (putative PHA depolymerase protein), K562_RS13470 (*gudD*, glucarate dehydratase), K562_RS16220 (DUF3025 domain-containing protein), K562_RS18550 (hypothetical protein), K562_RS28510 (hypothetical protein). Fitness values for each strain was calculated as the $\log_2$ (reads in experimental condition / reads in Time 0). Fitness value for each

gene was calculated as the arithmetic mean from the individual strain fitness values for each gene. Smoothing of fitness values was done using a genomic position using a moving window to deal with increased read count due to proximity to the replication forks (Wetmore et al. 2015). Gene fitness for the three replicates was calculated as the inverse-variance weighted mean. Spearman, Pearson, and Lin correlation coefficients across replicates for each condition were between 0.5 and 0.8. An independent two-sided Student's t-test was performed on each gene fitness values compared to the DMSO control for each condition.

2.18 BioCyc Pathway Perturbation Score and Pathway Enrichment

For BioCyc analysis, a text file containing locus tags for genes that had significant change in gene fitness, along with the said gene fitness value, was uploaded for each compound into a SmartTable. This was done separately for genes that had negative fitness scores and positive fitness scores. To calculate the pathway perturbation score, the cellular overview tool was used and, under Overlay Experimental Data, the data from SmartTable was imported, and the pathway perturbation score was calculated using the default settings. For pathway enrichment, in the SmartTable, use enrichment tool for pathways and use the default settings.

2.19 Unmarked Gene Deletions

A double homologous recombination method described previously (Flannagan et al. 2008; Hamad et al. 2010) was used to make unmarked gene deletions in *B. cenocepacia* K56-2. Approximately 350 bp of upstream and downstream regions were amplified and ligated using a *Hind*III restriction cut site. This ligated product was used to amplify the upstream and downstream regions fused together, which was then ligated into the pGPI-SceI plasmid using *Xba*I and *Xma*I

cut sites. These plasmids were then transformed into *E. coli* SY327 and conjugated into *B. cenocepacia* K56-2. Colony PCR was used to confirm insertion of the first recombination event of trimethoprim resistant clones. To encourage the second recombination event, pDAI-SceI-*sacB* was conjugated into these clones. Trimethoprim sensitive colonies were identified and colony PCR was used to confirm deletion. The pDAI-SceI-*sacB* plasmid was cured by patching onto LB (without NaCl) + 0.438 M sucrose. Colonies that grew on sucrose were screen for tetracycline sensitivity for successful curing of the plasmid.

2.20 Growth Detection of Glutathione Mutants

To measure the growth of the glutathione mutants, cultures were made in LB for wildtype and deletion mutants or in LB plus 100 μg/mL trimethoprim for the non-targeting strain or the *gshA1gshB* mutant. Once they reached stationary phase, each strain was back diluted to an OD_{600nm} of 0.01 in LB or LB Tp100 +/- 30.5 mM rhamnose in a 96-well plate. The plate was incubated at 37˚C with shaking for 18 hours. OD_{600nm} was then measured to determine the growth of each mutant. One-way ANOVA and Dunnett Test were performed using R studio.

2.21 ATP Detection of Exponential Phase Cells Exposed to MS-40 and MS-40S

An overnight culture of *B. cenocepacia* K56-2 was subcultured in 5 mL LB and incubated with shaking at 37˚C for 3 hours. After incubation, subculture was adjusted to an OD_{600nm} of 0.6. To a 384-well plate, *B. cenocepacia* K56-2 exponential phase cells were exposed to MS-40, MS-40S at 2x and 0.5x MIC, and tetracycline at 2x MIC, in duplicate. Cells were also exposed to 15 mM AsO_4 and a DMSO control and added to the plate in duplicate. *B. cenocepacia* K56-2 cells alone in LB were also added in duplicate, and LB only was added in duplicate as a blank. Plates

were incubated at 37˚C with shaking for 3 hours. After incubation, OD_{600nm} was measured, followed by addition of BacTiter-Glo™ Reagent to all wells. Plates were incubated in a BioTek Synergy 2 plate reader at 25˚C for 5 min, then luminescence was recorded. One-way ANOVA and Dunnett test were performed using R studio.

CHAPTER 3: RESULTS

3.1 Analogs of Auranofin have lower MICs than Auranofin

We tested the MIC auranofin and ten auranofin analogs (Figure 5), using the broth microdilution method, against a panel of Bcc bacteria, comprising of clinical isolates from CF patients and strains from environmental sources (See Table 3). Auranofin (Figure 5A) and the analogs belonging to group one (Figure 5B) were largely inactive against members of the Bcc (Table 4), with most of the MICs being 128 μg/mL or higher. Group one analogs have modifications of the thioglucose ligands, with some having the triethylphosphine (-PEt_3) replaced with trimethylphosphine (-PMe_3). Auranofin, however, showed high activity against *B. mallei* with MICs ranging from 0.25–1 μg/mL. In *B. pseudomallei*, auranofin had an MIC of 64 μg/mL. Auranofin and the group one analogs in this study were shown to have diverse activity in other Gram-negative and Gram-positive bacteria, but they were inactive or had low activity in *P. aeruginosa*, *Enterobacter cloacae*, and *K. pneumoniae* (Wu et al. 2019).

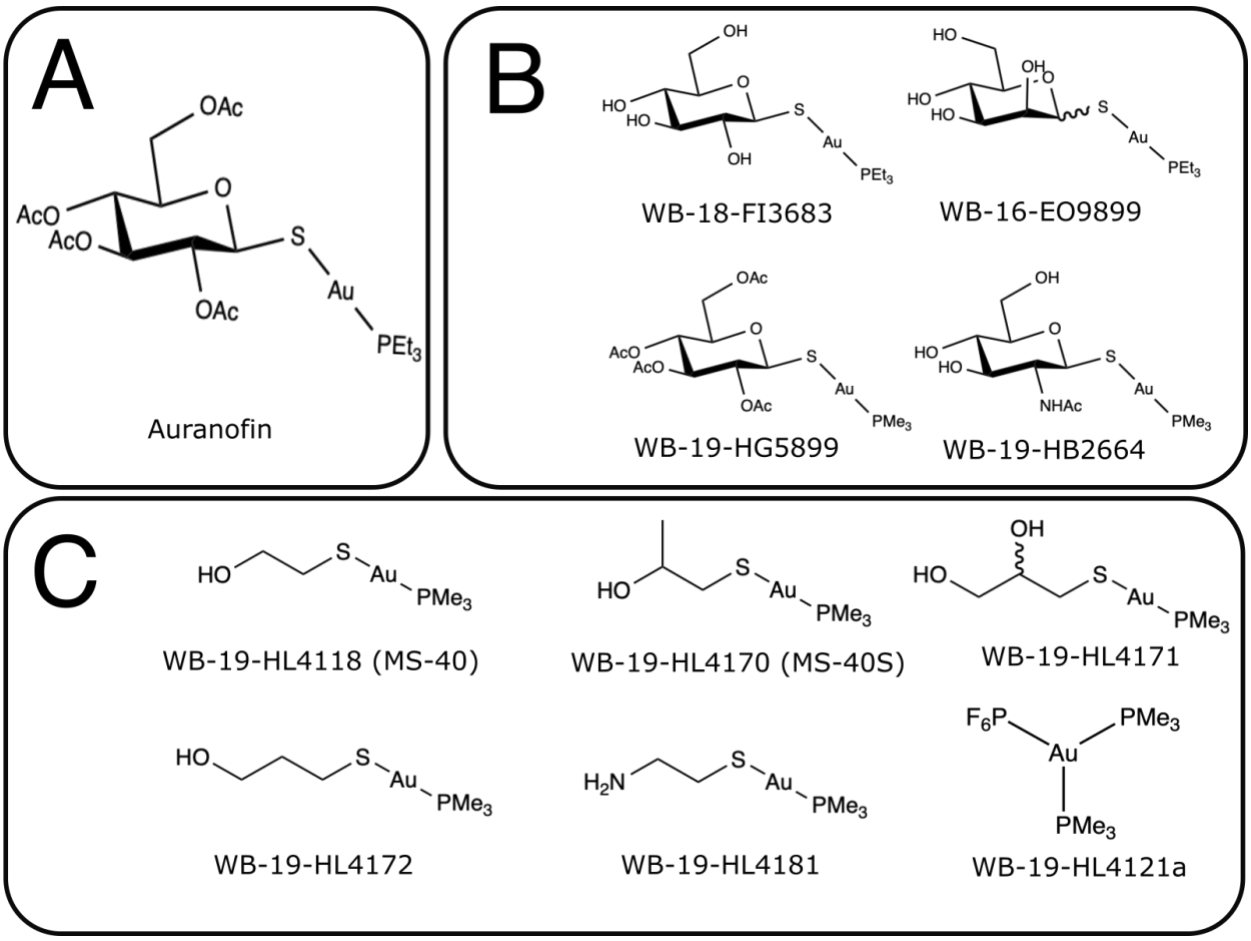

Figure 5. Chemical structure of auranofin and auranofin analogs.

(**A**) Auranofin. (**B**) Group one auranofin analogs containing modifications of the thioglucose and replacement of triethylphosphine ($P(CH_2CH_3)_3$; PEt_3) with trimethylphosphine ($P(CH_3)_3$; PMe_3). (**C**) Group two auranofin analogs, contains mercaptoethanol ($OHCH_2CH_2SH$) replacing the thioglucose, then with further modifications of the mercaptoethanol.

Table 4. Broth microdilution minimum inhibitory concentrations (MICs) of group one auranofin analogs against a panel of *Burkholderia cepacia* complex (Bcc) species .

Organism	**MIC (μg/mL)**				
	Auranofin	**WB-18-FI3683**	**WB-16-EO9899**	**WB-19-HG5899**	**WB-19-HB2664**
B. cenocepacia K56-2	>128	>128	>128	>128	>128
B. lata BCC6	128	128	128	128	128
B. contaminans MF16	128	128	128	128	128
B. contaminans FFH-2050MA	128	128	128	64	64
B. dolosa CEP021	>128	>128	>128	>128	>128
B. multivorans ATCC17616	128	128	128	128	128
B. cenocepacia 140485	128	64	32	128	128
B. ubonensis LMG 20358	>128	>128	>128	128	128
B. contaminans FFH-4004	>128	>128	>128	128	128
B. mallei China 5 (NBL 4)	0.25	ND	ND	ND	ND
B. mallei Ivan (NCTC 10230)	0.5	ND	ND	ND	ND
B. mallei China 7 (NBL 7)	1	ND	ND	ND	ND
B. pseudomallei 1710b	64	ND	ND	ND	ND
B. pseudomallei MSHR465a	64	ND	ND	ND	ND
B. pseudomallei HBPUB10134a	ND	ND	ND	ND	ND

The reported MIC values are from three biological replicates. In the case a 2-fold difference occurred, the higher value is reported.

Group two (Figure 5C) includes the analog WB-19-HL4118 (MS-40) which had shown a low MIC in Gram-negative and Gram-positive bacteria, such as in *A. baumannii, E. cloacae, E. coli,* and *S. aureus* with MICs ranging from 3-23 μM (Wu et al. 2019). Therefore, we synthetized additional analogs with similar structures to MS-40. Group two analogs showed lower MICs against members of the Bcc (Table 5) than group one (Table 4). Remarkably, MS-40 and WB-19-HL4170 (MS-40S) showed the strongest activity (Table 5). These two compounds also have high activity in *B. mallei* and *B. pseudomallei* strains as well. The remaining analogs from this group have moderate MICs, ranging from 8 to 64 μg/mL, with only WB-19-HL4171 against *B. ubonensis* LMG 20358 and WB-19-HL4121a against *B. dolosa* CEP021 and *B. ubonensis* LMG 20358 being 128 μg/mL or higher. The structures of the group two analogs have substitution of thioglucose ligands with mercaptoethanol ($HOCH_2CH_2SH$) or mercaptoethanol modification.

Next, we compared the MICs of MS-40S and MS-40 to common antibiotics used to treat CF patients infected with *Burkholderia* spp. Those include ceftazidime (Balwan et al. 2016; Kitt et al. 2016), meropenem (El-Laboudi et al. 2009; Gilchrist et al. 2012; Balwan et al. 2016; Kitt et al. 2016), doxycycline (Salizzoni et al. 2014), and tobramycin (El-Laboudi et al. 2009; Gilchrist et al. 2012; Kitt et al. 2016). The combination therapy ceftazidime–avibactam is considered the last resort treatment for those infected with *Burkholderia* species (Los-Arcos et al. 2019); therefore, we determined the MIC of ceftazidime–avibactam and these four antibiotics against the Bcc panel (Table 6). The MICs of MS-40 and MS-40S are much lower than the antibiotic tobramycin and are similar to the other antibiotics, including the last resort combination treatment ceftazidime–avibactam. Additionally, doxycycline, against some isolates from the Bcc, had MIC values as low as 1 and 2 μg/mL. Taken together, the initial MIC testing shows MS-40S and MS-

40 are comparable to antibiotics used currently in the clinic, having MICs lower than most and even have similar values to the combination therapy ceftazidime–avibactam.

Table 5. Broth microdilution minimum inhibitory concentrations (MICs) of group two auranofin analogs against a panel of *Burkholderia cepacia* complex (Bcc), *B. mallei* and *B. pseudomallei* .

Organism	MIC (µg/mL)						
	Auranofin	**WB-19-HL4118**	**WB-19-HL4170**	**WB-19-HL4171**	**WB-19-HL4172**	**WB-19-HL4181**	**WB-19-HL4121a**
B. cenocepacia K56-2	>128	4	8	32	32	32	128
B. lata BCC6	128	8	8	32	16	16	32
B. contaminans MF16	128	8	8	64	32	64	32
B. contaminans FFH-2050MA	128	4	16	32	16	32	32
B. dolosa CEP021	>128	16	32	64	32	64	128
B. multivorans ATCC17616	128	8	16	32	32	32	64
B. cenocepacia 140485	128	8	16	16	32	32	32
B. ubonensis LMG 20358	>128	16	16	>128	32	32	128
B. contaminans FFH-4004	>128	8	16	32	32	32	64
B. mallei China 5 (NBL 4)	0.25	0.12	0.12	ND	ND	ND	ND
B. mallei Ivan (NCTC 10230)	0.5	0.12	0.12	ND	ND	ND	ND
B. mallei China 7 (NBL 7)	1	0.25	0.25	ND	ND	ND	ND
B. pseudomallei 1710b	64	4	4	ND	ND	ND	ND
B. pseudomallei MSHR465a	64	4	4	ND	ND	ND	ND
B. pseudomallei HBPUB10134a	64	4	2	ND	ND	ND	ND
B. pseudomallei MSHR305	ND	2	ND	ND	ND	ND	ND

The reported MIC values are from three biological replicates. In the case a 2-fold difference occurred, the higher value is reported. ND; not determined.

Table 6. Broth microdilution minimum inhibitory concentrations (MICs) of MS-40 and MS-40S compared to clinical antibiotics used to treat CF patients.

Organism	MIC (µg/mL)							
	Auranofin	**MS-40**	**MS-40S**	**MEM**	**TOB**	**CAZ**	**DOX**	**CZA[a]**
B. cenocepacia K56-2	>128	4	8	16	512	32	4	4
B. lata BCC6	128	8	8	4	128	64	4	16
B. contaminans MF16	128	8	8	8	32	32	16	8
B. contaminans FFH-2050MA	128	4	16	4	128	8	2	4
B. dolosa CEP021	>128	16	32	8	128	16	16	8
B. multivorans ATCC17616	128	8	16	4	64	16	2	8
B. cenocepacia 140485	128	8	16	16	128	8	1	8
B. ubonensis LMG 20358	>128	16	16	16	128	16	4	4
B. contaminans FFH-4004	>128	8	16	8	64	8	8	4

[a]8 µg/mL avibactam. The reported MIC values are from three biological replicates. In the case a 2-fold difference occurred, the higher value is reported. MEM, meropenem; TOB, tobramycin; CAZ, ceftazidime; DOX, doxycycline; CZA, ceftazidime avibactam.

3.2 MS-40 and MS-40S have Broad Bactericidal Activity from

Individuals with CF are commonly infected by multiple bacteria, causing polymicrobial infections (Huang and LiPuma 2016; Cribbs and Beck 2017). For MS-40S and MS-40 to be effective antimicrobials, it is imperative for these compounds to kill additional CF pathogens. Common bacteria that cause CF lung infections, besides *Burkholderia* spp., are *Pseudomonas aeruginosa*, *Staphylococcus aureus*, *Stenotrophomonas maltophilia*, and *Achromobacter xylosoxidans* (Huang and LiPuma 2016; Vandeplassche et al. 2019). Other pathogenic Gram-negative bacteria that were shown to, although rarely, cause CF pulmonary infections include *Escherichia coli* (Edwards et al. 2020), *Escherichia vulneris* (Burns et al. 1998), *Klebsiella pneumoniae (Vandeplassche et al. 2019)*, and *Acinetobacter* species (Burns et al. 1998).

We thus tested MS-40 and MS-40S against CF pathogens to determine their MIC and MBC (minimum bactericidal concentration) (Table 7). MS-40 and MS-40S have low MICs for the Gram-positive bacterium *S. aureus*, one of which is an MRSA strain. MS-40 and MS-40S is also bactericidal against the other Gram-negative bacteria tested with MICs in the range of 1–16 μg/mL and most of the MBCs were between 1- and 4-fold of their respective MICs. *P. aeruginosa* is a common multi-drug resistant bacterium (Pang et al. 2019), with some strains/clinical isolates being extensively-drug resistant (Horcajada et al. 2019) and has moderate MIC values between 16 and 64 μg/mL and its MBCs between 2- and 16-fold higher than its MICs. Overall, the MICs/MBCs against CF pathogens show MS-40 and MS-40S have broad-spectrum bactericidal activity, indicating their potential as a therapeutic option for CF patients.

Table 7. MS-40 and MS-40S are bactericidal against other bacteria that infect CF patients from broth microdilution assay.

Organism	MIC (μg/mL)		MBC (μg/mL)	
	MS-40	**MS-40S**	**MS-40**	**MS-40S**
Burkholderia cenocepacia K56-2	4	8	8	16
Stenotrophomonas maltophilia DH57	1	2	4	8
Stenotrophomonas maltophilia K279a	2	2	2	8
Pseudomonas aeruginosa PA01	16	32	128	256
Pseudomonas aeruginosa PA7	32	64	64	128
Escherichia coli 120955	4	4	32	64
Escherichia vulneris CEP511	2	4	2	4
Klebsiella pneumoniae 120310	2	4	4	8
Acinetobacter baumannii ATCC 17978	2	2	4	8
Staphylococcus aureus ATCC 27700	0.25	0.5	2	2
Staphylococcus aureus 107094	0.25	0.25	1	1
Achromobacter xylosoxidans ACH03	8	16	8	32

The reported MIC values are from three biological replicates. In the case where a 2-fold difference occurred, the higher value was taken.

3.3 MS-40 and MS-40S do not Select for Multistep Resistant Mutants

We characterized the occurrence of resistance to MS-40 and MS-40S due to repeated exposure and continuous growth (AbdelKhalek et al. 2018). Bacteria grown in the presence of subinhibitory concentrations of each compound (0.5 x MIC) were subcultured and grown overnight in lysogeny broth (LB). These cultures were then used for the next MIC test, and this process was repeated for a total of 24 days (Figure 6A). We performed this procedure for MS-40, MS-40S and the antibiotics meropenem and doxycycline. These antibiotics were chosen because they are commonly used to treat cystic fibrosis patients infected with *Burkholderia* species (El-Laboudi et al. 2009; Gilchrist et al. 2012; Salizzoni et al. 2014; Balwan et al. 2016; Kitt et al. 2016), and they have different mechanisms of action and resistance (Kohanski et al. 2010; Munita and Arias 2016). Meropenem is a β-lactam and inhibits cell wall synthesis (Zhanel et al. 2007). Doxycycline inhibits protein synthesis by binding to the 30S ribosome (Grossman 2016).

Figure 6B shows that resistance against meropenem and doxycycline arose quickly. While their starting MICs values were 16 and 4 μg/mL, respectively, both MICs reached 256 μg/mL after 12–16 days. Remarkably, no apparent increase in their MICs was observed for MS-40 and MS-40S, demonstrating a desired property as a potential therapeutic agent.

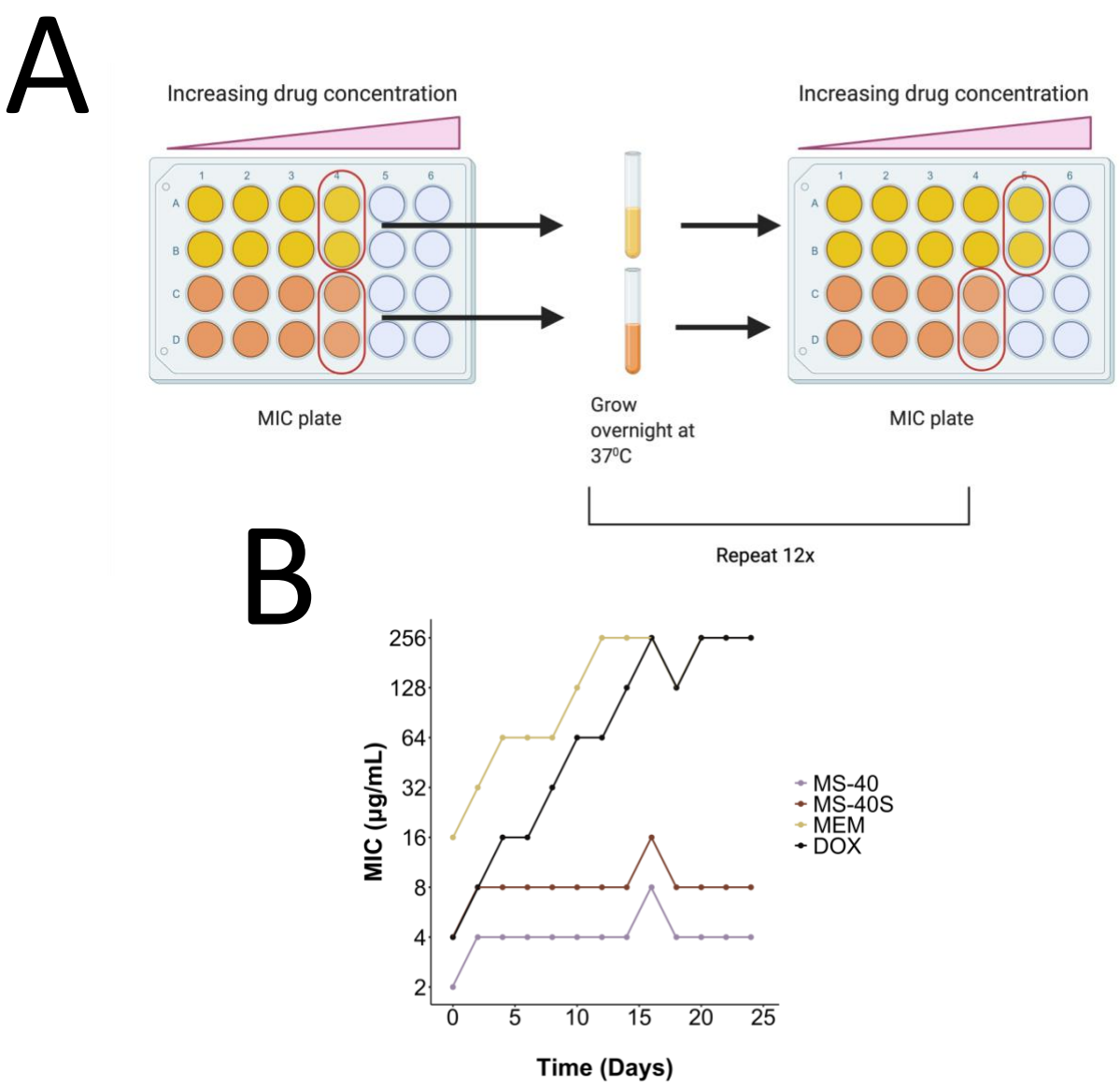

Figure 6. Mutational resistance is not generated to MS-40 and MS-40S from spontaneous resistance assay.

Repeated exposure of a *B. cenocepacia* K56-2 continuously grown culture to sub-lethal concentrations of the antimicrobials were achieved by determining the MIC of the compound. Then, for each compound, 30 µL of bacteria from the well with growth with the highest concentration of compound was grown overnight and used in the next MIC test. This was repeated over 24 days, with the MIC tested every second day. MEM, meropenem; DOX, doxycycline.

3.4 MS-40 and MS-40S are Bactericidal against Both Replicating and Non-Replicating Cells by Time Kills

Antibiotics are classified either as bactericidal, if they kill cells and reduce the population by 99.99%, or bacteriostatic, if they prevent cell growth/division, but do not kill more than 99.99% of the population (Kohanski et al. 2007, 2010). It is common for antibiotics to only target actively dividing cells because their targets are involved in replication or other energy-dependent processes (Kohanski et al. 2010), rendering them less effective when cells are not replicating or respiring (Corona and Martinez 2013). In time kill experiments, we found MS-40 and MS-40S to be bactericidal to both exponential (replicating) and stationary (non-replicating) phase cells (Figure 7). Interestingly, MS-40S is more effective at killing stationary phase than exponential phase cells, reducing the culture by approximately three $\log_{10}$ units and nine $\log_{10}$ units at 4x MIC in the exponential and stationary phase, respectively. For comparison purposes, we show that doxycycline and ceftazidime–avibactam are both unable to kill cells in stationary phase (Figure 7) and ceftazidime–avibactam is slow at killing exponential phase cells, regardless of the concentration (Figure 7).

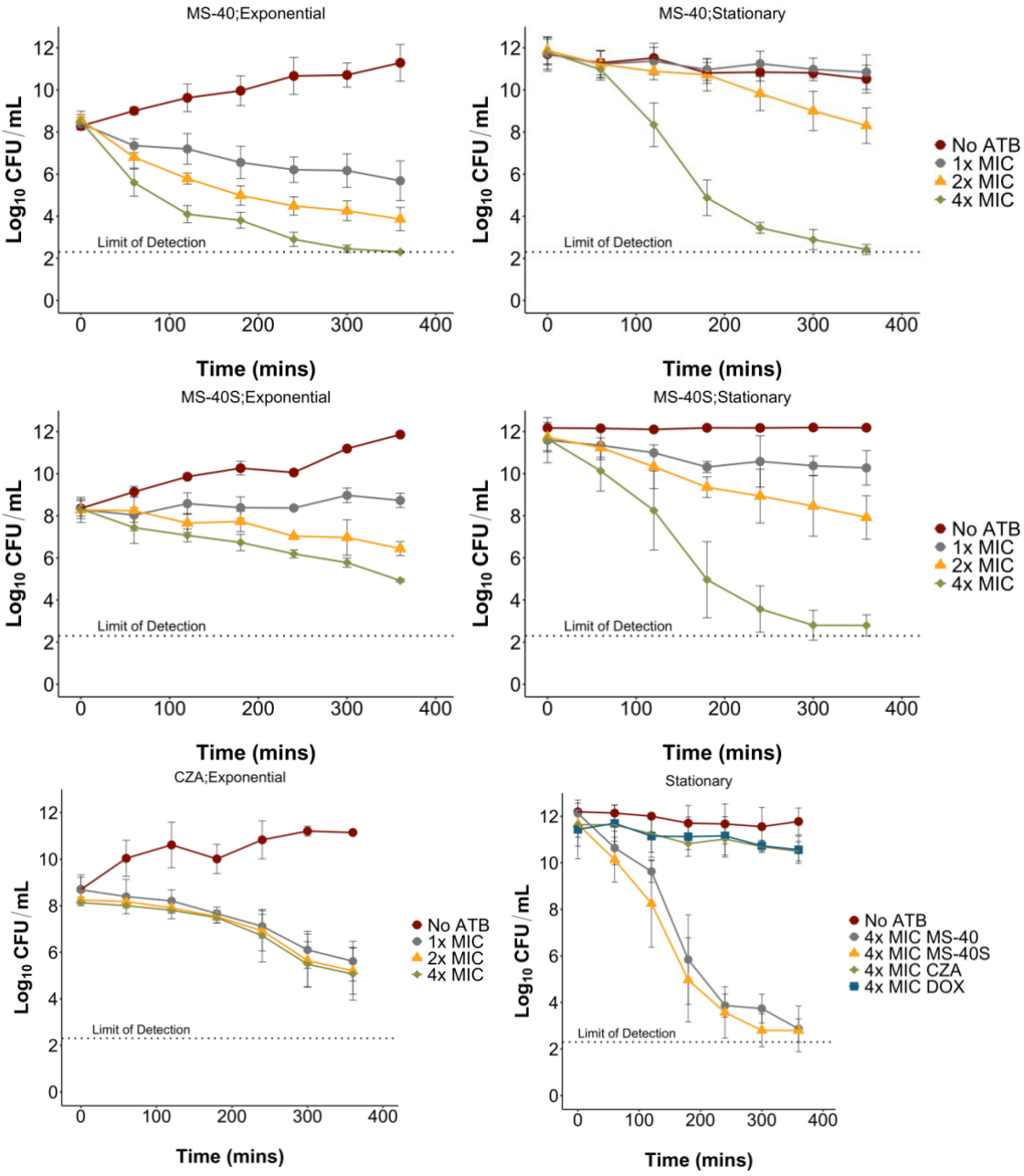

Figure 7. Exponential and stationary time kills of *Burkholderia cenocepacia* K56-2.

Exponential and stationary time kills of *Burkholderia cenocepacia* K56-2. The compounds used were MS-40, MS-40S, and ceftazidime–avibactam (CZA) at 1 x, 2 x, and 4 x MIC, as well as doxycycline (DOX) at 4 x MIC. The cultures were grown overnight for stationary phase cells or grown overnight, subcultured, and grown to early exponential phase. Samples were taken every hour for six hours to determine CFU/mL by spot plating. No ATB; no antibiotic.

3.5 MS-40 and MS-40S Kill and Inhibit the Formation of Persister Cells from Time Kills and Persister Frequency Assays

Persister cells, a subpopulation that is not killed by an antimicrobial, are hypothesized to be a common cause of relapses in infections and persistent infections (Wood et al. 2013; Brauner et al. 2016). Persisters are thought to form via randomly overexpressing a resistance factor, decreased growth rate, decreased cellular energy, and/or a slower lag phase (Brauner et al. 2016; Wilmaerts et al. 2019). Once the antibiotic is removed, they will begin to grow normally, without inherited resistance, termed "persister awakening" (Wilmaerts et al. 2019). A stationary phase population has increased amounts of persisters because it is slower growing and is metabolically dormant (Wood et al. 2013).

MS-40 and MS-40S can kill stationary phase cells effectively, so we reasoned that the compounds might kill persister cells. We exposed an exponentially growing *B. cenocepacia* K56-2 population to 5x MIC of ciprofloxacin (MIC, 2 μg/mL) for 3 hours. The surviving population of cells are now enriched in persisters. After the treatment, surviving cells were washed and collected in PBS to prevent persister awakening (Bahar et al. 2015), then exposed to the MS-40 and MS-40S. Figure 8A show persister cells, in the presence of MS-40 and MS-40S, are killed to a concentration below/close to the limit of detection, whereas the persister cells re-exposed to ciprofloxacin or those without antibiotics are not killed. This demonstrates that MS-40 and MS-40S can indeed kill persister cells created by other antibiotics.

To determine the amount of persisters remaining after 24 hours of exposure, we performed a persister frequency assay (Ross et al. 2018). We exposed a culture with a CFU/mL of 1×10^8, to one of the antimicrobials for 24 hours. Compounds tested included MS-40S, meropenem, ceftazidime–avibactam, and MS-40. The remaining cells, enriched in persisters, were plated on

LB to determine CFU/mL and percent survival was calculated by the log10 CFU/mL values. After 24 hours, no persisters were formed after exposure to 10x MIC MS-40S, and a very low persister frequency with 5x MIC MS-40S (Figure 8B). No persisters were formed exposed to 5x and 10x MIC of MS-40 and meropenem also produced a low amount of persisters at both concentrations tested. The last resort combination therapy ceftazidime–avibactam (CZA) produced the most persisters in this assay, with approximately 30% (+/-26.2) of the culture enriched in persisters surviving after treatment. CZA treatment produced large error bars because one replicate, there were no surviving cells.

Taken together, these results show MS-40S, as well as MS-40, can kill persister cells created by other antibiotics and can inhibit persister cell formation. This suggests that MS-40S, as well as MS-40, have the potential to effectively eradicate an infection, reducing the risk of a relapse in infection after the treatment regime.

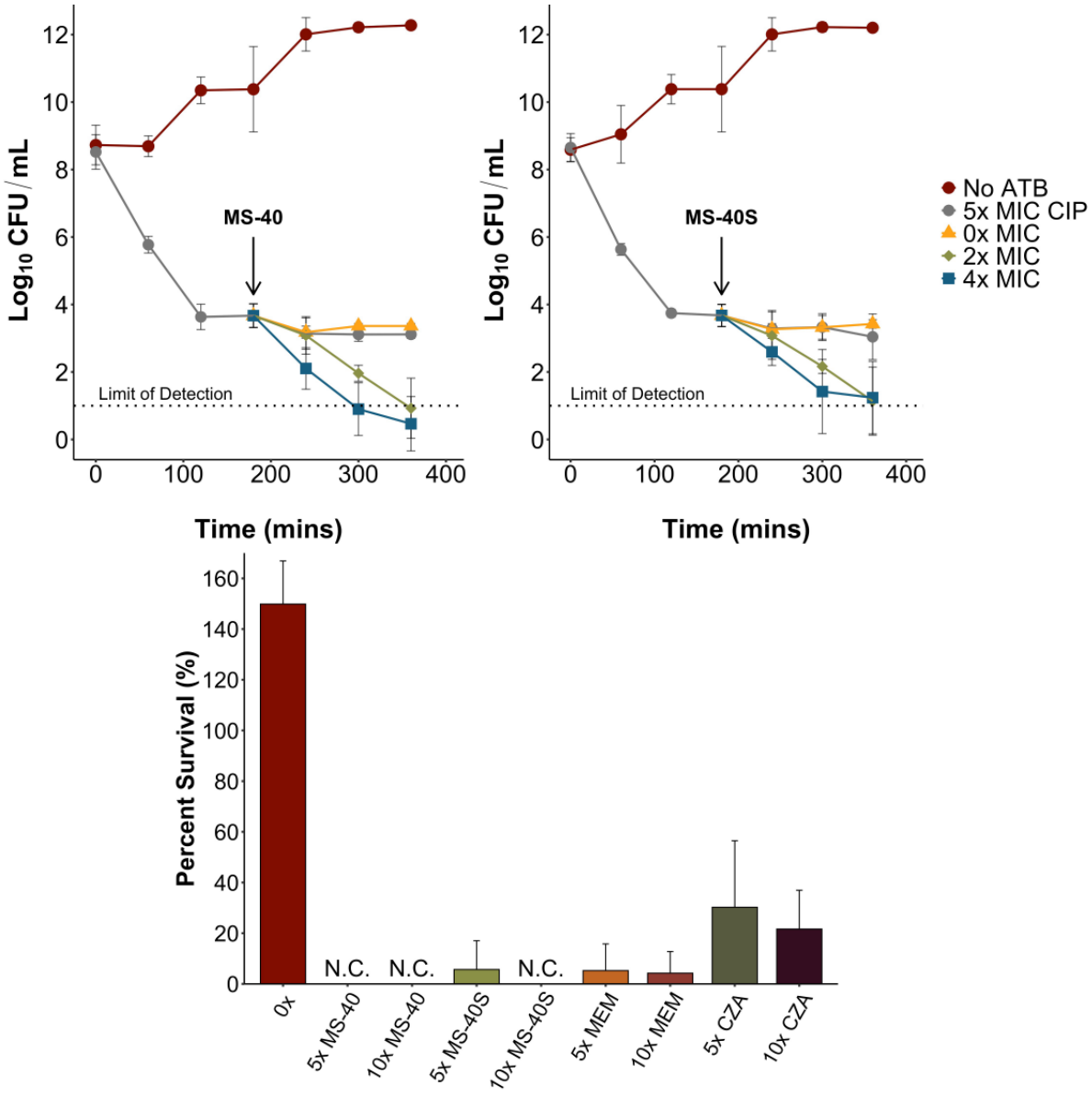

Figure 8. MS-40 and MS-40S kills and inhibits the formation of persister cells from persister time kills and persister frequency assays.

(**A and B)** An exponential phase culture with approximately 1×10^8 CFU/mL was exposed to 5x MIC ciprofloxacin (CIP) to generate persister cells. At three hours post-exposure, persister cells were washed, resuspended in PBS and exposed to 0x, 2x, or 4x MIC of MS-40 (**A**) and MS-40S (**B**) for an additional three hours. No ATB; no antibiotic. Dots represent mean from three biological replicates, error bars show standard deviation. (**C**) An overnight culture of *B. cenocepacia* K56-2 was incubated with the corresponding antimicrobial, MS-40, MS-40S, meropenem (MEM), or ceftazidime–avibactam (CZA). Percent survival was calculated by the $\log_{10}$ CFU/mL of the surviving population/$\log_{10}$ CFU/mL of the initial population. N.C., no

colonies. Bars represent mean from three biological replicates and error bars represent standard deviation.

3.6 MS-40 and MS-40S are non-toxic in *C. elegans* and *G. mellonella* Model Toxicity Assay's

In preliminary cytotoxicity tests, MS-40 was shown to have lower toxicity in human A549 cells than auranofin, with auranofin's IC_{50} being approximately 12 μM and MS-40's being approximately 50 μM (Wu et al. 2019); however, the novel compound, MS-40S, has not been tested. To show that these compounds are safe for eukaryotic cells in the range of their MIC values, we first used *Caenorhabditis elegans* as a model organism. We performed a survival assay with *C. elegans* exposed to MS-40 and MS-40S, and three clinical antibiotics: the combination ceftazidime–avibactam, meropenem, and doxycycline (Table 8). We calculated the Survival100/MIC value, which is a ratio of the highest concentration with 100% survival to the compound's MIC (Selin et al. 2015). This is a preliminary view to a compound's therapeutic index. MS-40S has similar Survival100/MIC values as clinical antibiotics, with MS-40S, doxycycline, and ceftazidime–avibactam having values of 8, 16, and 32, respectively, and MS-40 and meropenem having a value of 4.

Similar to *C. elegans*, *Galleria* larvae were also well tolerated to MS-40 and MS-40S (Table 9). This was compared to MS-40 and a clinical antibiotic, doxycycline, which has similar MIC values to MS-40S and MS-40. Concentrations used ranged from 10 to 1 mg/kg. MS-40 and MS-40S were safe for the larvae at concentrations of 10 mg/kg with a percent survival of approximately 80% and higher. This was similar as the clinical antibiotic, doxycycline. Taken together, *C. elegans* and *Galleria* toxicity models show that MS-40 and MS-40S have low toxicity in these eukaryotic organisms. However, its bioaccumulation is not known.

Table 8. Percent survival of *C. elegans* exposed to MS-40, MS-40S, and clinical antibiotics by a *C. elegans* toxicity assay.

Antibiotic	Concentrations (μg/mL)								$Survival_{100}$/ MIC ratio*
	256	**128**	**64**	**32**	**16**	**8**	**4**	**DMSO control**	
MS-40	74.4	81.8	94.7	92.9	100	100	100	100	4
MS-40S	85.7	97.6	100	100	100	100	100	100	8
MEM	93.2	97.4	100	100	100	100	100	100	4
DOX	79.5	91.5	100	98.2	100	97.4	100	100	16
CZA[a]	88.2	100	100	100	100	100	100	100	32

The values in bold indicate percent survival of the compound at its MIC value. *The $Survival_{100}$/MIC ratio is calculated as the highest concentration in which there is 100 percent survival divided by the compound's MIC. [a]Ceftazidime with 8 μg/mL avibactam. Values reported are representative of three experimental replicates.

Table 9. Percent survival of *Galleria mellonella* larvae exposed to doxycycline (DOX) MS-40, and MS-40S by a *Galleria* toxicity assay.

		***Galleria* Survival**		
Compound	**Dose Concentration (mg/kg)**	**24 h**	**48 h**	**72 h**
DOX	10.0	93.3	93.3	93.3
	5.0	93.3	90.0	90.0
	2.0	93.3	93.3	93.3
	1.0	96.7	96.7	96.7
MS-40	10.0	90	83.3	80.0
	5.0	96.7	93.3	90.0
	2.0	90.0	80.0	80.0
	1.0	100	96.7	96.7
MS-40S	10.0	90.0	76.7	76.7
	5.0	93.3	86.7	86.7
	2.0	83.3	83.3	83.3
	1.0	96.7	86.7	86.7
DMSO	10.0	93.3	86.7	86.7

Data reported are representative of three survival curves (n=30) for each concentration. The survival differences between the DMSO control and treatments were not statistically different (log-rank test).

3.7 Auranofin may be Inactive in *Burkholderia cenocepacia* Due to High Efflux and not the Presence of Glutathione Reductase

Auranofin and other auranofin analogs were shown to inhibit mammalian thioredoxin reductase (Epstein et al. 2019) and thioredoxin reductase from *Staphylococcus aureus* and *Mycobacterium tuberculosis* (Harbut et al. 2015). Auranofin is thought to be inactive in Gram-negatives for one of two reasons: 1) the presence of the secondary antioxidant system, the glutathione system, or 2) due to the low permeability of the cell envelope. We hypothesized that MS-40 and MS-40S are bactericidal in *B. cenocepacia* because they target thioredoxin reductase and the structurally and functionally similar protein, glutathione reductase (GOR) of the glutathione system, while auranofin is not bactericidal because it only inhibits thioredoxin reductase.

To confirm that auranofin, MS-40 and MS-40S share the same target, the *trxB* gene was expressed and the protein was purified from *B. cenocepacia* K56-2 and the enzymatic activity of TrxB was tested. The *trxB* gene (K562_RS14600) was amplified via PCR and ligated into the pET-24b+ expression vector via restriction digestion, this plasmid was then transformed into *E. coli* BL21 (DE3)-Gold cells. To check to see if the TrxB protein was being expressed, we grew the *E. coli* until an OD of 0.6, then induced expression by adding IPTG at 1 mM for 3 hours. After induction, cells were lyzed by sonication and the pellet and supernatant were separated by centrifugation and ran on an acrylamide gel (Figure 9). We can see TrxB being expressed in pET-24b-TrxB, and thus we moved to the purification using a nickel column. The *E. coli* was grown in the same conditions as the expression trial; however, a larger volume was used. After induction, the culture was pelleted and resuspended in lysis buffer (see Material and Methods) and lyzed using an emulsiflex and the soluble and insoluble fractions were separated by centrifugation and

the soluble fraction was ran through the nickel column. After washes, the protein was eluted with elution buffer (see Material and Methods) and all washes/elutions were ran on an acrylamide gel (Figure 10). From the gel, we saw that TrxB was in high concentration. After elution, the protein was concentrated using a protein concentrator (BioRad) and the elution buffer was replaced with a gel filtration buffer (see Material and Methods). Size exclusion chromatography (SEC) was then done to further purify the TrxB protein (Figure 11). The SEC showed that TrxB was in single species, and we collected the samples that eluted in the range of 50-70 mL. Resulting samples from the SEC were also run on an acrylamide gel to ensure there's only one size of protein present (Figure 12). From all this, we saw that we successfully purified TrxB in single species.

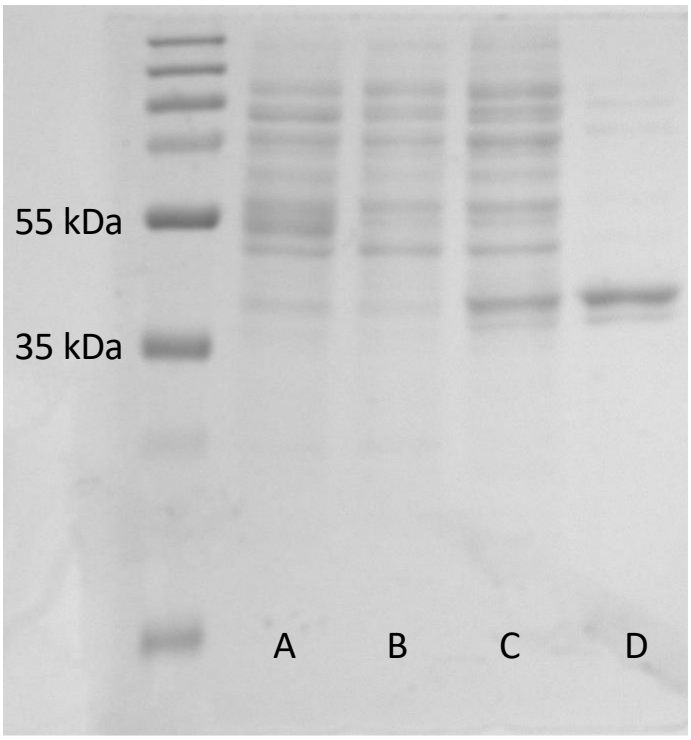

Figure 9. Expression Trial of pET-24b-TrxB.

E. coli containing pET-24b+ (empty vector) and pET-24b-TrxB were grown until an OD of 0.6 then induction was started by the addition of 1 mM IPTG for half the samples. Induction was done for three hours. Resulting cultures were pelleted and resuspended in lysis buffer: 50 mM TRIS, 500 mM NaCl, 25 mM imidazole, pH 7.5. Lysis was done using sonication and after sonication, soluble fraction was collected by centrifugation and ran on a 10% acrylamide gel. (A) pET-24b+ empty vector without induction. (B) pET-24b+ empty vector with induction. (C) pET-24b-TrxB without induction. (D) pET-24b-TrxB with induction.

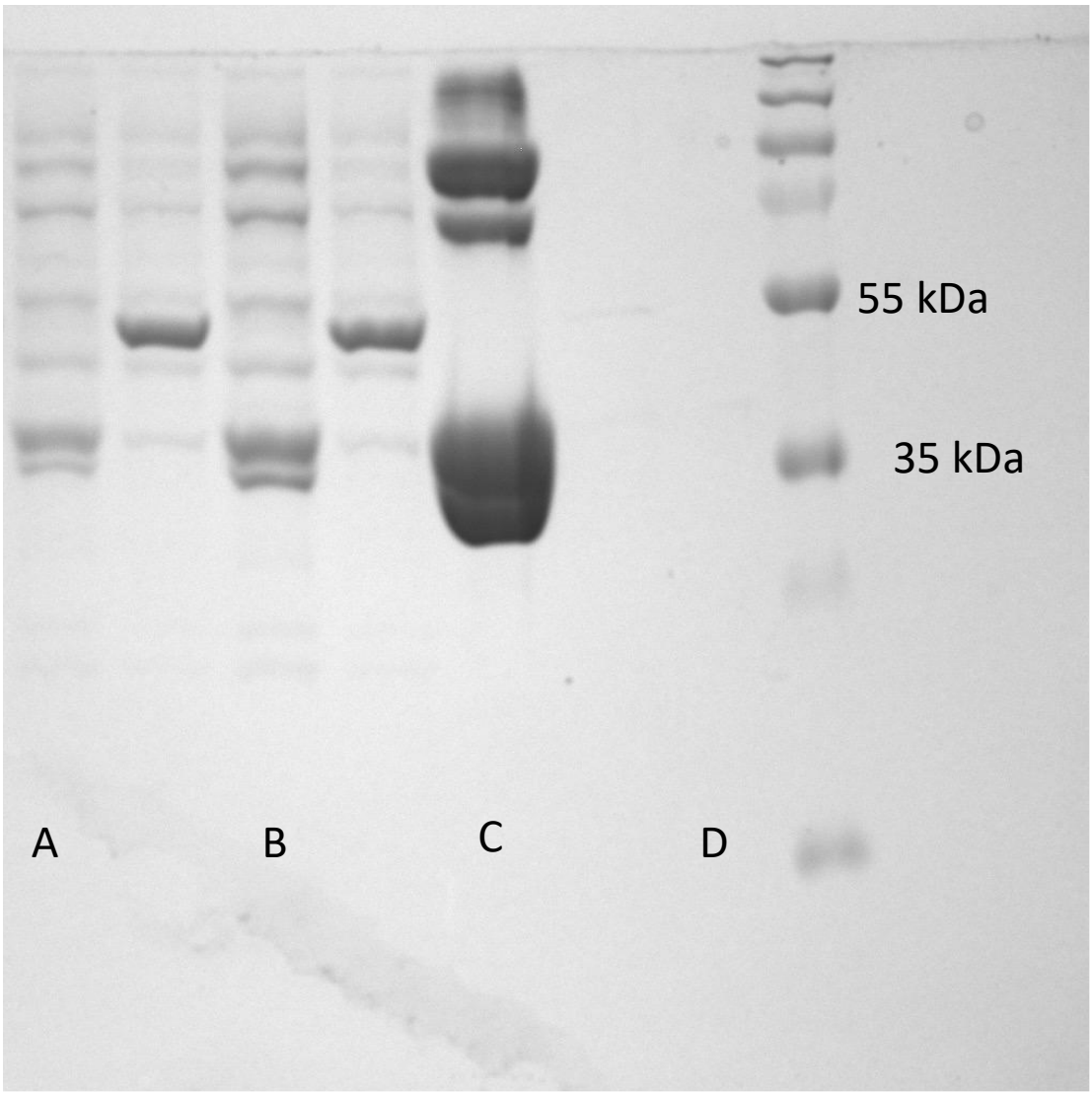

Figure 10. Purification of TrxB.

E. coli containing pET-24b-TrxB were grown until an OD of 0.6 then induction was started by the addition of 1 mM IPTG for half the samples. Induction was done for three hours. Resulting cultures were pelleted and resuspended in lysis buffer: 50 mM TRIS, 500 mM NaCl, 25 mM imidazole, pH 7.5. Lysis was done using an emulsiflex and after the soluble fraction was collected by centrifugation ran through a nickel affinity column. (A) pET-24b-TrxB flow through. (B) pET-24b-TrxB wash. (C) pET-24b-TrxB elution. (D) pET-24b-TrxB second wash.

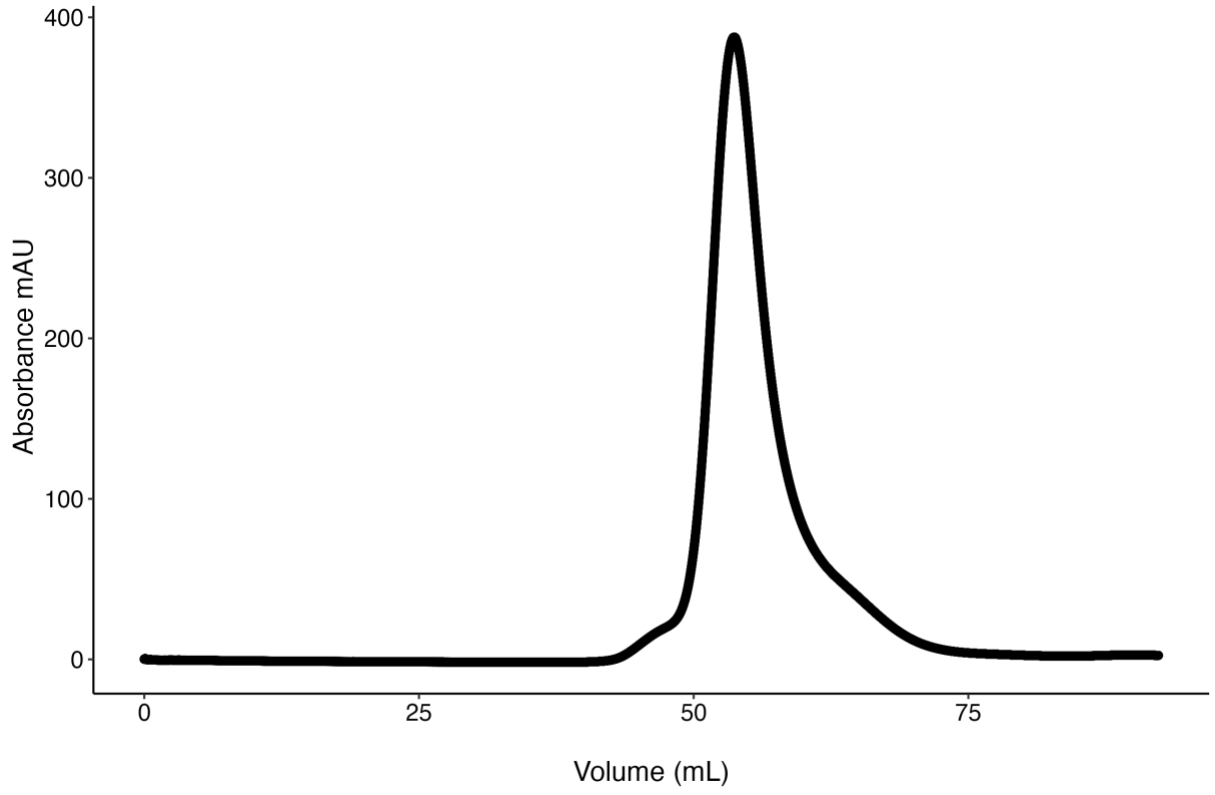

Figure 11. Size exclusion chromatography of TrxB.

After elution, the TrxB protein was concentrated and the elution buffer was replaced with a gel filtration buffer (20 mM Tris pH 7.5, 150 mM sodium chloride, and 1 mM β-ME). The concentrated protein was then run through an AKTA for SEC.

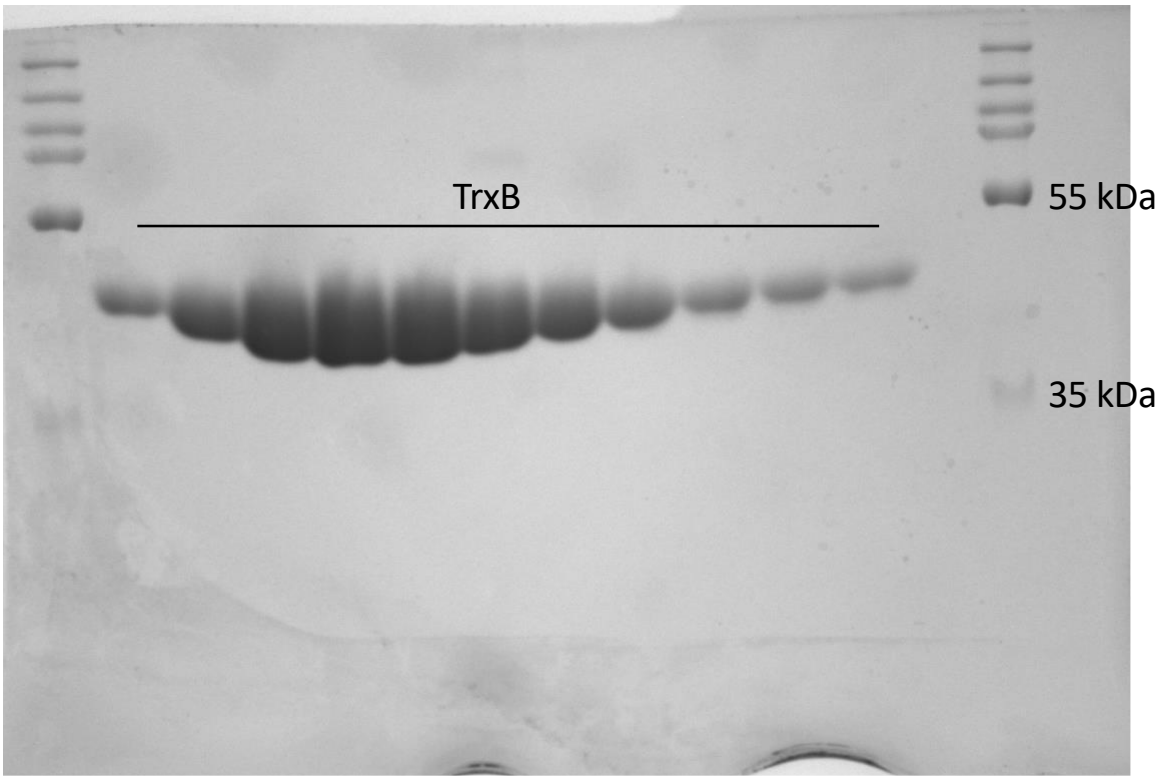

Figure 12. Size exclusion chromatography of TrxB on an acrylamide gel.

After elution, SEC and the resulting fractions were run on a 10% acrylamide gel.

The TrxB enzymatic reaction used 5,5'-Dithiobis(2-nitrobenzoic) acid (DTNB) which is converted to 5-thio-2-nitrobenzoic acid (TNB) by thioredoxin reductase, with electrons supplied by NADPH. TNB is detectable at an optical density of 412 nm and if TrxB is functional, we should see an increase in TNB. Auranofin, MS-40, and MS-40S were shown to inhibit the function of TrxB *in vitro* in the nanomolar range (Figure 13A), indicating that these three compounds are potent inhibitors of the essential protein thioredoxin reductase. We next investigated the effect of a *trxB* knockdown mutant on the growth inhibition activity of auranofin, MS-40, and MS-40S. A *trxB* CRISPRi mutant was created with a CRISPRi system adapted for *Burkholderia* (Hogan et al. 2019), where a rhamnose-inducible dCas9 is expressed and produces a *trxB* gene knockdown. The *trxB* CRISPRi mutant showed slight enhanced susceptibility to MS-40 and MS-40S under gene silencing conditions, with the MIC decreasing 2-fold (Figure 13B), which confirmed its role in the mechanism of action (MOA). However, the *trxB* CRISPRi mutant did not show any MIC changes to auranofin compared to MS-40 and MS-40S, suggesting auranofin may not reach the cytoplasmic target due to the cell envelope barrier.

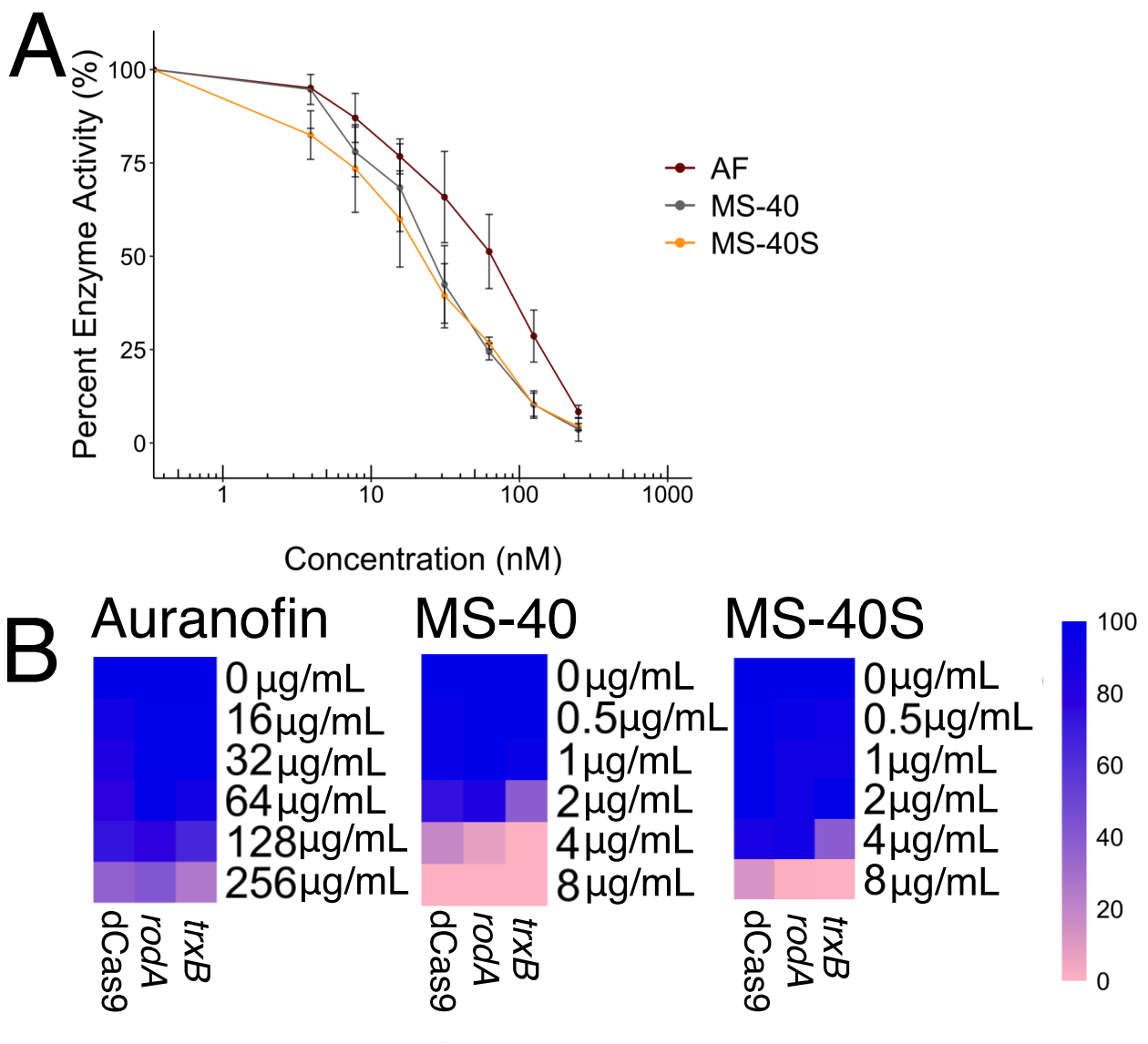

Figure 13. Auranofin inhibits TrxB *in vitro* but not *in vivo* from TrxB inhibition assays and enhanced susceptibility assays.

(**A**) TrxB *in vitro* assay. Purified TrxB from *B. cenocepacia* K56-2 in the presence of substrate, DTNB, is reduced to TNB, with NADPH as a source of electrons, producing a fluorescent product. This reaction was performed in the presence of a concentration gradient of auranofin, MS-40, and MS-40S ranging from 250 nM to 3.906 nM. (**B**) CRISPRi mutant of *trxB* gene as well as the dCas9 non-targeting control and *rodA* gene, as a functionally unrelated essential gene control, was exposed to a concentration gradient of auranofin ranging from 256 µg/mL to 0 µg/mL, and MS-40 and MS-40S ranging from 8 µg/mL to 0 µg/mL in the presence of 30.5 mM rhamnose. 100 percent growth is represented as blue and 0% growth is represented as pink.

Alternatively, auranofin could be inactive in *B. cenocepacia* because glutathione reductase (GOR) can compensate for the lack of TrxB, while auranofin analogs are active because the analogs could also inhibit GOR. To determine if GOR is a target of MS-40 and MS-40S the *gor* gene was overexpressed and the protein was purified from *B. cenocepacia* K56-2. The *gor* gene from *B. cenocepacia* K56-2 was amplified via PCR, digested, and ligated into pET-22, containing a C-terminal 6x His-tag, creating pET-22-GOR. This plasmid was then transformed into *E. coli* BL21 (DE3)-Gold cells. To ensure that the GOR protein was being expressed, we ran an expression trial. We grew the *E. coli* until an OD of 0.6, then induced expression by adding IPTG at 1 mM for 3 hours. The cultures were pelleted and resuspended in lysis buffer (see Material and Methods) after induction. Lysis was accomplished by sonication and the pellet and supernatant were separated by centrifugation and ran on an acrylamide gel (Figure 14). From this gel, we saw that GOR was being expressed from pET-22-GOR, thus, we moved to the purification using a nickel affinity column. The *E. coli* was grown in the same conditions as the expression trial; however, a larger volume was used. The resulting induced cultures were pelleted and resuspended in lysis buffer (see Material and Methods) and lyzed using an emulsiflex. The soluble and insoluble fractions were separated by centrifugation and the soluble fraction was ran through the nickel column. The protein was eluted with elution buffer (see Material and Methods) after washes. All flow throughs were run on an acrylamide gel (Figure 15). From the gel, we saw that GOR was purified, but not as high concentration as TrxB. After elution, the protein was concentrated using a protein concentrator (BioRad) and the elution buffer was replaced with a gel filtration buffer (see Material and Methods). Size exclusion chromatography (SEC) was then done to further purify the GOR protein (Figure 16). SEC showed that GOR was present in multiple species. We collected volume that eluted in the range of approximately 50-60 mL. Resulting samples from the SEC were

also run on an acrylamide gel to ensure there's only one size of protein present (Figure 17). From all this, we saw that we successfully purified GOR in single species.

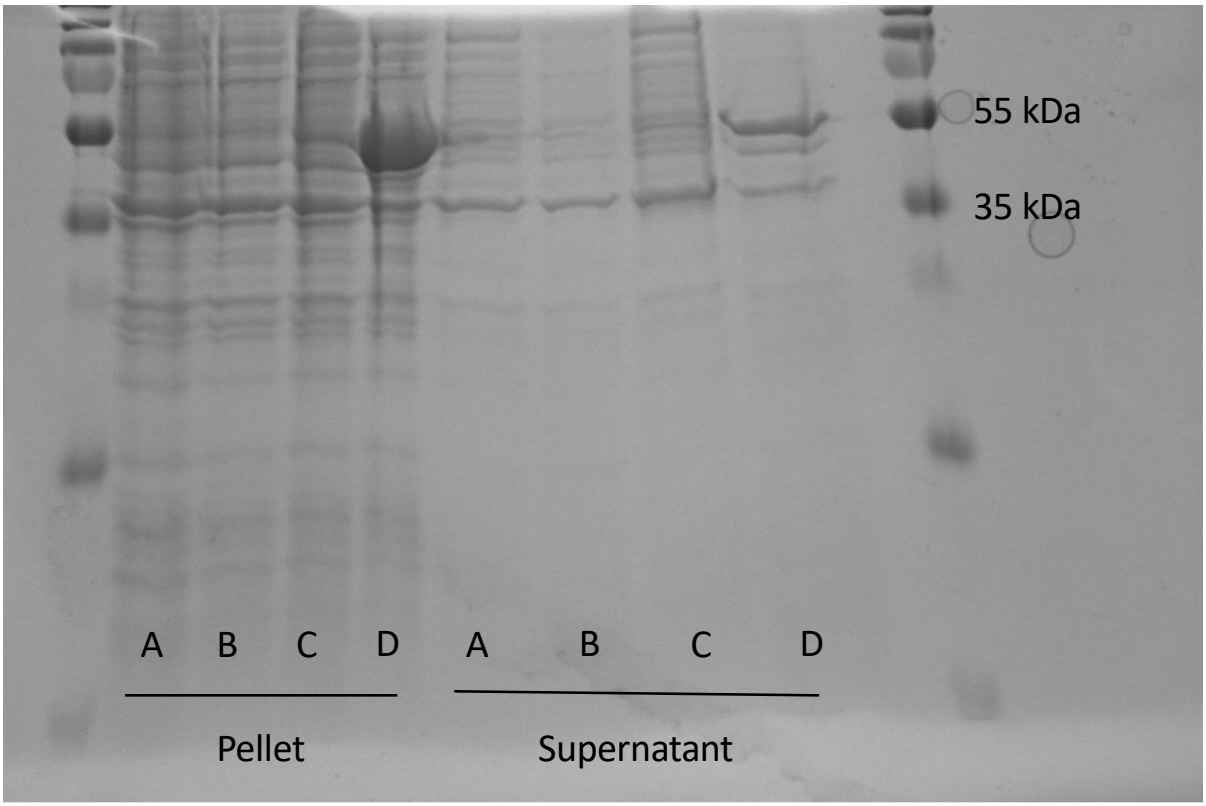

Figure 14. Expression Trial of pET-22-GOR.

E. coli containing pET-22 (empty vector) and pET-22-GOR were grown until an OD of 0.6 then induction was started by the addition of 1 mM IPTG for half the samples. Induction was done for three hours. Resulting cultures were pelleted and resuspended in lysis buffer: 50 mM TRIS, 500 mM NaCl, 25 mM imidazole, pH 7.5. Lysis was done using sonication and after sonication, soluble fraction was collected by centrifugation and ran on a 10% acrylamide gel. (A) pET-22 empty vector without induction. (B) pET-22 empty vector with induction. (C) pET-22-GOR without induction. (D) pET-22-GOR with induction.

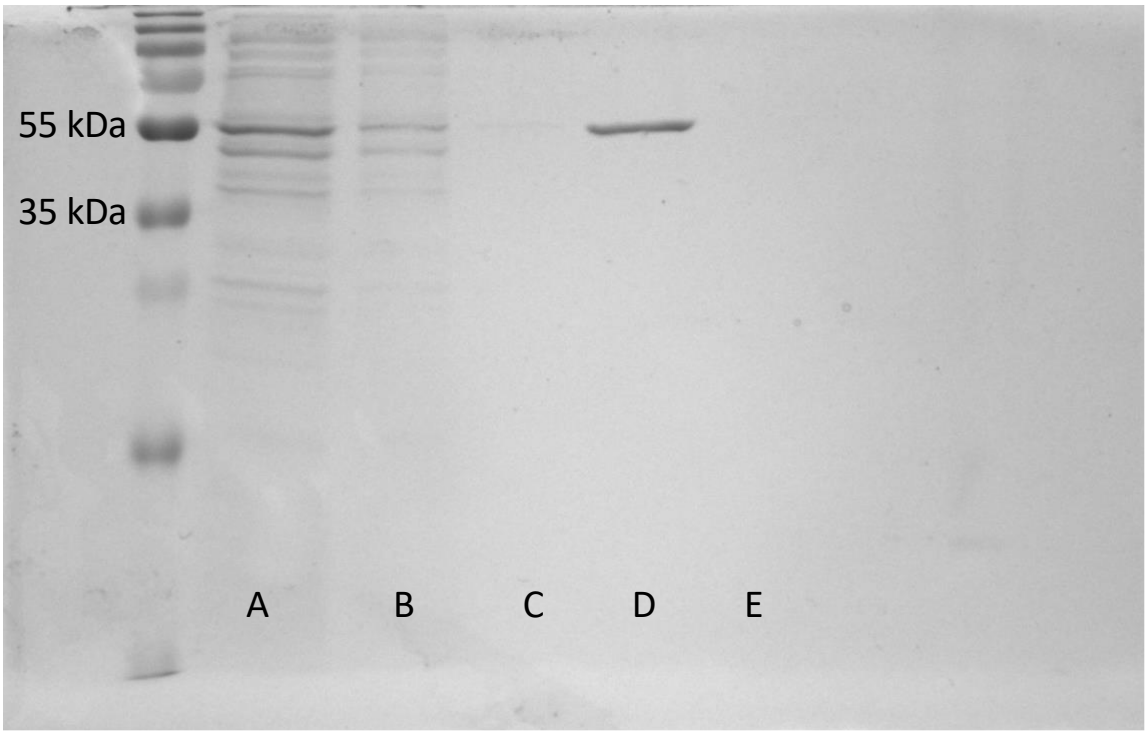

Figure 14. Purification of GOR.

E. coli containing pET-22-GOR was grown until an OD of 0.6 then induction was started by the addition of 1 mM IPTG for half the samples. Induction was done for three hours. Resulting cultures were pelleted and resuspended in lysis buffer: 50 mM TRIS, 500 mM NaCl, 25 mM imidazole, pH 7.5. Lysis was done using an emulsiflex and after , soluble fraction was collected by centrifugation ran through a nickel affinity column. (A) pET-22-GOR flow through. (B) pET-22-GOR wash. (C) pET-22-GOR wash. (D) pET-22-GOR elution. (E) pET-22-GOR wash, after elution.

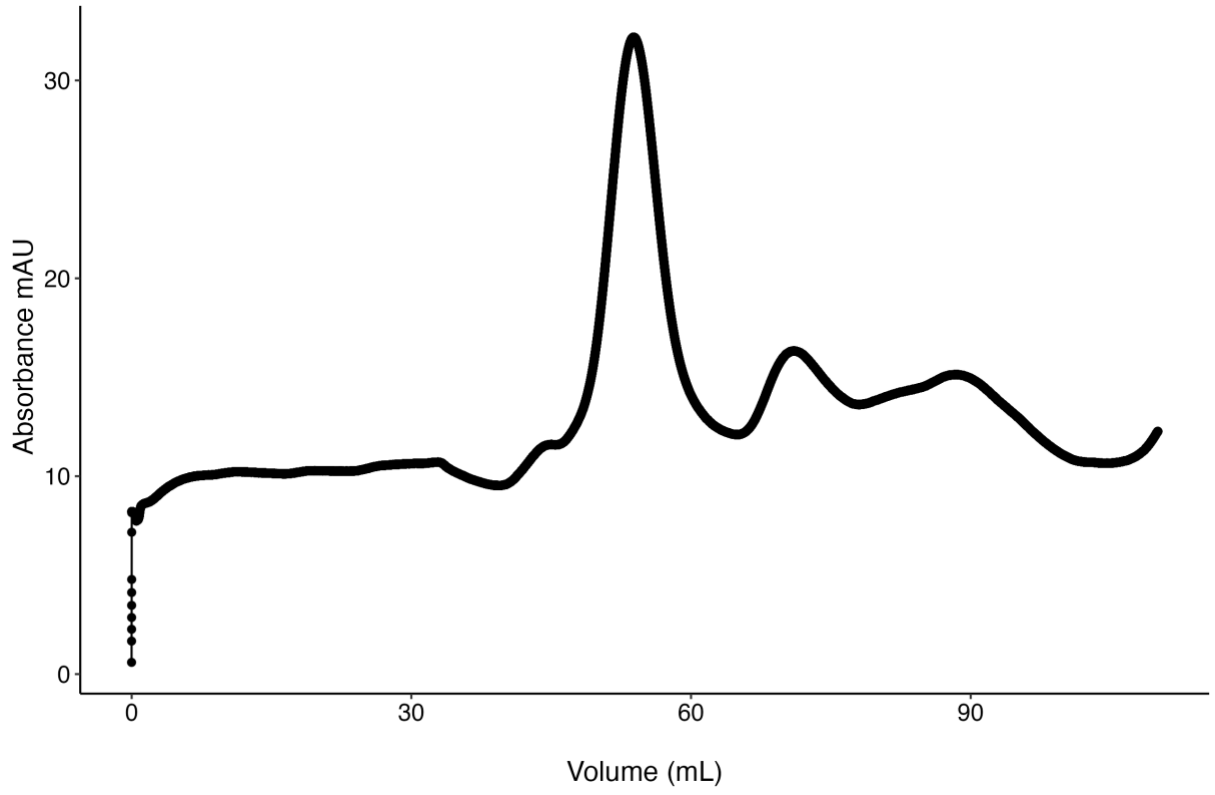

Figure 15. Size exclusion chromatography of GOR.

After elution, the GOR protein was concentrated and the elution buffer was replaced with a gel filtration buffer (20 mM Tris pH 7.5, 150 mM sodium chloride, and 1 mM β-ME). The concentrated protein was then run through an AKTA for SEC.

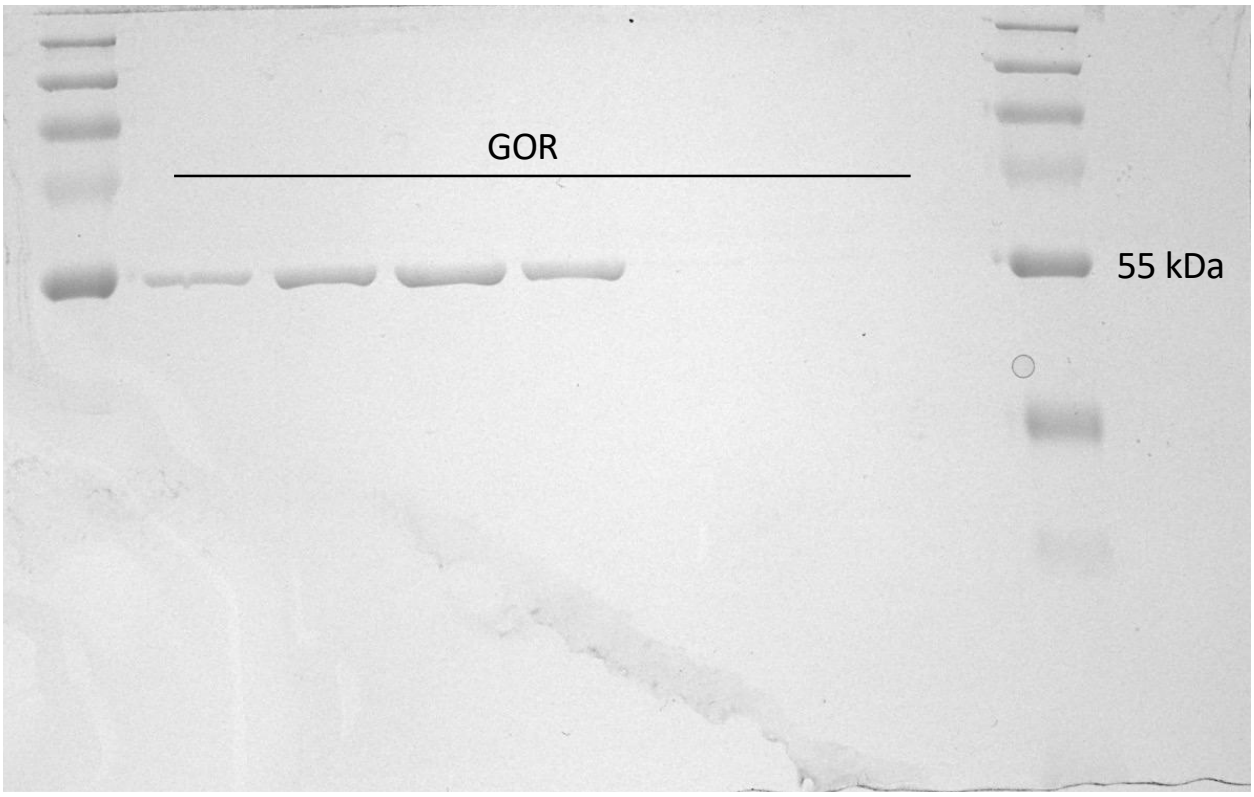

Figure 16. Size exclusion chromatography of GOR on an acrylamide gel.

After elution, SEC and the resulting fractions were run on a 10% acrylamide gel.

The inhibition assay with GOR used oxidized glutathione which is converted to reduced glutathione in the presence of GOR, with electrons supplied by NADPH (Carmel-Harel and Storz 2000; Smirnova and Oktyabrsky 2005; Couto et al. 2016). Enzyme activity was determined by tracking the amount of NADPH at an optical density of 340 nm (Kedrowski et al. 2014). We reasoned that if the enzyme was functioning, we should see a decrease in NADPH, as it is oxidized to $NADP^+$. However, with the addition of auranofin, MS-40, and MS-40S, up to a concentration of 250 μM, we did not see inhibition of GOR, indicating that this is not a target of auranofin nor auranofin analogs (Figure 17). Thus, auranofin may be inactive in *B. cenocepacia*, and other Gram-negatives, because of lack of uptake.

B. cenocepacia has many genes that may influence the permeability of its cellular envelope, such as the *mla* system (Bernier et al. 2018), which plays a role in movement of phospholipids between the inner and outer membrane (Abellon-Ruiz 2023). Other examples are *lolA*, a chaperone that moves lipoproteins from the inner to the outer membrane (Tajima et al. 1998; Kaplan et al. 2018), *hpnN* encoding a hopanoid transporter that shuttles hopanoids to the outer membrane (Kumar et al. 2017), and *shc*, which is involved in hopanoid biosynthesis (Schmerk and Valvano 2013), providing membrane stability (Schmerk et al. 2011). The LPS also provides resistance to antibiotics by affecting permeability (Simpson and Trent 2019), and *hldD* is involved in synthesis of the LPS (Loutet et al. 2006). Lastly, *B. cenocepacia* has many RND efflux pumps that lead to resistance, two of which are BpeAB-OprB (RND-4) and BpeEF-OprC (RND-10) (Somprasong et al. 2021).

Previously, through BarSeq, our lab found some transporters and membrane integrity elements that lead to altered susceptibility to antibiotics with molecular mass above 500 (Hogan et al. 2023), which is above the cut off for Lipinski's rule of five (Benet et al. 2016), such as the

antibiotic erythromycin. This suggests that mutants of these genes will have higher cell envelope permeability (Hogan et al. 2023). Auranofin's molecular weight is also above 500 g/mol, 678.13 g/mol to be exact, while MS-40 and MS-40S are 350.01 and 364.03 g/mol, respectively, thus, genes that lead to increased susceptibility to erythromycin for example, may lead to increased susceptibility to auranofin. If auranofin is inactive because it cannot gain entry to the cell, we should see higher auranofin growth inhibition activity in mutants with increased permeability. We thus created CRISPRi mutants of these genes and tested the MIC of auranofin, MS-40 and MS-40S (Figure 17B).

Silencing transporters did not lead to susceptible changes to MS-40 and MS-40S indicating that MS-40 and MS-40S are not affected by the permeability of the membrane and efflux and can thus passively diffuse into the cell. However, silencing *hpnN* and *bpeABoprB* led to minor susceptibility changes to auranofin and knockdown of these genes lead to the largest change in susceptibility to auranofin. These CRISPRi mutants were assessed for outer membrane permeability using an NPN-uptake assay (Figure 17C). Interestingly, silencing the *mlaFEDvacJ* operon and *hldD, lolA,* and *shc* lead to high permeabilization of the membrane, but only lead to small susceptibility changes to auranofin. Also, silencing *hpnN* did not lead to permeabilization, and thus, the effect we are seeing with the *hpnN* knock-down in terms of auranofin susceptibility is not due to general permeability. Thus, this provides evidence that high efflux may be why auranofin is inactive in *B. cenocepacia* K56-2.

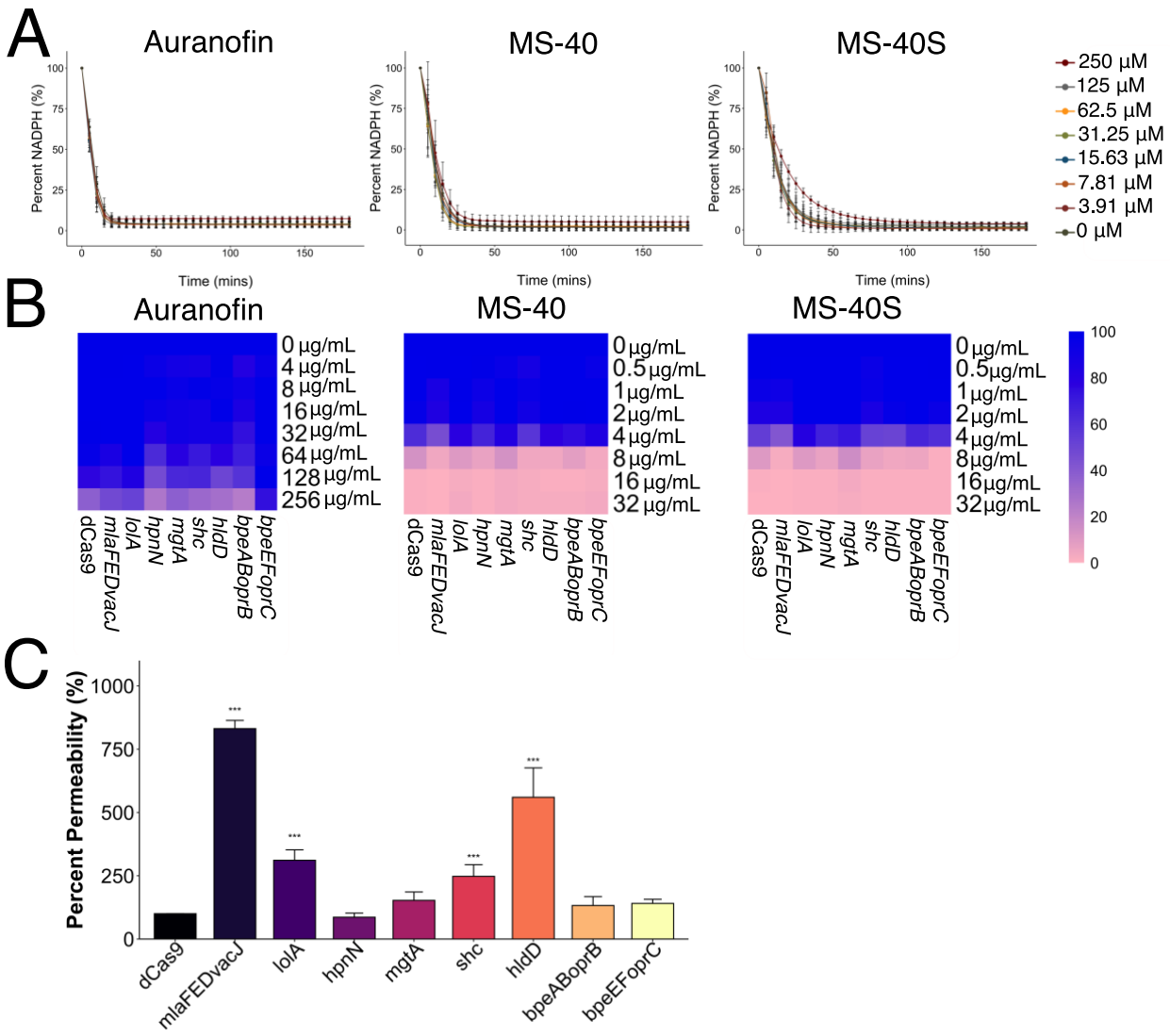

Figure 17. Auranofin, MS-40, nor MS-40S inhibit GOR and auranofin may be inactive due to high efflux from CRISPRi susceptibility assays.

(**A**) Purified GOR from *B. cenocepacia* K56-2 in the presence of substrate, oxidized glutathione, is reduced to reduced glutathione, with NADPH as a source of electrons. This reaction tracks the usage of NADPH, which is detectable at 340 nm. This reaction was performed in the presence of a concentration gradient of auranofin, MS-40, and MS-40S ranging from 250 µM to 3.906 µM. (**B**) MIC of transporters in the presence of auranofin, MS-40, and MS-40S. (**C**) CRISPRi mutants were subcultured in LB Tp100 and 30.5 mM rhamnose until an OD of approximately 1.0. Cells were then washed and resuspended in 5mM HEPES pH 7.2 with 10 mM NaN_3 for 30 minutes. The cells were then added to a plate and were incubated with NPN at 40 µM. Fluorescence was measured on a Synergy2 plate reader. *** indicates $P < 0.0001$ from a one-way ANOVA and Dunnett post-hoc.

3.8 MS-40 and MS-40S Cause an Increase in Reactive Oxygen Species (ROS)

We showed that MS-40 and MS-40S inhibit TrxB *in* vitro, and the thioredoxin system is involved in detoxifying ROS (Lu and Holmgren 2014), thus we hypothesized that MS-40 and MS-40S may cause an increase in reactive oxygen species (ROS). We examined if *B. cenocepacia* K56-2 had an increase in ROS after exposure to MS-40 and MS-40S using the cell-permeant indicator dye 2',7'-dichlorodihydrofluorescein diacetate (H_2DCFDA). H_2DCFDA diffuses into cells in a non-fluorescent form, where it is oxidized by ROS (mainly H_2O_2, ROO•, and $ONOO^-$) to the fluorescent 2',7'-dichlorofluorescein (DCF). We found that tetracycline, our antibiotic control that has been shown to not be related to ROS (Hoeksema et al. 2018), did not cause an increase in ROS (Figure 18A). However, MS-40 and MS-40S at a concentration four-fold higher than MIC, caused a significant increase in ROS compared to the DMSO solvent control, validating that ROS plays a role in the MOA of these compounds. The increase in ROS was also showed using microscopy, in which cells fluoresced only when exposed to MS-40 and MS-40S at 5 times the MIC (Figure 18B).

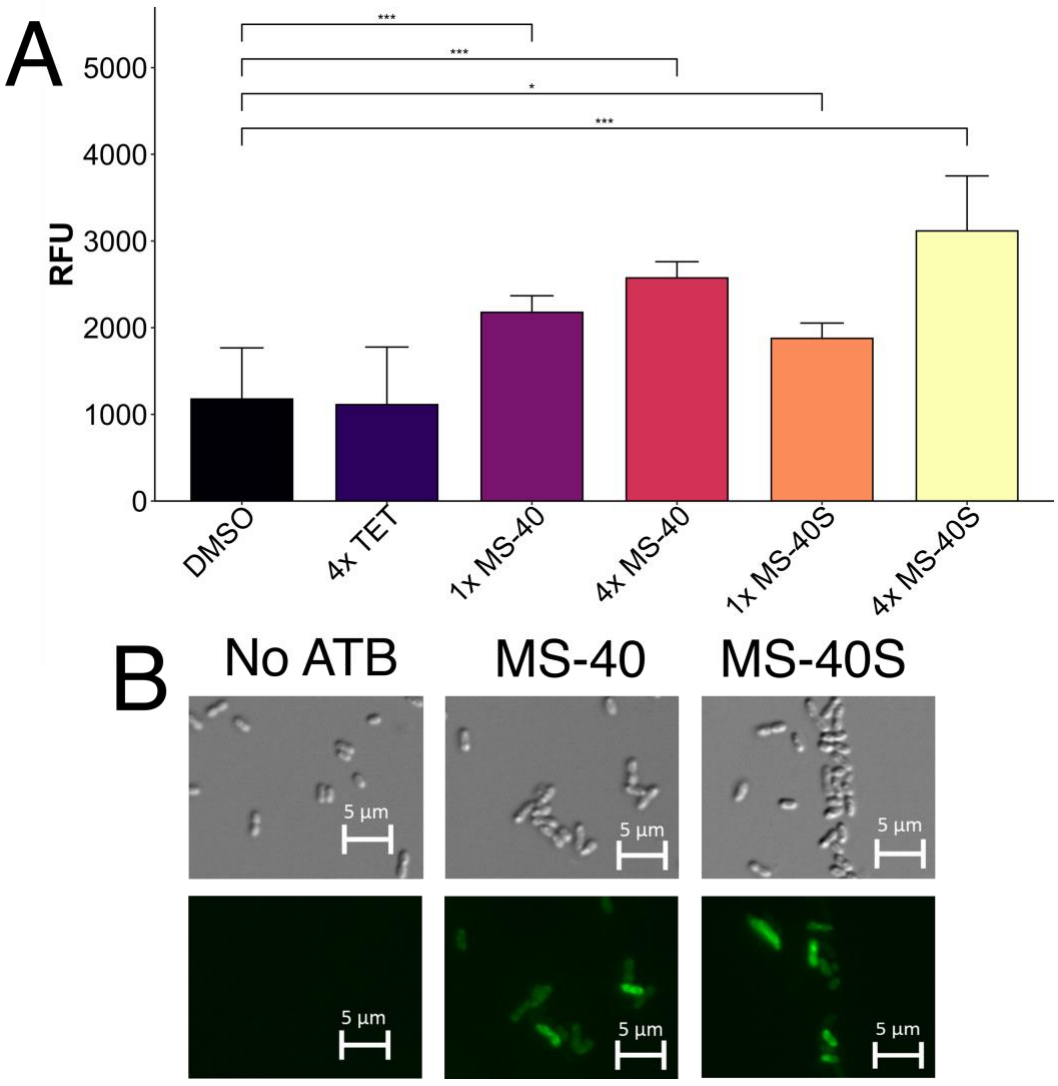

Figure 18. ROS Detection of *B. cenocepacia* K56-2 exposed to MS-40 and MS-40S.

(**A**) ROS detection of MS-40 and MS-40S. An OD_{600nm} of 0.3 wild type K56-2 were incubated with H_2DCFDA for 45 mins at 37˚C, then exposed to the corresponding antimicrobial. Fluorescence was measured on a synergy two plate reader. * indicates $P < 0.05$ and *** indicates $P < 0.0001$ from a one-way ANOVA and post-hoc Dunnett Test. (**B**) Microscopy of wild type K56-2 cells stained with H_2DCFDA dye then exposed to MS-40 and MS-40S.

3.9 BarSeq Analysis of Cells Exposed to MS-40, MS-40S, and other ROS Inducers

To investigate the full global response due to exposure to MS-40 and MS-40S we used randomly barcoded transposon sequencing (BarSeq) to find what other processes in the cell have a role in the mechanism of action. A barcoded transposon mutant library in *B. cenocepacia* K56-2 containing more than 330,000 unique mutants in over 6,400 protein coding genes (Hogan et al. 2023) was exposed to the IC_{25} of MS-40, MS-40S and ROS inducers (As_2O_3, diamide, H_2O_2, and paraquat) (Table 10) for 8 hours. These additional ROS inducers were included as benchmarks for comparison to find the MOA of MS-40 and MS-40S. The BarSeq was done to find which gene disruptions led to altered susceptibility to these compounds, implicating those genes in a compound's MOA or resistance. Barcode abundance served as proxy for mutant abundance (Wetmore et al. 2015). Fitness for each gene was then calculated as the $\log_2$ fold change of number of reads in experimental condition to time zero (Wetmore et al. 2015; Pierce et al. 2021). When compared to the DMSO solvent control, the change in gene fitness for each individual mutant can be calculated. A positive gene fitness score indicates the mutant was more abundant following treatment, while a negative fitness score indicates those mutants were more depleted following treatment.

Table 10. Inhibitory Concentrations of ROS inducers, with known mechanism of action, used in BarSeq.

Compound	**IC_{25}**	**Mechanism of Action**
MS-40	5.0 μM	Inhibits TrxB, increase in ROS production
MS-40S	8.0 μM	Inhibits TrxB, increase in ROS production
As_2O_3	40.0 μM	Heavy metal, may cause ROS (Carney 2008)
Diamide	1.30 mM	ROS and thiol stress (Cumming et al. 2004; Pöther et al. 2009)
H_2O_2	0.12 mM	ROS (Imlay 2008)
Paraquat	0.38 mM	ROS (Ezraty et al. 2017)

We analyzed data for known interactions with As_2O_3, diamide, H_2O_2, and paraquat (Figure 19). One of the most depleted mutants for H_2O_2 was one in which *dyp-type peroxidase* was disrupted, which plays a role in ROS scavenging (Figure 19). Additionally, mutants in known arsenic efflux and arsenic tolerance proteins were identified as being more susceptible to As_2O_3 (Figure 19). These arsenic resistance genes include *arsH*, which encodes for a flavoprotein that uses NADP+ to oxidize As(III) to As(V), conferring resistance (Ben Fekih et al. 2018), and *acr3 family arsenite efflux transporter*, which is involved in the efflux of arsenite from the cell (Ben Fekih et al. 2018). In summary, our results confirm that the BarSeq can reliably detect genetic elements that are part of ROS-inducers mechanism of action.

We generated a genetic network map to visualize how similar each of the compounds were, in terms of which genes had a significant change in gene fitness compared to the DMSO control (Figure 20A). Transposon disruption of 825 genes resulted in significant changes (from an independent two-sided Student's t-test) in gene fitness in the presence of MS-40, with 216 exclusive interactions. These genes were related to the glyoxylate shunt, octane oxidation, and general degradation/utilization/assimilation. For MS-40S, we observed significant changes in fitness for 788 genes, with 178 exclusive to MS-40S. These genes were related to L-glutamate, L-aspartate, and sugar degradation. There were 17 genes with differential fitness for all six compounds used in the BarSeq. Interestingly, one of these genes was glutathione reductase, an element in the glutathione system, and this gene had positive fitness scores for all compounds, except diamide. Another gene found in all six is a LysR type transcriptional regulator, which had a negative fitness for all ROS inducers. This regulator has, so far, an unknown function in *B. cenocepacia* K56-2. Additionally, an Upset plot shows how many interactions are shared between multiple conditions (Figure 20B). Unsurprisingly, MS-40 and MS-40S had the most similar

interaction profiles compared to any other compound, with 162 genes shared between these two. Genes in this subset are related to phosphonate/phosphorous metabolism and aerobic respiration.

There were 37 interactions shared between just MS-40, MS-40S, and As_2O_3, with these genes being related to the NAD salvage pathway, purine nucleotide biosynthesis, and glycerol degradation. There were also 37 interactions shared between just MS-40, MS-40S, and diamide, with these genes being related to glutathione biosynthesis and L-selenocysteine biosynthesis. For MS-40, MS-40S, and H_2O_2, there were 26 shared interactions with the genes being involved in pyrroloquinoline quinone biosynthesis and glutathione biosynthesis. Lastly, there were 31 interactions shared between MS-40, MS-40S, and paraquat, with the genes being involved in flavin biosynthesis and glycerophosphodiester degradation. Comparison to the benchmarking compounds shows that MS-40 and MS-40S shared the most interactions with diamide and the fewest with H_2O_2 (Figure 20C). MS-40 and MS-40S shared 110 genes with As_2O_3, 133 with diamide, 102 with H_2O_2, and 113 with paraquat (Figure 20D). However, these are all very small number of differences in the number of mutants that had altered susceptibility, compared to the DMSO solvent control, thus, we can conclude that all ROS inducers tested have similar BarSeq fitness profiles.

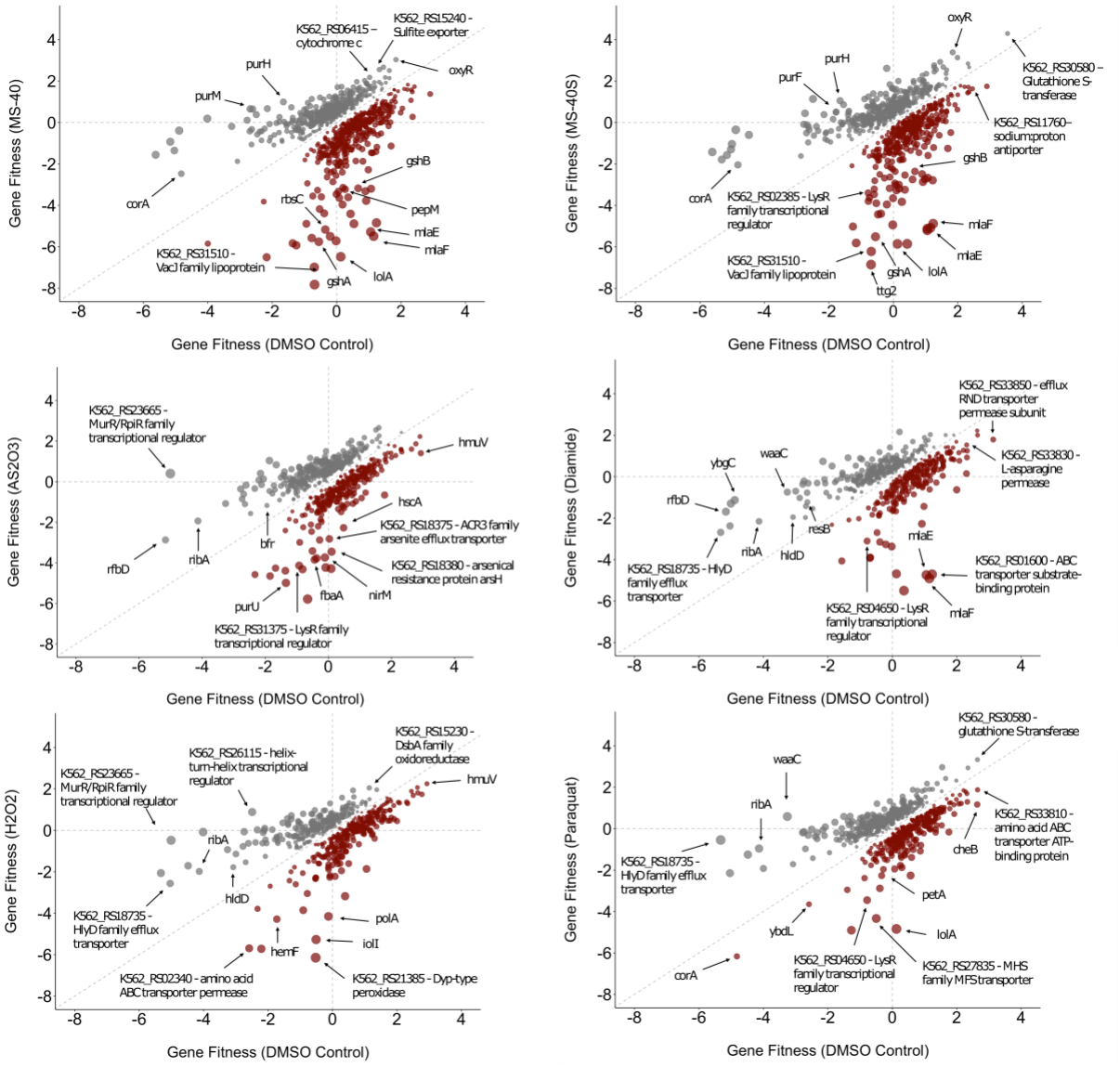

Figure 19. Mutants with significant altered fitness scores for each compound used in BarSeq.

Each dot represents a gene that, when disrupted, had altered sensitivity to the corresponding compound compared to the DMSO control ($P < 0.05$). Grey dots represent those that had a positive change in gene fitness, red indicates those with negative change in gene fitness. Select genes are indicated with their gene name or locus tag.

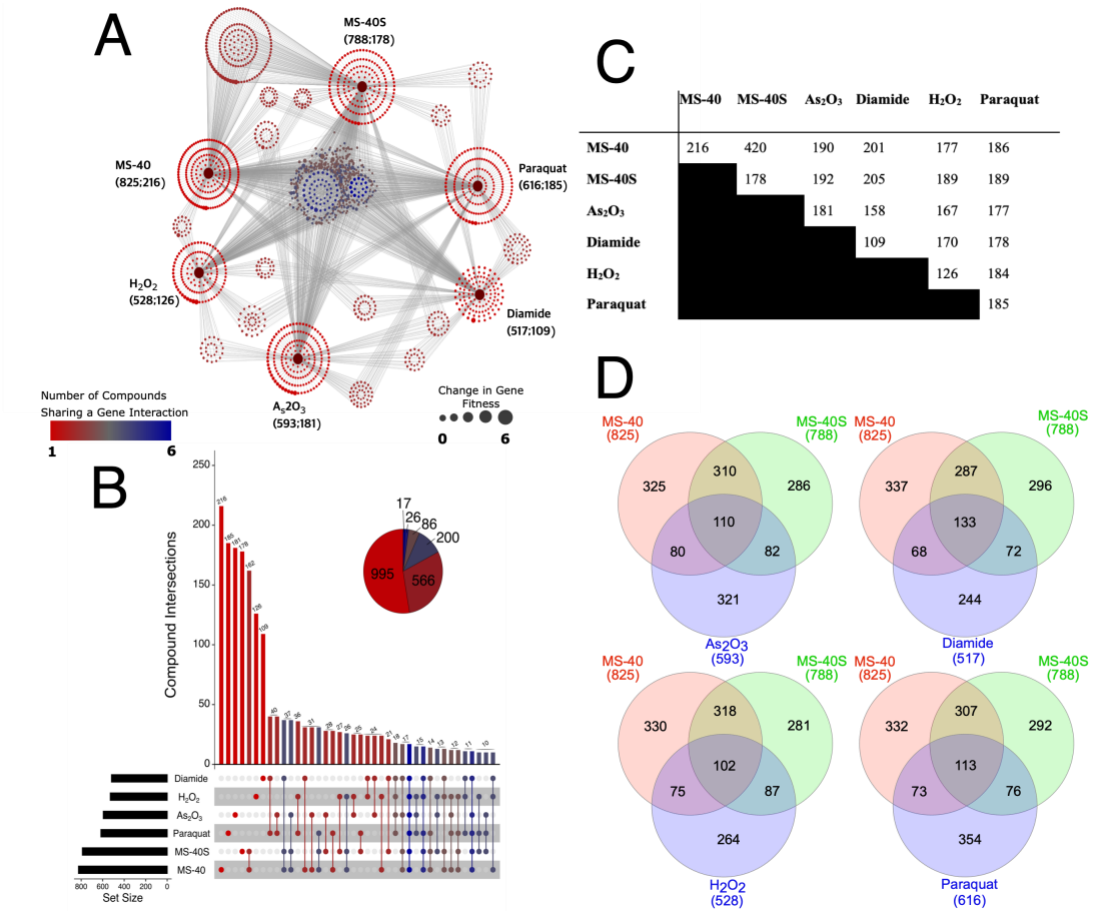

Figure 20. Comparison of BarSeq data of MS-40 and MS-40S with the benchmarking compounds.

(**A**) Genetic network map showing gene connectedness between compounds used in the BarSeq figure made using Cytoscape. This figure shows how many genes were identified as significant for each compound and how many genes were only identified in that condition. Large burgundy dots represent each compound and grey lines connect each compound to a smaller node that represents a gene, which is coloured based on how many compounds that gene when disrupted had altered sensitivity. (**B**) Upset plot showing how many mutants had altered sensitivities in each condition. (**C**) How many genes that had significant changes in gene fitness between two compounds used in BarSeq. (**D**) Venn diagrams of genes that had significant changes in gene fitness between MS-40, MS-40S and a ROS inducing compound that was used in the BarSeq. Venn diagrams were generated from Venny 2.1.

3.10 BioCyc Analysis Identifies Glutathione and Purine Biosynthesis in the MOA of MS-40 and MS-40S

After validating BarSeq as a powerful method to capture the global response to ROS inducers, we set to identify pathways that were important for MS-40 and MS-40S's mechanism of action. To help narrow down which cellular processes highly affect each compound used in BarSeq, analysis from BioCyc was used (Karp et al. 2019). Pathway enrichment (Figure 21 and 22) was used to find if the BarSeq data was enriched in mutants in any specific pathways. This analysis finds which pathways were enriched or depleted in the set of genes that had a significant change in gene fitness (positive gene fitness represents that mutant was more abundant than time zero, and a negative gene fitness represents that mutant was less abundant than time zero), compared to the entire genome of *B. cenocepacia* K56-2, without taking the amplitude of the gene fitness value into consideration. For genes that had a positive fitness (Figure 21), the gene set was especially enriched in genes related to nucleoside and nucleotide metabolism, specifically purine metabolism, include 5-aminoimidazole ribonucleotide biosynthesis. For diamide and paraquat, they also had pyrimidine biosynthesis as an enriched pathway. Alternatively, for genes that had a negative fitness for MS-40 and MS-40S (Figure 22) the gene set was enriched in genes in amine and polyamine degradation, glutathione biosynthesis, and phosphorus compound metabolism.

Another analysis from BioCyc, pathway perturbation score (PPS) was calculated as the weighted average of each gene's fitness belonging to that pathway (Karp et al. 2019). For genes that had a positive gene fitness, the top perturbed pathways for MS-40 and MS-40S was two component alkanesulfonate monooxygenase (Figure 23), which is involved in using alkanesulfonates as a source of sulfur (Eichhorn et al. 1999). Other perturbed pathways in this analysis were related to purine metabolism, such as biosynthesis and salvage and the other ROS

inducers used in the BarSeq also had purine or pyrimidine synthesis/salvage as their most perturbed pathways. Additionally, pyruvate decarboxylation to acetyl-CoA was a pathway that was in the top perturbed pathways for MS-40S and diamide, suggesting a role of central metabolism on the MOA of these compounds. On the other hand, for genes that had a negative gene fitness, the top 15 perturbed pathways are shown in Figure 24. Glutathione biosynthesis was one of the most perturbed pathways for MS-40, MS-40S, As_2O_3, and diamide, suggesting that this pathway is highly responsible for scavenging ROS in the cell exposed to oxidative stress.

BioCyc analysis helped identify which cellular processes are putatively involved in the mechanism of action of MS-40 and MS-40S and these are marked with an asterisk in Figures 21-24. Glutathione biosynthesis was the most perturbed pathway in mutants that had negative fitness for MS-40 and MS-40S and was present in analyses with some of the other ROS inducers as well, so we wanted to explore this avenue further. Additionally, purine metabolism was a process that was found to cause decreased susceptibility to all ROS inducers, a novel mechanism in ROS susceptibility, so we wanted to investigate this as well.

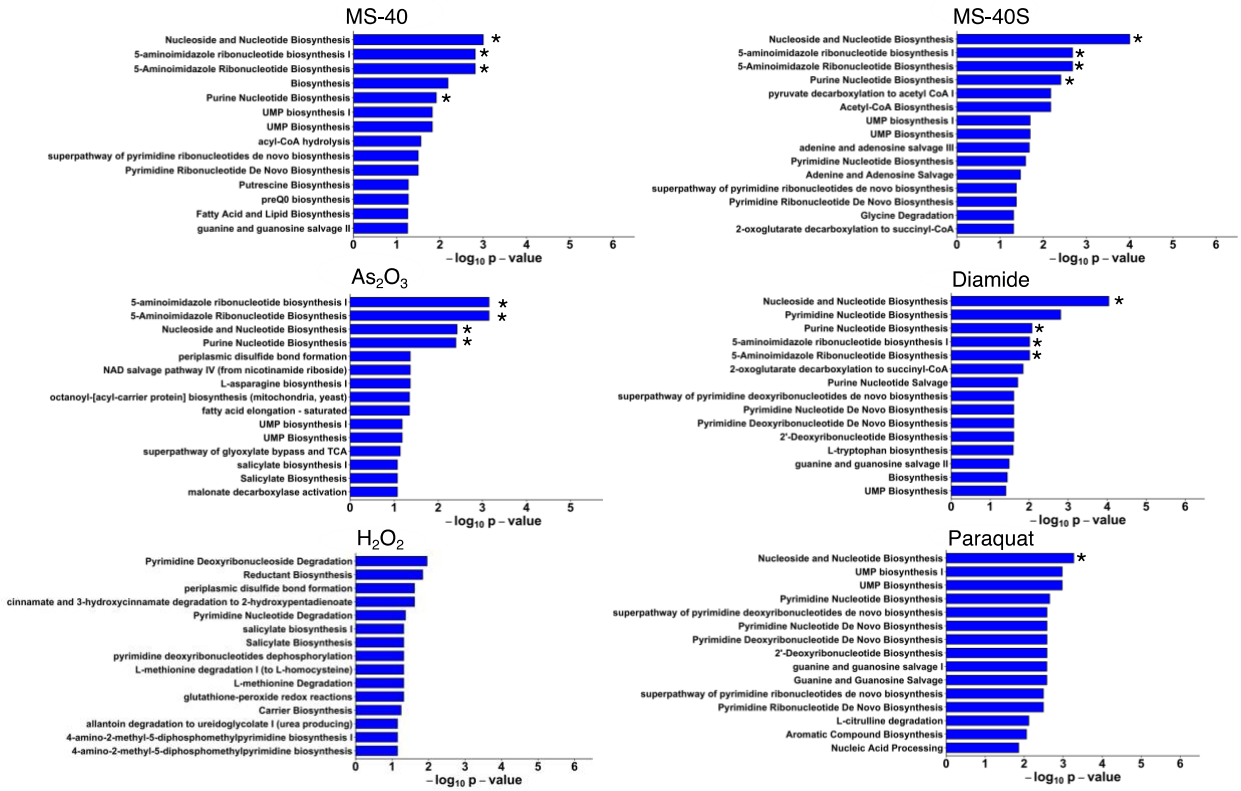

Figure 21. BioCyc pathway enrichment with BarSeq data with positive fitness.

Genes that had significant positive changes in fitness were uploaded to BioCyc Smart Tables for analysis. Pathway enrichment was done using the Fisher Exact test using the *B. cenocepacia* K56-2 database to create the -$\log_{10}$ p-value. Top 15 perturbed pathways are shown. * indicates cellular processes we explored.

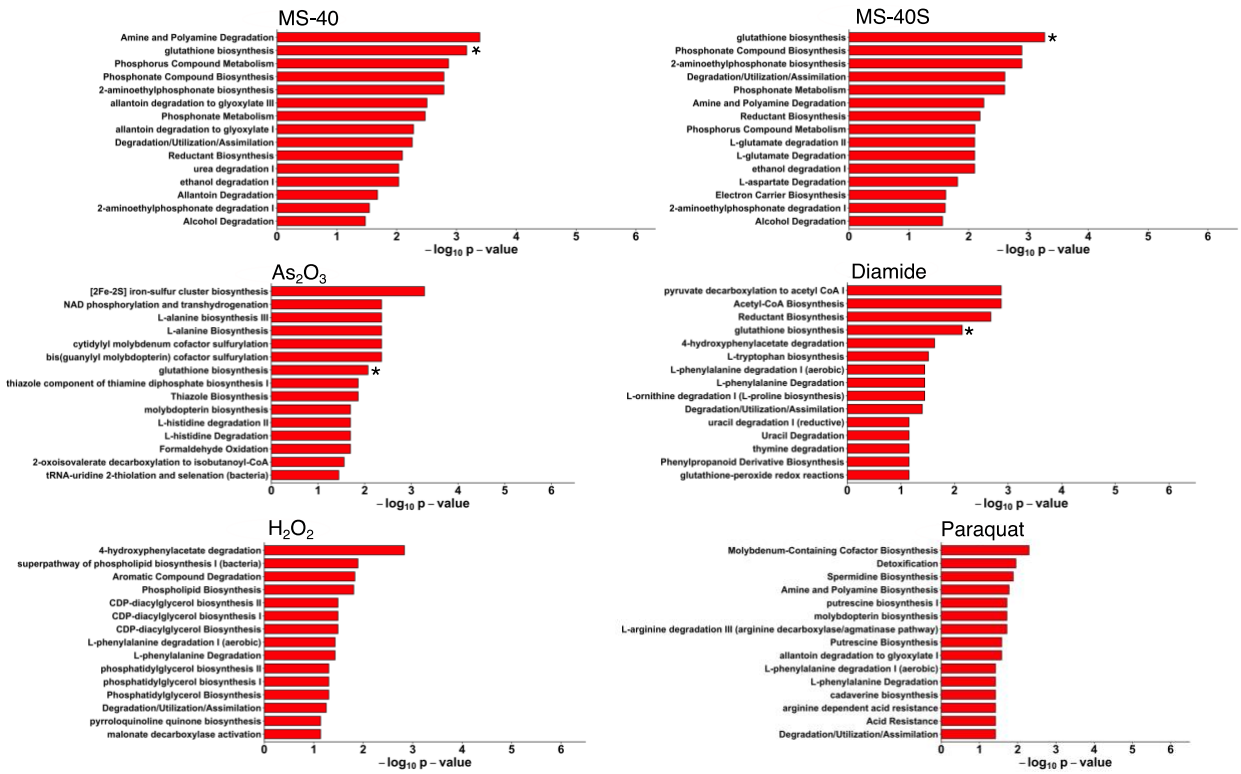

Figure 22. BioCyc pathway enrichment with BarSeq data with negative fitness

Genes that had significant negative changes in fitness were uploaded to BioCyc Smart Tables for analysis. Pathway enrichment was done using the Fisher Exact test using the *B. cenocepacia* K56-2 database to create the -$\log_{10}$ p-value. Top 15 perturbed pathways are shown. * indicates cellular processes we explored.

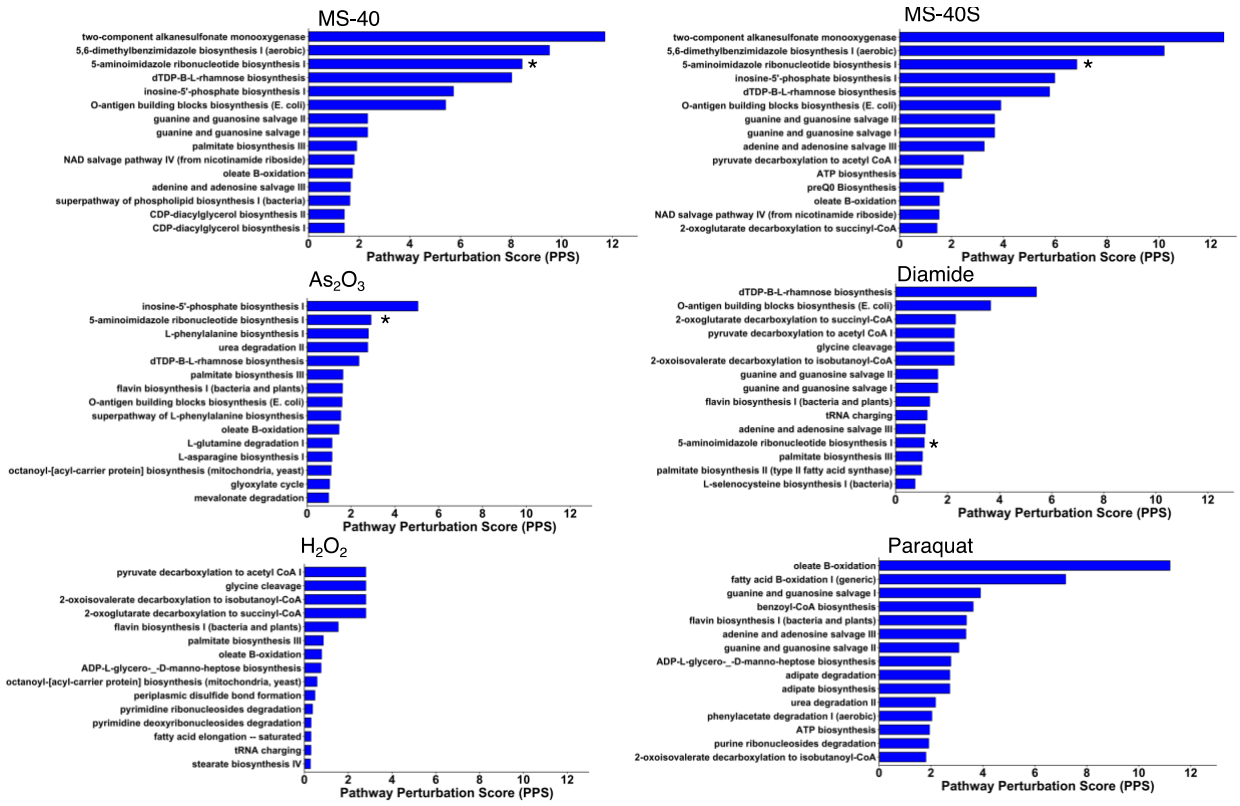

Figure 23. BioCyc pathway perturbation score with BarSeq data with positive fitness.

Genes that had significant positive changes in fitness were uploaded to BioCyc Smart Tables for analysis. Pathway perturbation score was performed from cellular overview on BioCyc under the *Burkholderia cenocepacia* K56-2 database. Top 15 perturbed pathways are shown. * indicates cellular processes we explored.

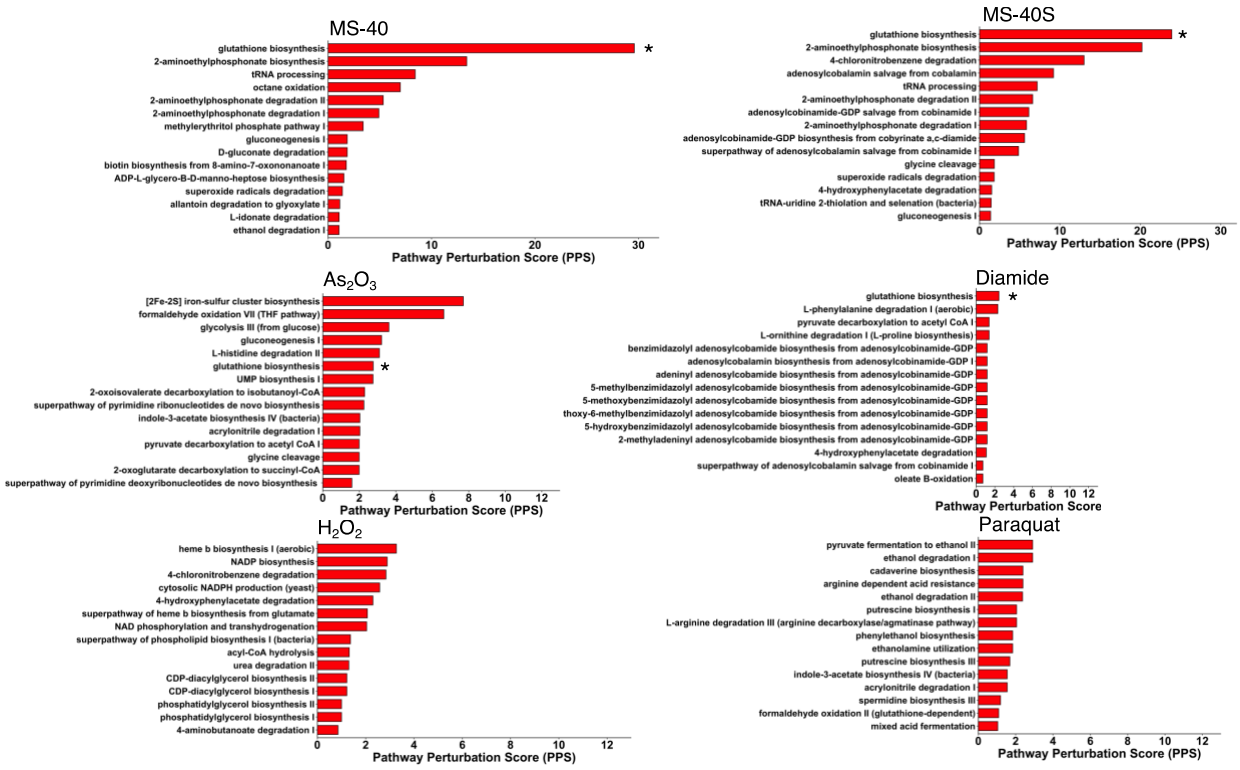

Figure 24. BioCyc pathway perturbation score with BarSeq data with negative fitness.

Genes that had significant negative changes in fitness were uploaded to BioCyc Smart Tables for analysis. Pathway perturbation score was performed from cellular overview on BioCyc under the *Burkholderia cenocepacia* K56-2 database. Top 15 perturbed pathways are shown. * indicates cellular processes we explored.

3.11 Reactive Oxygen Species Related Genes and their Fitness Values in BarSeq

There are many genes in bacteria that help detoxify reactive oxygen species (ROS) in the cell. First are superoxide dismutase genes, *sodB* and *sodC*, both responsible for clearing superoxide anions in the cell (Imlay 2008). Another set of ROS detoxifying genes are catalases and peroxidases, which clear hydrogen peroxide inside the cell (Imlay 2003, 2008). A transcriptional regulator that is involved in the ROS response is encoded by the *oxyR* gene, which activates the expression of other ROS scavenging genes, such as catalases (Imlay 2015), this gene is present in *B. cenocepacia* (Van Acker et al. 2016). Similarly to *oxyR*, *soxR* is also a transcriptional regulator which senses superoxide anions and ultimately activates superoxide dismutases (Imlay 2015). The alkyl hydroperoxide reductase system, encoded by *ahpCF* converts lipid hydroperoxides to alcohols, using NADPH or NADH (Carmel-Harel and Storz 2000). Lastly, protein product of the *organic hydroperoxide resistance (ohr)* gene in *Pseudomonas aeruginosa* acts as a hydroperoxide reductase (Lesniak 2002), also contributing to ROS-scavenging. All of these help clear ROS inside the bacterium, and thus, when deleted, an increase in cellular ROS should occur and the bacterium may become more susceptible to ROS producing compounds. However, of these, only *sodC* has been deleted/interrupted in *B. cenocepacia* before to confirm its function (Keith and Valvano 2007), thus, the function of other ROS-scavengers are based on protein homology to other species whose function has been validated. It has only been shown, however, via an *oxyR::lux* fusion, that the expression of *oxyR* increases in the presence of H_2O_2 (Van Acker et al. 2016).

MS-40 and MS-40S were shown to cause an increase in reactive oxygen species (ROS) (Figure 18) so we first looked at mutants in ROS related genes, mentioned above, and their corresponding fitness values, a measure of how the mutant grew. Figure 25 shows which ROS scavenging genes were identified by BarSeq. Some genes, when disrupted lead to increased

susceptibility to MS-40 and MS-40S, including *katG* and *katE*, *organic hydroperoxide resistance (ohr) family peroxidase* (K562_RS31135), *sodC*, *ahpC*, and various peroxidases. Interestingly, the ROS regulator *oxyR*, as well as *ahpD* and *ahpF*, when disrupted lead to the opposite effect, decreased susceptibility, even though in *E. coli* these systems are known to help clear ROS inside of the cell (Imlay 2008, 2015).

Based on hierarchical clustering, MS-40 and MS-40S are most similar to H_2O_2 (Figure 25), suggesting that hydrogen peroxide is the ROS produced by MS-40 and MS-40S. The next similar compound is diamide, which causes thiol-stress, suggesting that MS-40 and MS-40S also cause thiol stress, which might lead to an accumulation of hydrogen peroxide in the cell. To further explore these findings, CRISPRi mutants were made of some ROS genes and their susceptibility was measured against MS-40 and MS-40S, however, no major change was seen (Figure A15).

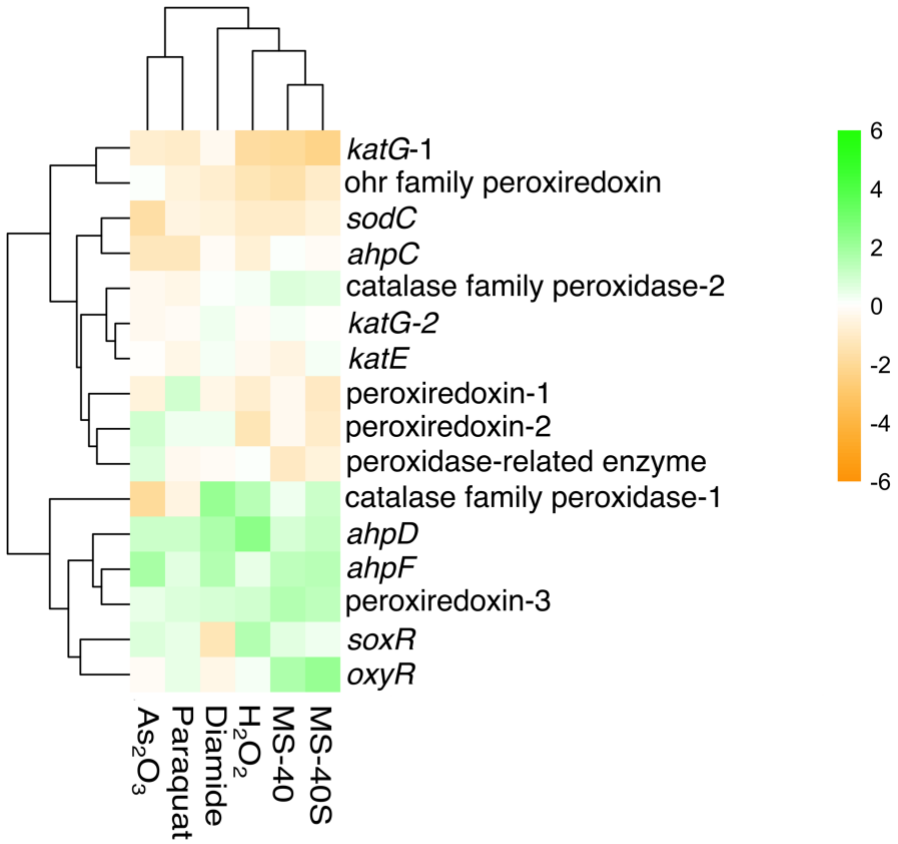

Figure 25. Mutant fitness profile for ROS related mutants in BarSeq.

Heatmap of ROS-related genes and their corresponding gene fitness values for each compound used in BarSeq. Heatmap was generated on RStudio using the pheatmap package. Green represents positive fitness and orange represents negative fitness.

3.12 Glutathione biosynthetic pathway is involved in protection against MS-40 and MS-40S

The putative glutathione biosynthesis pathway, based on sequence similarity to *E. coli*, is shown in Figure 26A. The role of this system is to create glutathione, which can be used to detoxify ROS inside the cell (Smirnova and Oktyabrsky 2005; Couto et al. 2016). The genes *gshA* and *gshB* encode for the glutathione synthetic enzymes, *grxC* and *grxD* encode glutaredoxins, and *gpo* encode for a glutathione peroxidase (Smirnova and Oktyabrsky 2005).

In our BarSeq, transposon disruptions of *gshA*1, *gshA2*, and *gshB*, resulted in gene fitness between -4 to -6 in the presence of MS-40 and MS-40S, indicating these mutants become depleted compared to time zero (Figure 26B). Transposon mutants of *gshA1*, *gshA2*, and *gshB* also decreased in abundance to the other ROS-inducing compounds used in the BarSeq experiment; however, the interactions were not as strong as with MS-40 and MS-40S. Thus, we deleted these three genes in *B. cenocepacia* K56-2, as well as two glutaredoxins, *grxC* and *grxD*, and exposed the mutants to MS-40 and MS-40S. The mutants Δ*gshA1* and Δ*gshB* were more susceptible to MS-40 and MS-40S, with the MIC's dropping 2- and 4-fold respectively (Figure 26C). This both validates the BarSeq method and indicates the involvement of the glutathione system in the mechanism of action of MS-40 and MS-40S.

The genes *gshA1* and *gshB* are in an operon in *B. cenocepacia* K56-2, and thus, to investigate the effect of silencing both in *B. cenocepacia* K56-2, we used CRISPR interference to simultaneously knockdown these genes. The growth of this knockdown mutant was then measured in tandem with Δ*gshA1* and Δ*gshB* (Figure 26D). Neither Δ*gshA1* nor Δ*gshB* had a growth defect compared to wild-type K56-2, but the *gshA1B* CRISPRi mutant had a major growth defect in the presence of rhamnose, with the percent growth being 30% that of the non-targeting control (Figure 15D).

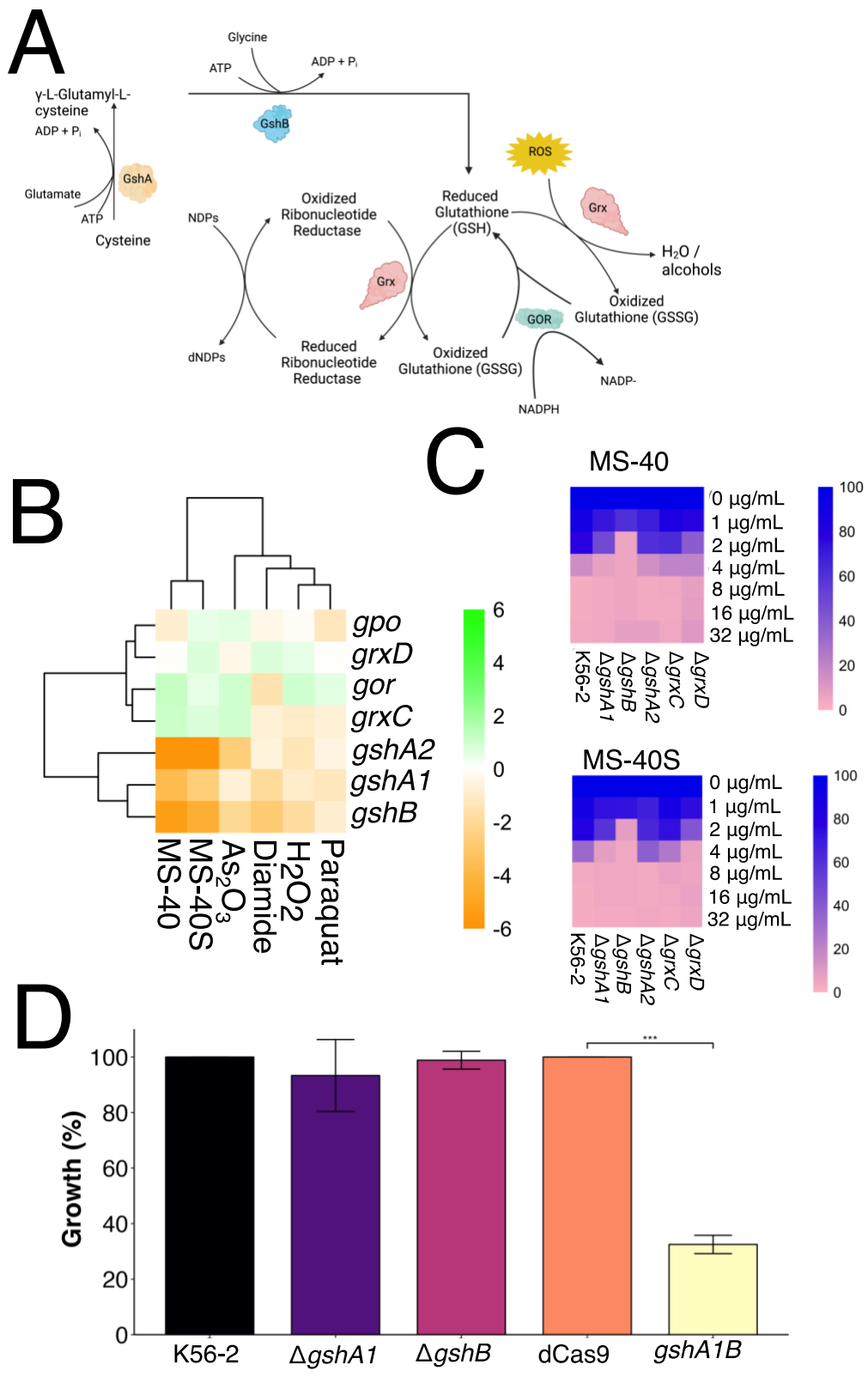
A
Glycine
ATP
ADP + Pi
GshB
γ-L-Glutamyl-L-cysteine
ADP + Pi
GshA
Glutamate
ATP
Cysteine
ROS
Grx
H2O / alcohols
Oxidized Glutathione (GSSG)
GOR
NADP-
NADPH
Reduced Glutathione (GSH)
Oxidized Ribonucleotide Reductase
NDPs
dNDPs
Reduced Ribonucleotide Reductase
Grx
Oxidized Glutathione (GSSG)
B
gpo
grxD
gor
grxC
gshA2
gshA1
gshB
MS-40
MS-40S
As2O3
Diamide
H2O2
Paraquat
6
4
2
0
-2
-4
-6
C
MS-40
0 μg/mL
1 μg/mL
2 μg/mL
4 μg/mL
8 μg/mL
16 μg/mL
32 μg/mL
K56-2
ΔgshA1
ΔgshB
ΔgshA2
ΔgrxC
ΔgrxD
100
80
60
40
20
0
MS-40S
0 μg/mL
1 μg/mL
2 μg/mL
4 μg/mL
8 μg/mL
16 μg/mL
32 μg/mL
K56-2
ΔgshA1
ΔgshB
ΔgshA2
ΔgrxC
ΔgrxD
100
80
60
40
20
0
D
Growth (%)
100
80
60
40
20
0
***
K56-2
ΔgshA1
ΔgshB
dCas9
gshA1B

Figure 26. Glutathione system may be involved in the MOA of MS-40 and MS-40S.

(**A**) Schematic of the glutathione system showing the roles of each protein, their respective reactions. (**B**) Fitness profile of glutathione related genes from BarSeq. Heatmap of ROS-related genes and their corresponding gene fitness values for each compound used in BarSeq. Heatmap was generated on RStudio using the pheatmap package Green represents positive fitness and orange represents negative fitness. (**C**) Percent growth (100% growth blue, 0% growth pink) of glutathione related deletion mutants and wildtype against MS-40 and MS-40S. OD values were taken from MIC testing using broth microdilution assay and converted to percent growth. (**D**) Growth of each strain was measured after 18 hours after grown in LB (for K56-2 wildtype, Δ*gshA*, and Δ*gshB*) or LB Tp100 + 30.5 mM rhamnose (for dCas9 non-targeting control and *gshA1gshB* CRISPRi mutant). *** indicates $P < 0.0001$ from one-way ANOVA and post-hoc Dunnett Test.

To see if silencing the *gshA1gshB* operon could potentiate the activity of other antibiotics, the minimum inhibitory concentration and minimum bactericidal concentrations were measured in the dCas9 non-targeting strain and the *gshA1B* knock-down strain in cation-adjusted Mueller Hinton broth, with 100 μg/mL trimethoprim and 30.5 mM rhamnose (Table 11). Interestingly, silencing both *gshA1* and *gshB* did not change the MIC to MS-40 and MS-40S but the MIC of ceftazidime decreased from 32 μg/mL to 4 μg/mL and decreased the MBC for ciprofloxacin, ceftazidime, and meropenem between 2- and 4- fold, compared to wild type *B. cenocepacia* K56-2.

Table 11. Minimum inhibitory concentration and minimum bactericidal concentration of *gshA1B* CRISPRi mutant against bactericidal antibiotics using broth microdilution assays.

	MIC (µg/mL)		**MBC (µg/mL)**	
Strain	**dCas9***	***gshA1B***	**dCas9***	***gshA1B***
Ciprofloxacin	2	2	**16**	**4**
Doxycycline	4	4	>16	>16
Meropenem	32	32	**64**	**32**
Ceftazidime	**32**	**4**	**64**	**32**
MS-40	8	8	16	16
MS-40S	8	8	16	16

*non-targeting control. The reported MIC values are from three biological replicates. Assays done in the presence of 7.61 mM rhamnose.

3.13 Disrupting Purine Metabolism Leads to Decreased Susceptibility to MS-40 and MS-40S

Purine metabolism is present in all domains of life because it synthesizes purines that are used to make up DNA, as well as for energy metabolism, in the form of ATP, and cell signaling (Chua and Fraser 2020). The purine biosynthesis pathways start with phosphoribosyl pyrophosphate and ends with inosine monophosphate (IMP), a precursor for both adenosine 5'-monophosphate and guanosine 5'-monophosphate (Pedley and Benkovic 2017). Purine metabolism has previously been implicated in antibiotic killing in *E. coli*. It was found that deletions in purine biosynthesis reduced killing by ampicillin and ciprofloxacin, but increased killing by gentamycin (Yang et al. 2019).

Purine/nucleotide metabolism was a pathway that was enriched in our BarSeq data and was a highly perturbed pathway, from the Pathway perturbation analysis (Figure 27), leading to decreased susceptibility to ROS inducers, so, we wanted to explore this further. Figure 27A shows various genes that were identified from the BarSeq and their gene fitnesses. Most of the genes had statistically significant positive gene fitness scores for MS-40 and MS-40S, as well as the other compounds used in the BarSeq experiment (Figure 27A). This suggested that disrupting purine metabolism may reduce susceptibility to oxidative stress. The pathway for purine metabolism from *E. coli* is shown in Figure 27B. CRISPRi mutants were also made to knock-down a few genes involved in purine metabolism, but there were no changes in their MIC values (Figure A15).

Of the control compounds, MS-40 and MS-40S clustered most closely to As_2O_3 for purine related genes (Figure 27A). It is known that heavy metals, such as gold and arsenic can bind to ATP (Hainfeld et al. 1999; Shen et al. 2013), causing them to be degraded, suggesting the effect MS-40 and MS-40S is having on purine metabolism may be due to gold binding ATP. We performed an ATP detection assay, which is based on a luciferase assay to see the effect MS-40

and MS-40S have on ATP levels upon treatment. Surprisingly, our control antibiotic tetracycline caused an increase in cellular ATP (Figure 27C). We also included AsO_4 as another heavy metal control as this has been shown previously to deplete ATP (Shan et al. 2017); however, we did not see any depletion in our assay. Both MS-40 and MS-40S caused a slight decrease in ATP levels compared to the DMSO solvent control (Figure 27C), however, it is not a significant change, possibly indicating that ATP bound by heavy metals in *B. cenocepacia* can be salvaged.

Because MS-40 and MS-40S didn't have any effect on the levels of ATP in the cell, we tested the purine metabolism CRISPRi mutants on their ROS production, to see if they have decreased ROS production, as an explanation why the mutants are more tolerant to ROS inducers. However, none of the CRISPRi mutants in purine metabolism gene had significant changes in ROS production, compared to the non-targeting dCas9 control (Figure 27D).

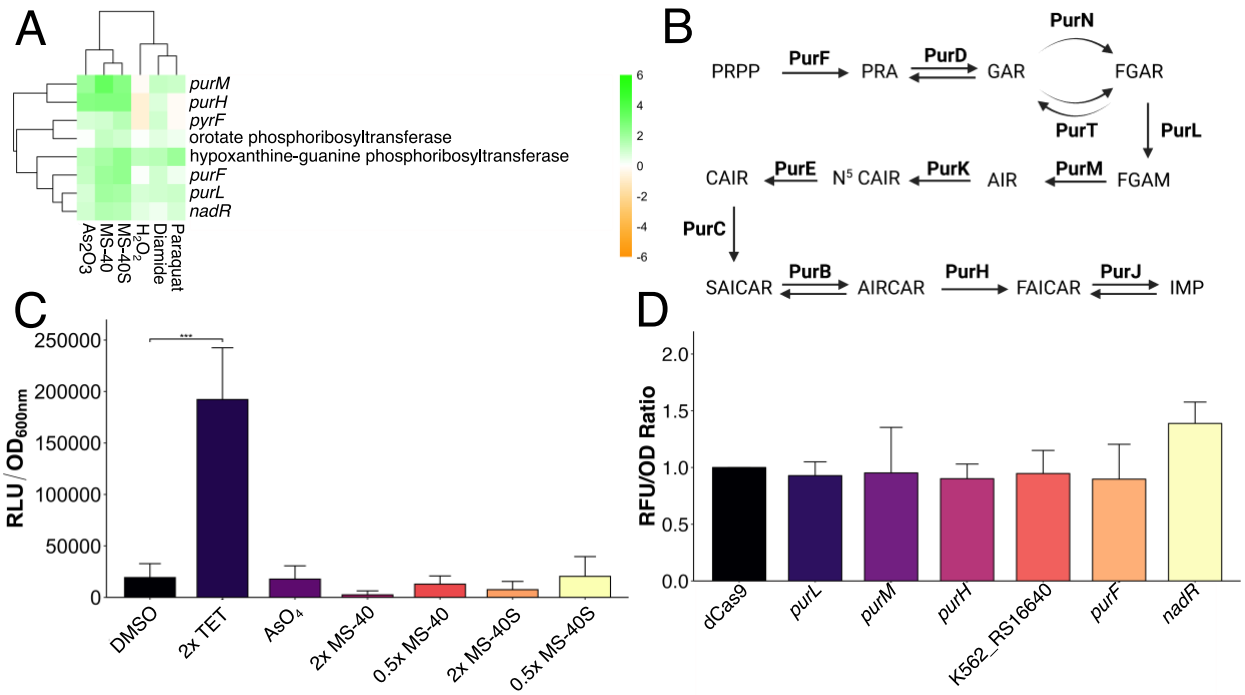

Figure 27. Disrupting purine biosynthesis leads to decreased susceptibility to MS-40 and MS-40S.

(**A**) Fitness profile of purine/pyrimidine related mutants in BarSeq. Heatmap of ROS-related genes and their corresponding gene fitness values for each compound used in BarSeq.Green represents positive fitness and orange represents negative fitness. (**B**) Simple schematic of the purine biosynthesis pathway. (**C**) ATP detection of *B. cenocepacia* K56-2 exposed to antibiotics. An OD_{600nm} of 0.6 wild type K56-2 were incubated with corresponding antibiotics, 15 mM AsO_4, and a DMSO solvent control for three hours. BacTiter Glo was then added to all wells and luminescence was recorded. *** indicates $P < 0.0001$ from a one-way ANOVA and post-hoc Dunnett Test. (**D**) Exponential phase cells were subcultured for 3 hours in 30.5 mM rhamnose, washed, then resuspended in PBS before being exposed to 10 mM of H_2DCFDA dye. Fluorescence ($\lambda_{ex}485/\lambda_{em}528$) and OD_{600} readings were taken every 5 minutes for 2 hours to calculate relative ROS production compared to the non-targeting control (dCas9).

CHAPTER 4: DISCUSSION

4.1 Identification of MS-40 and MS-40S and their activity

Here, we started by exploring the antibiotic properties of two auranofin analogs, MS-40 and the novel compound MS-40S, against the cystic fibrosis pathogen *B. cenocepacia* K56-2. The antibiotic properties were explored in parallel with common antibiotics prescribed to CF patients infected with *Burkholderia* species, specifically, doxycycline, meropenem, and ceftazidime–avibactam. One difference between MS-40 and MS-40S and the clinical antibiotics used in this study is the ability of MS-40 and MS-40S to eliminate non-replicating cells. It is common for antibiotics to act on essential processes, such as those involved in cell wall synthesis, DNA replication, and translation (Kohanski et al. 2010). In stationary phase, most of these processes are decreased, preventing the antibiotics from acting upon the cell. We confirmed this with two antibiotics with different mechanisms of action (MOA): doxycycline, a tetracycline that binds to the 30s subunit of the ribosome, preventing translation elongation (Grossman 2016), and ceftazidime–avibactam, a cephalosporin–β-lactamase inhibitor combination that inhibits cell wall synthesis (Shirley 2018). These two antibiotics did not kill cells in stationary phase. Our data show that MS-40 and MS-40S are bactericidal against both replicating and non-replicating cells. Interestingly, MS-40S was shown to kill a greater amount of stationary phase cells than exponential phase, unlike MS-40. This suggests that the MOA of these two compounds may be slightly different.

B. cenocepacia strains are inherently resistant to many available antibiotics (Ostermann et al. 2016; Rhodes and Schweizer 2016; Scoffone et al. 2017), leaving only a few available for treatment. As shown in the resistance studies, resistance is not easy to achieve for MS-40 and MS-

40S. Mutational resistance can be achieved by altering the antibiotic gene targets, decreasing the binding affinity of the antimicrobial to the gene product, decreasing the uptake/increase in efflux, or, lastly, by changing global responses such as changing a metabolic pathway (Munita and Arias 2016). Meropenem and doxycycline quickly generated multistep resistance, possibly by one of the mechanisms listed above; however, resistance did not emerge for MS-40 and MS-40S. This might be due to MS-40 and MS-40S not being affected by the change of porins/efflux pumps that can cause resistance to other antimicrobials (Munita and Arias 2016), especially in *Burkholderia* species (Guglierame et al. 2006; Rhodes and Schweizer 2016; Scoffone et al. 2017). Alternately, mutations in the gene targets of MS-40 and MS-40S could have resulted in a reduced fitness of the resistant mutant cell, preventing the mutant from outcompeting the sensitive cells (Hughes and Andersson 2017; Durão et al. 2018).

Additionally, MS-40 and MS-40S can clear difficult-to-eradicate persister cells which commonly cause relapses in infections (Brauner et al. 2016). This suggests these compounds could eradicate the difficult-to-treat persistent infections in the CF lung, helping CF patients infected with *Burkholderia* species become eligible for lung transplants (Dupont 2017). MS-40 and MS-40S were shown to eliminate persister cells in two ways. The first way was by killing an enriched population of ciprofloxacin-generated persisters, reducing the population by a further 1–2 $\log_{10}$ CFU/mL. The second way was from a stationary-phase population of bacteria exposed solely to MS-40 and MS-40S, with MS-40S only having a small amount of persisters at 5x MIC and MS-40 producing no persisters. Alternatively, the persister frequency was low for meropenem (5–7%), and approximately 30% for ceftazidime–avibactam, similar to the amount produced by *Burkholderia pseudomallei* exposed to ceftazidime (Ross et al. 2018). Therefore, MS-40 and MS-

40S could be used on their own to eliminate infections, or in tandem with current antibiotics to help eradicate infections (Zheng et al. 2020).

We have also showed MS-40 and MS-40S have low toxicity in *C. elegans* and *G. mellonella*. One limitation of these compounds is that we did not observe *in vivo* antibiotic activity in *C. elegans* and *G. mellonella* infected with *B. cenocepacia* K56-2 (data not shown). To help explain why we were not seeing a protective effect, we tested the MIC of MS-40 and MS-40S in 50% human serum. In the presence of 50% human serum, the MICs of both compounds increased to 128 μg/mL, suggesting these compounds bind non-specifically to proteins, which could decrease their antimicrobial activity. To increase the efficacy of these potent antimicrobials, a drug delivery system must be developed. One possible route is the creation of an MS-40/MS-40S-loaded liposome, as has been shown with rifampicin in the treatment of pulmonary *Mycobacterium abscessus* infections (Rinaldi et al. 2021). Creating an aerosolized antimicrobial therapy would also allow us to achieve higher concentrations of the drug, and increase lung penetration, which is especially important for CF pulmonary infections (Chalmers et al. 2021).

4.2 Mechanism of Action of MS-40 and MS-40S

Auranofin, and previously published auranofin analogs, inhibit thioredoxin reductase, an enzyme that plays a role in thiol-homeostasis in the cell (Harbut et al. 2015; Epstein et al. 2019). However, it is unknown whether MS-40 and MS-40S share the same target with auranofin or if they have any other additional targets. It is assumed that the active component of auranofin is the gold atom, which binds the sulfur in the active site of thioredoxin reductase, inhibiting the formation of the critical disulfide bond, disrupting the function of the enzyme (Kean et al. 1997; Epstein et al. 2019). Auranofin was shown to have other effects on the bacterial cell, such as

inhibiting DNA, protein, and cell wall synthesis. Thus, thioredoxin reductase may not be the sole antimicrobial target (Thangamani et al. 2016). It is assumed that MS-40 and MS-40S will have similar effects inside the cell as auranofin, possibly having a multi-target mechanism of action. The lack of multi-step resistance may support this multi-target mechanism of action because multiple mutations would be needed to generate resistance. The other potential targets of auranofin and auranofin analogs are not known. Other factors in the mechanism of action of the antimicrobials, which can explain differences in activity among compounds with slightly different structures, can be associated efflux pumps and transporters.

We have shown that MS-40 and MS-40S inhibit thioredoxin reductase, which is as expected as auranofin and other analogs were shown to inhibit this enzyme (Harbut et al. 2015; Epstein et al. 2019). We hypothesized that MS-40 and MS-40S would also inhibit the structurally and functionally similar protein glutathione reductase, as both contain two key cysteine amino acids in their active site (Carmel-Harel and Storz 2000; Lu and Holmgren 2014). However, this was not the case, as MS-40 and MS-40S were shown to have no affect on the activity of GOR. Although, deleting the *gor* gene in *B. cenocepacia* K56-2 caused a 2-fold increase in the MIC of MS-40 and MS-40S. If MS-40 and MS-40S, due in fact increase reactive oxygen species, as hypothesized, the decreased susceptibility of the Δ*gor* mutant might be related to the fact that deleting *gor* lead to a decrease in ROS (Figure A16). This raises the question, why does deleting GOR lead to an decrease in ROS while this protein plays a role in detoxifying ROS? One hypothesis is that another protein, in the absence of GOR, can maintain reduced/oxidized glutathione homeostasis, such as glutaredoxins (Tuggle and Fuchs 1985).

We have also found that auranofin may be inactive in *Burkholderia cenocepacia* because of efflux. Interesingly, silencing the *mlaFEDvacJ* operon, *lolA*, and *hldD* lead to increased

permeability of the *B. cenocepacia* K56-2 membrane, but this only lead to slightly increased sensitivity to auranofin, suggesting that auranofin is already able to permeate into the WT cell. However, silencing the major efflux system in *B. cenocepacia* K56-2, *bpeAB-oprB* lead to the largest change in susceptibility to auranofin, suggesting that efflux plays a role in why auranofin is inactive in *B. cenocepacia*. Silencing this efflux system had no effect on the activity of MS-40 and MS-40S, suggesting these compounds are not effluxed by the bacterium. Also, silencing *hpnN* and *shc*, in hopanoid biosynthesis, lead to increased susceptibility. It has been shown that deleting hopanoid biosynthesis decreases efflux activity (Sáenz et al. 2015), and this is why we think silencing *hpnN* and *shc* lead to increased sensitivity to auranofin.

To determine the factors involved in susceptibility and tolerance to two novel antimicrobials, MS-40 and MS-40S, as well as other ROS producing compounds as benchmarking controls, we used a randomly barcoded transposon mutant library. This library was created previously in our lab in *B. cenocepacia* K56-2 (Hogan et al. 2023). This allowed us to have a genome-wide look at which mutants, when the gene is disrupted by a transposon, had altered susceptibilities after exposure to MS-40, MS-40S, and other ROS inducers. Looking at which compounds have the most mutants in common for having altered susceptibility, MS-40 and MS-40S are most similar to diamide and As_2O_3.This suggests that the mechanism of action (MOA) of these novel therapeutics involve thiol stress and heavy metal toxicity.

There are a lot of specific mutants that are shared between MS-40 and MS-40S that disrupting alters sensitivity, such as *gshA* and *gshB*, which are involved in glutathione biosynthesis, *oxyR*, a regulatory for oxidative stress, and *purH*, *purL*, and *purM* in purine biosynthesis. This is expected because MS-40 and MS-40S are structurally very similar. This suggests that the MOA of MS-40 and MS-40S include the glutathione system, which can detoxify

reactive oxygen species (ROS) and maintain thiol homeostasis in the cell (Couto et al. 2016), oxidative stress, and purine metabolism/biosynthesis. This is also shown in the pathway perturbation score and pathway enrichment analysis, which again pointed us towards glutathione biosynthesis and purine metabolism/biosynthesis.

We validated some of the BarSeq findings by making gene deletions in the glutathione biosynthesis pathway, *gshA1*, *gshA2*, and *gshB*, as well as in two glutaredoxins, *grxC* and *grxD*. The BarSeq found that disrupting glutathione biosynthesis genes lead to increased sensitivity to the compounds. Deleting the genes in *B. cenocepacia* K56-2 also lead to increased sensitivity to MS-40 and MS-40S. This allows us to trust the BarSeq method in accurately representing mutant's sensitivities to MS-40 and MS-40S. CRISPRi mutants were made in several genes in various pathways and processes, such as purine metabolism, electron transport chain, ROS scavenging genes, and some in the thioredoxin system. However, we did not see any changes in sensitivity of these mutants to MS-40 and MS-40S. This may be because when grown clonally, compared to in a pool, the mutant's fitness is not as affected.

The genes *gshA1* and *gshB* are in an operon in *B. cenocepacia* K56-2 and we attempted to delete this operon but were unsuccessful, suggesting a new synthetic lethal combination. We thus created a CRISPR interference mutant of this operon in which we could tune the level of suppression, silencing both *gshA1* and *gshB*. CRISPRi is a method for gene silencing and is polar, such that if we silence the first gene in an operon, the subsequent genes are also silenced. Through this, we identified a new synthetic lethal combination, which could be used to develop a combinational therapy targeting both these proteins in *B. cenocepacia* K56-2. This is the first instance of identifying this combination as a synthetic lethal pair. Only silencing both genes resulted in any growth defect, i.e., deleting either of the genes alone do not produce a growth

defect. This causes us to suggest that individually, each protein can play the role of both in synthesizing glutathione and thus deleting both is needed to completely abolish glutathione biosynthesis.

We wanted to see if knocking down these two genes would enhance the antibacterial activity of other antibiotics and saw that the MIC of ceftazidime decreased and the MBC of ceftazidime, ciprofloxacin, and meropenem also decreased. We believed that the change in MIC and MBC we see with the *gshA1B* CRISPRi mutant for ceftazidime, meropenem and ciprofloxacin may be due to the increase in ROS this mutant has (Figure A16). However, a checkerboard assay with these antibiotics and hydrogen peroxide showed no interaction. Thus, the effect must be due to depletion of cellular glutathione and another role it plays in the cell, besides scavenging ROS.

For ROS related genes, in hierarchical clustering, MS-40 and MS-40S were more similar to H_2O_2 and diamide, which might suggest that the ROS produced by MS-40 and MS-40S is H_2O_2 and may also cause thiol-stress. Additionally, disrupting *oxyR* lead to increased tolerance to MS-40 and MS-40S in the BarSeq data and deleting this gene validated this interaction, in which the deletion mutant was more tolerant to MS-40, MS-40S, and H_2O_2. This is the opposite of what we were expecting because *oxyR* is an activator of ROS scavenging genes in many bacteria (Imlay 2008, 2015), however, less commonly, it can act as a negative repressor in some bacteria (Imlay 2015). It has been shown that *oxyR* transcription increases upon exposure to ROS in *Burkholderia cenocepacia* (El-Halfawy and Valvano 2014) but whether it is a positive or negative regulator is not known.

MS-40 and MS-40S clustered with As_2O_3 for purine biosynthesis and related genes, suggesting the the effect MS-40 and MS-40S has on purine metabolism/ATP is related to the presence of the gold heavy metal. Arsenic, in our assay, did not deplete ATP as previously reported

(Shen et al. 2013), this may be due to *B. cenocepacia* being able to salvage ATP that is bound to a heavy metal that other bacteria cannot. Additionally, tetracycline caused an increase in ATP. We believe that tetracycline causes an increase in ATP because tetracycline inhibits protein synthesis which is a highly ATP consuming process. As MS-40 and MS-40S inhibits the protein thioredoxin reductase, thioredoxins in the cell become unuseable. This may also explain why there is a slight decrease in cellular ATP, because thioredoxin is used as a reducing equivalent in the ribonucleotide reductase enzyme, which creates deoxyribonucleotides from ribonucleotides (Sengupta and Holmgren 2014; Lu and Holmgren 2014).

CHAPTER 5: CONCLUSION AND FUTURE DIRECTIONS

The aims of this work were to identify auranofin analogs that are active against the cystic fibrosis pathogen *Burkholderia cenocepacia* K56-2 and determine the active antimicrobial's mechanism of action. We tested auranofin and ten auranofin analogs and identified two with low MICs and found that these compounds, MS-40 and MS-40S, are bactericidal to *B. cenocepacia* K56-2 and other CF pathogens, do not select for resistance, and can kill metabolically dormant cells, such as persister cells. However, these compounds could not save *C. elegans* and *Galleria* worms infected with *B. cenocepacia* K56-2. We found that MS-40 and MS-40S inhibit the protein thioredoxin reductase, and not the structurally and functionally similar protein, glutathione reductase, and cause an increase in reactive oxygen species. Also, deleting glutathione biosynthesis led to increased susceptibility and disrupting purine metabolism led to decreased susceptibility to MS-40 and MS-40S.

Future work would be to create a drug delivery system for MS-40 and MS-40S, so that it gets to the site of infection and able to clear the bacteria in infection models. MS-40 and MS-40S were well tolerated, similar to the DMSO control, by the models tested in this work, *C. elegans* and *Galleria*, but they could not save the worms infected with *Burkholderia cenocepacia* K56-2, possibly because MS-40 and MS-40S were binding other cellular proteins, and thus, less were available to kill the bacteria. Another avenue that could be followed is the *gshA1B* synthetic lethal combination. Deleting both lead to an unviable cell, and thus, if a compound (or two compounds) inhibits these two proteins, that could lead to a new class of antibiotics with a novel mechanism of action with no known resistance.

CHAPTER 6: APPENDIX

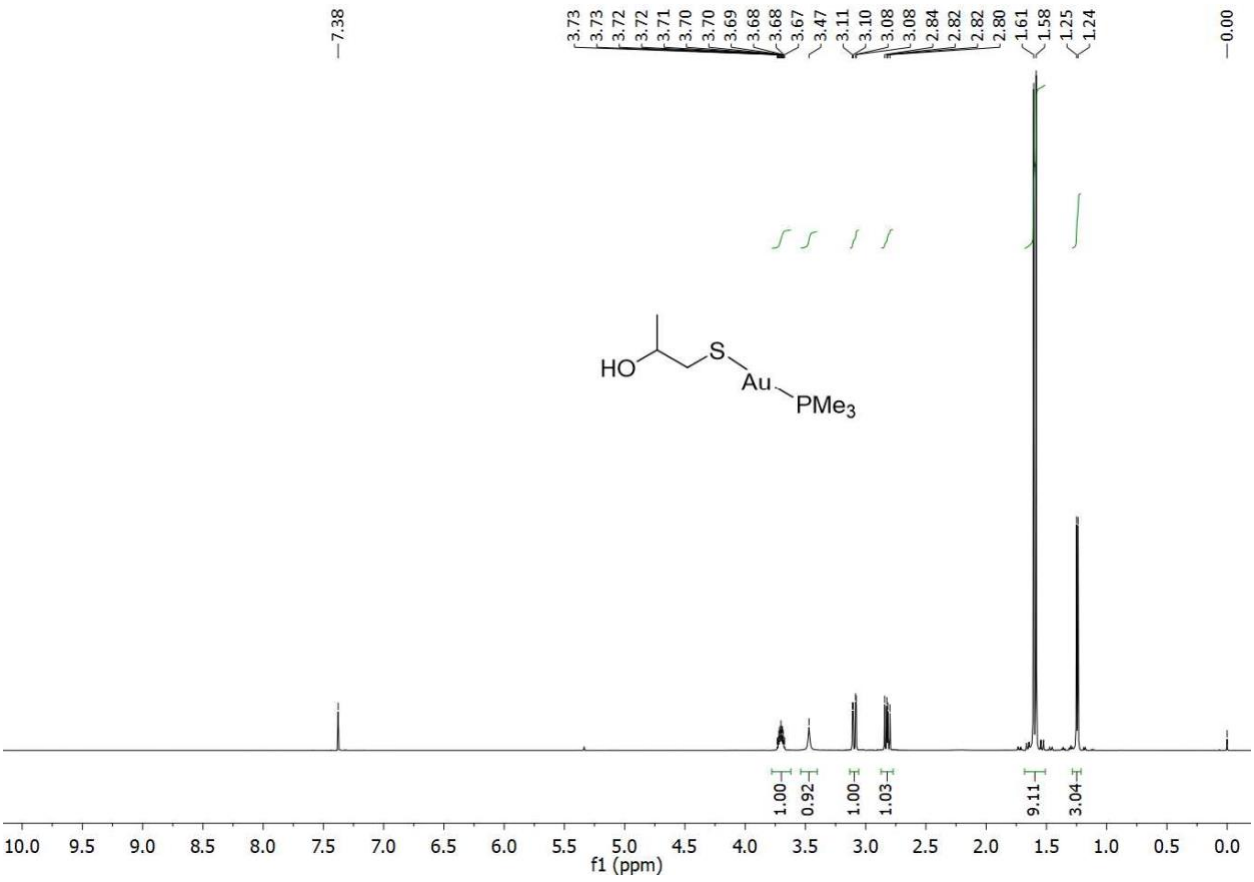

Figure A1. ^{1}H NMR spectrum of compound WB-19-HL4170 (MS-40S) in $CDCl_3$.

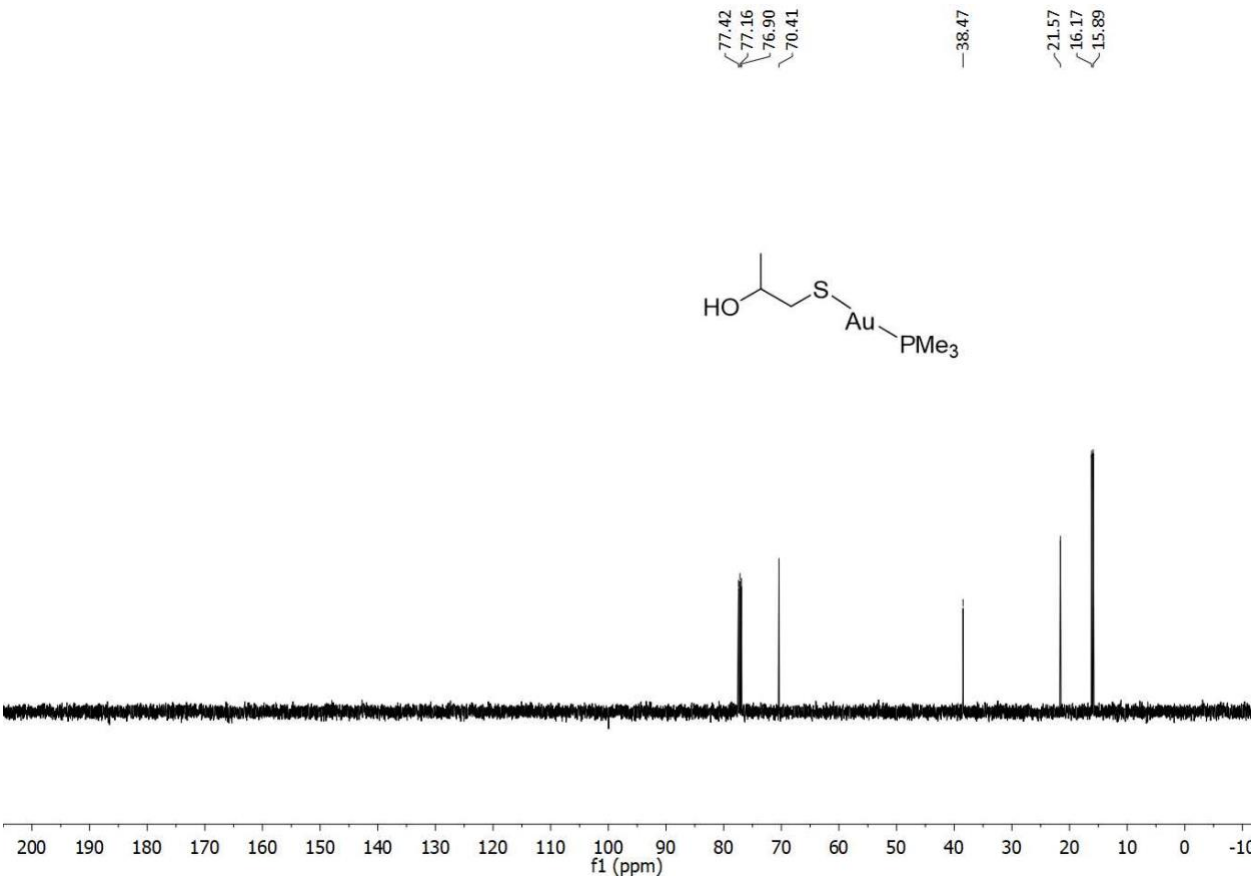

Figure A2. ^{13}C NMR spectrum of compound WB-19-HL4170 (MS-40S) in $CDCl_3$.

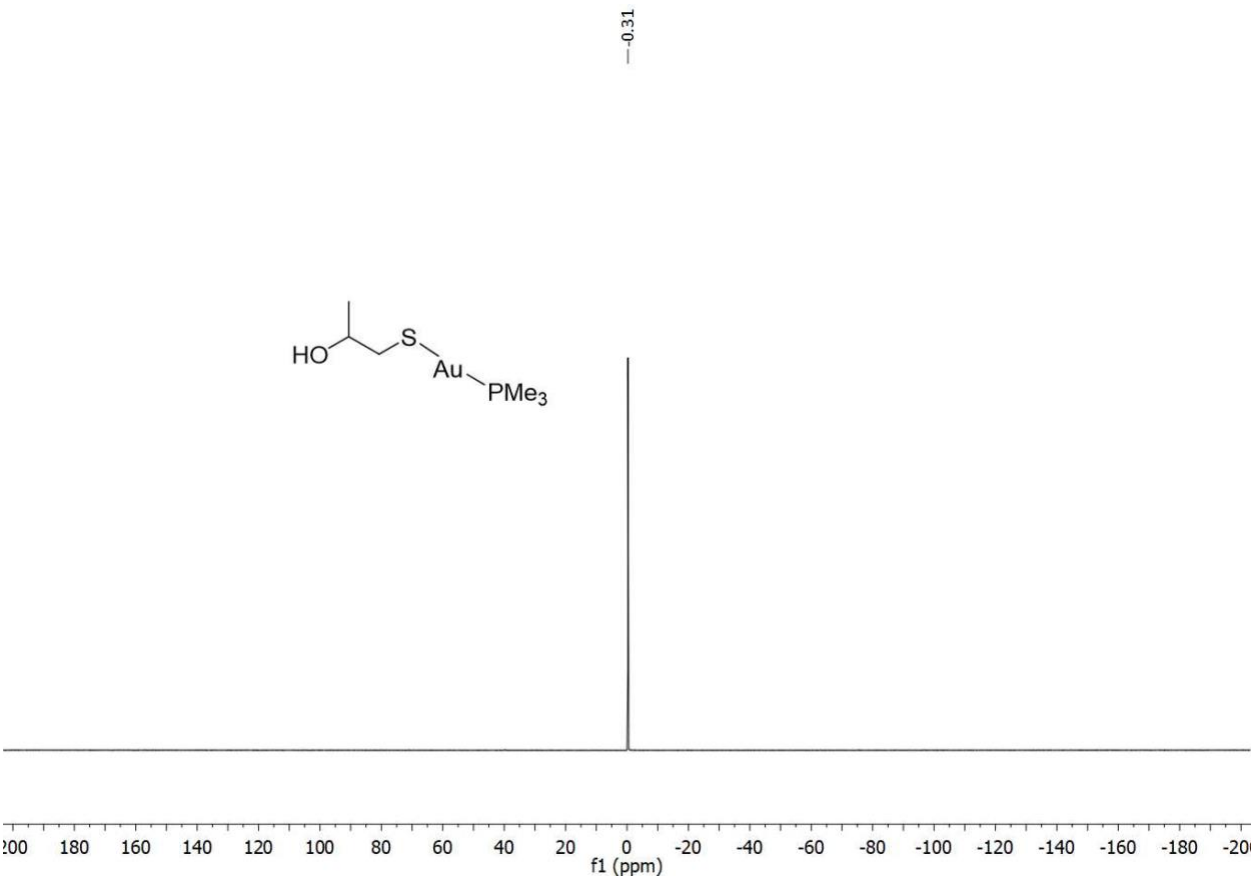

Figure A3. ^{31}P NMR spectrum of compound WB-19-HL4170 (MS-40S) in $CDCl_3$.

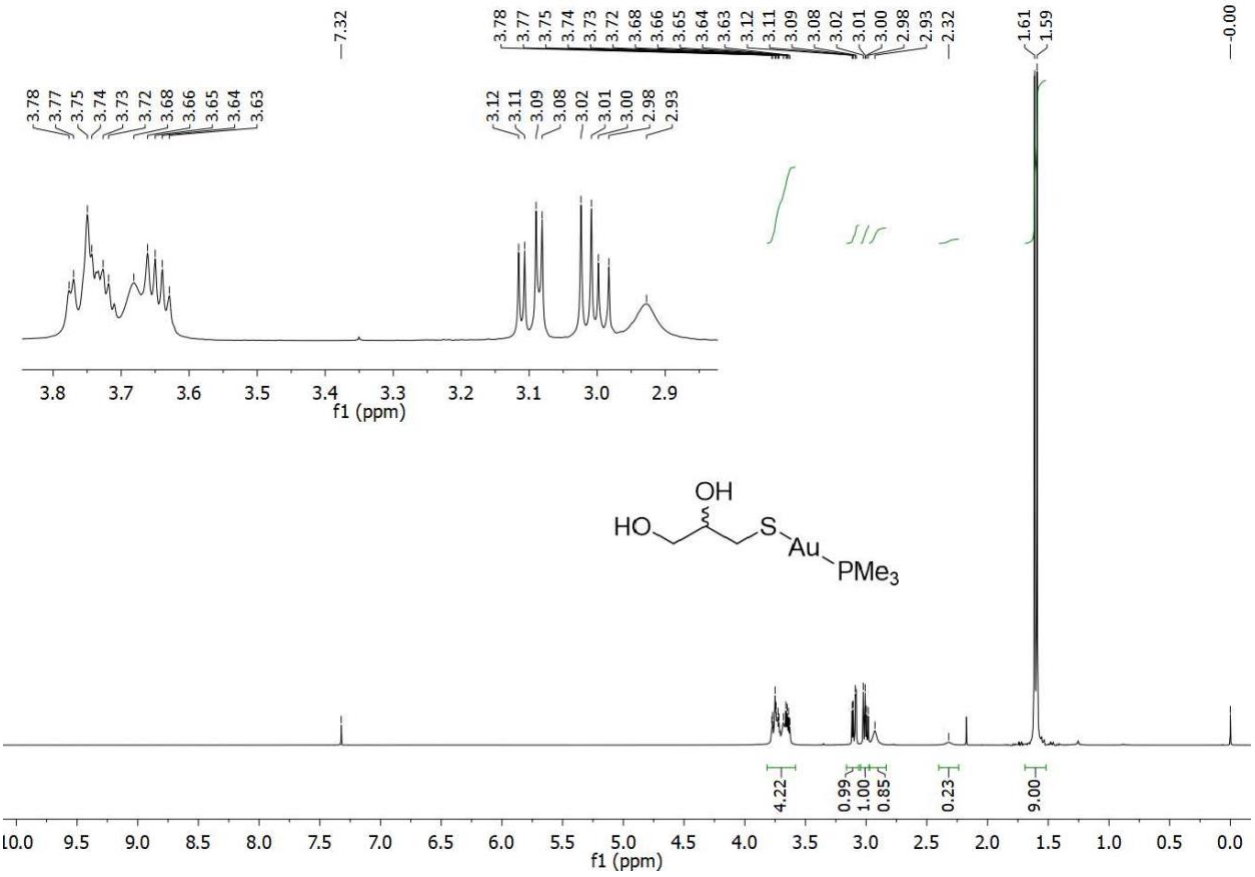

Figure A4. ^{1}H NMR spectrum of compound WB-19-HL4171 in $CDCl_3$.

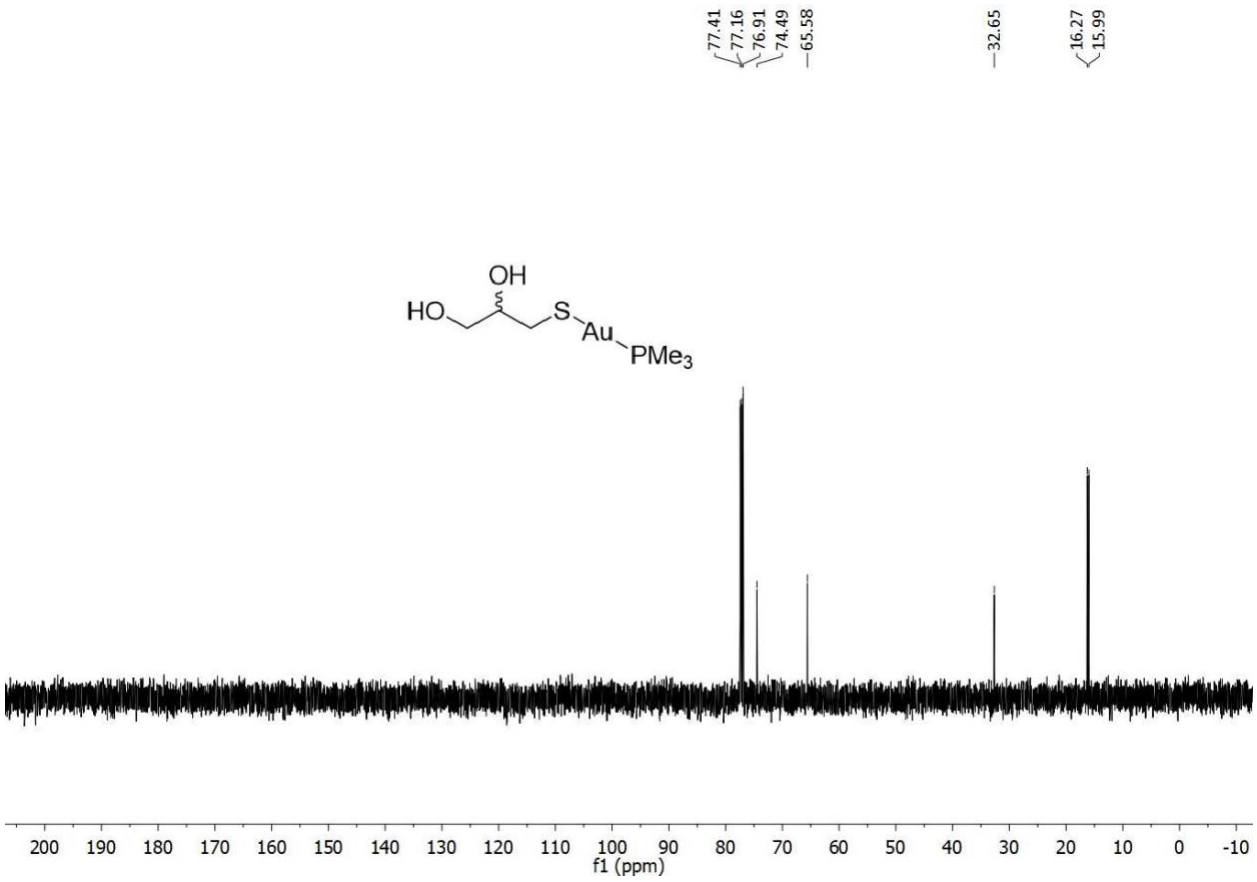

Figure A5. ^{13}C NMR spectrum of compound WB-19-HL4171 in $CDCl_3$.

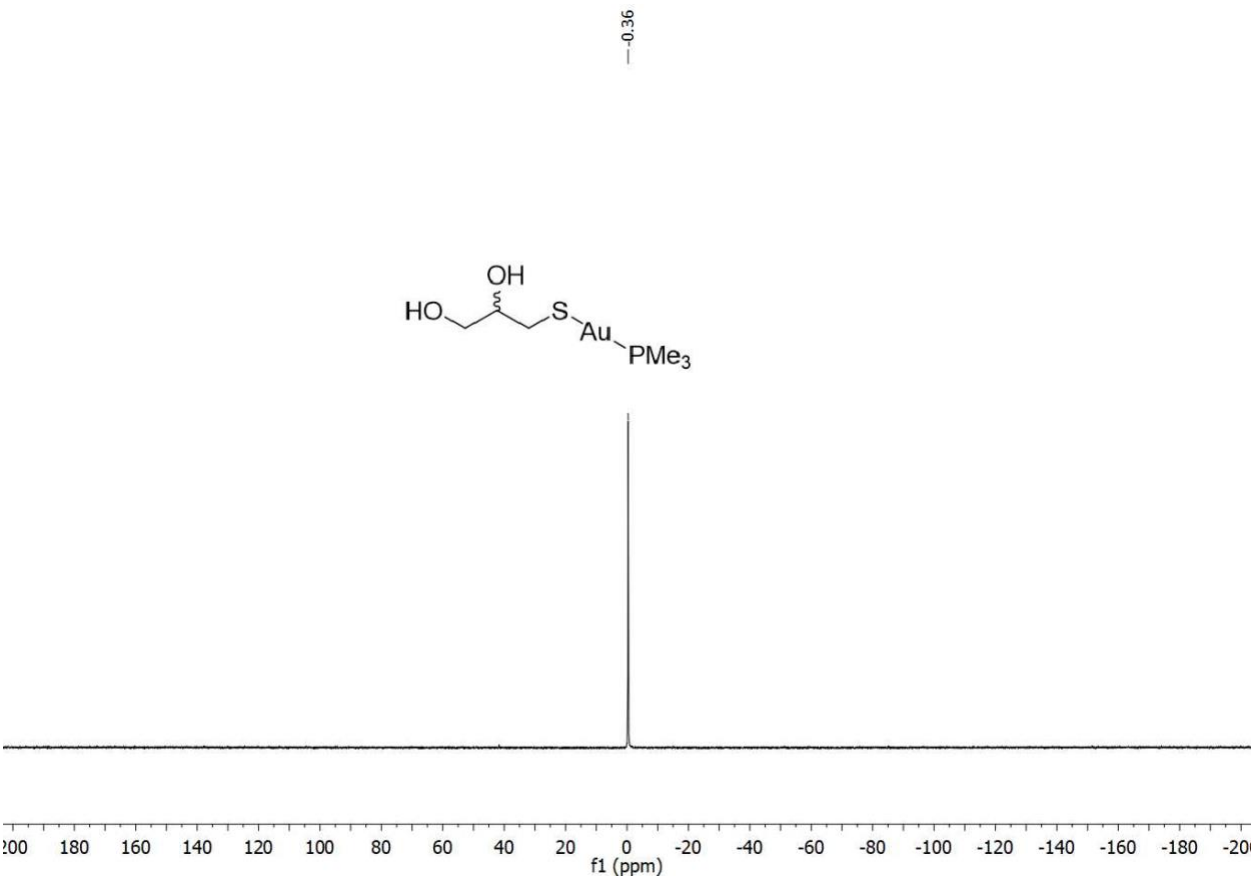

Figure A6. ^{31}P NMR spectrum of compound WB-19-HL4171 in $CDCl_3$.

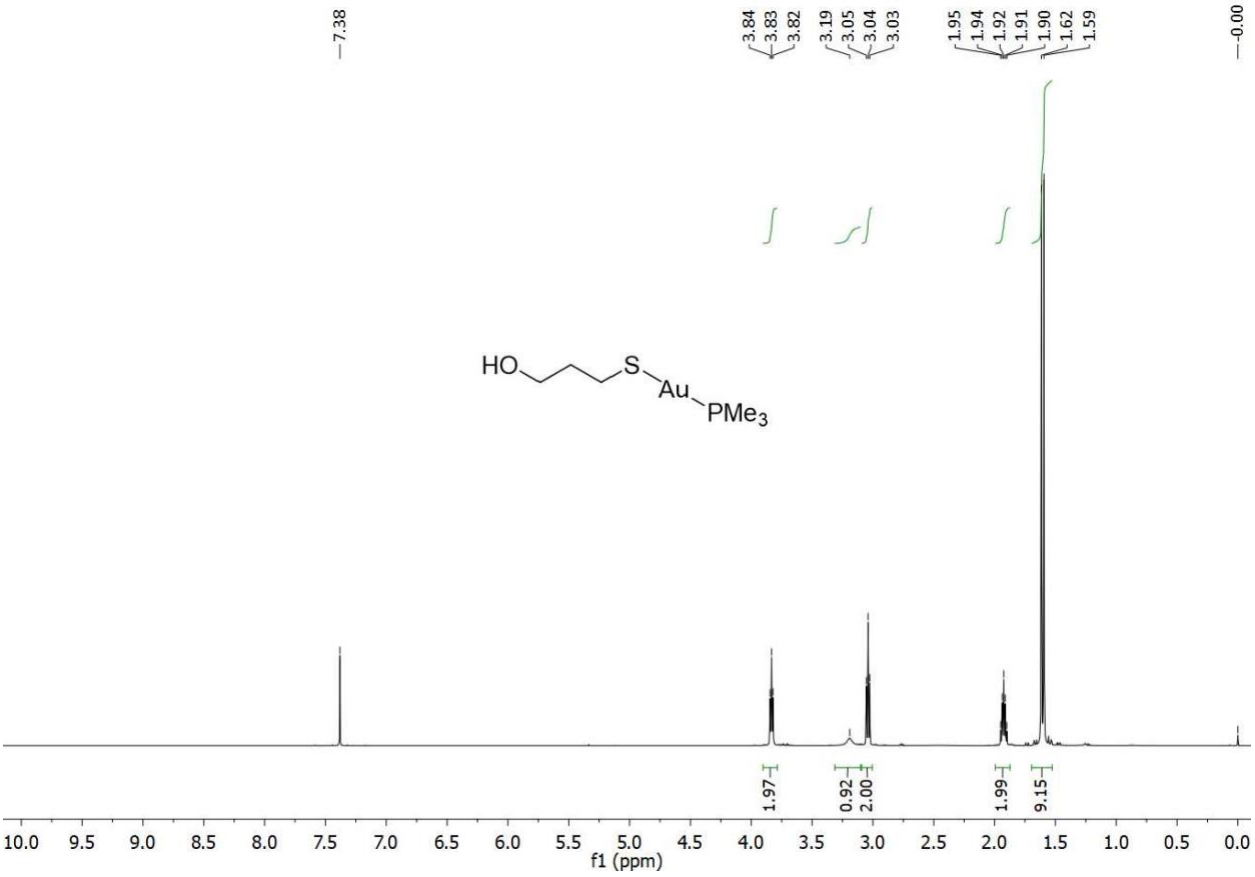

Figure A7. ^{1}H NMR spectrum of compound WB-19-HL4172 in $CDCl_3$.

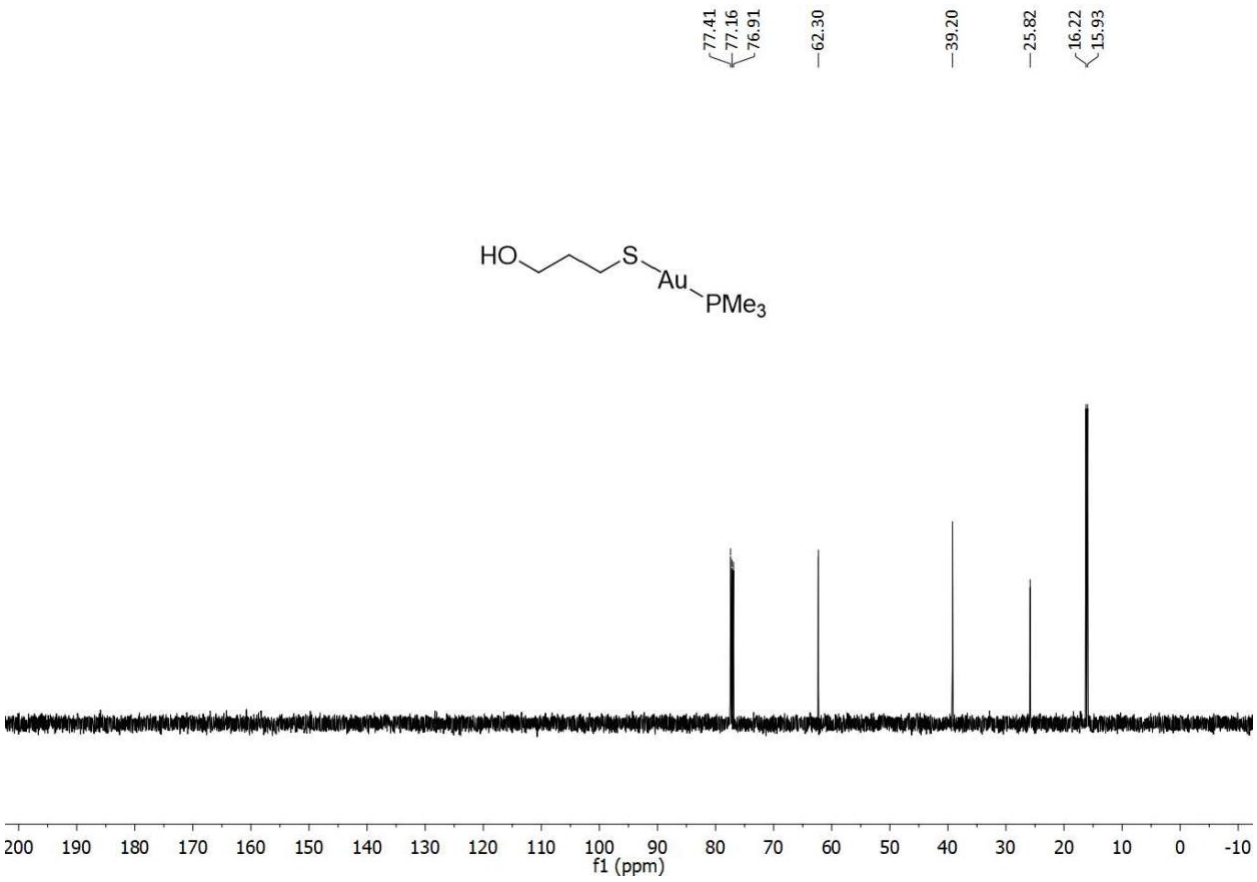

Figure A8. ^{13}C NMR spectrum of compound WB-19-HL4172 in $CDCl_3$.

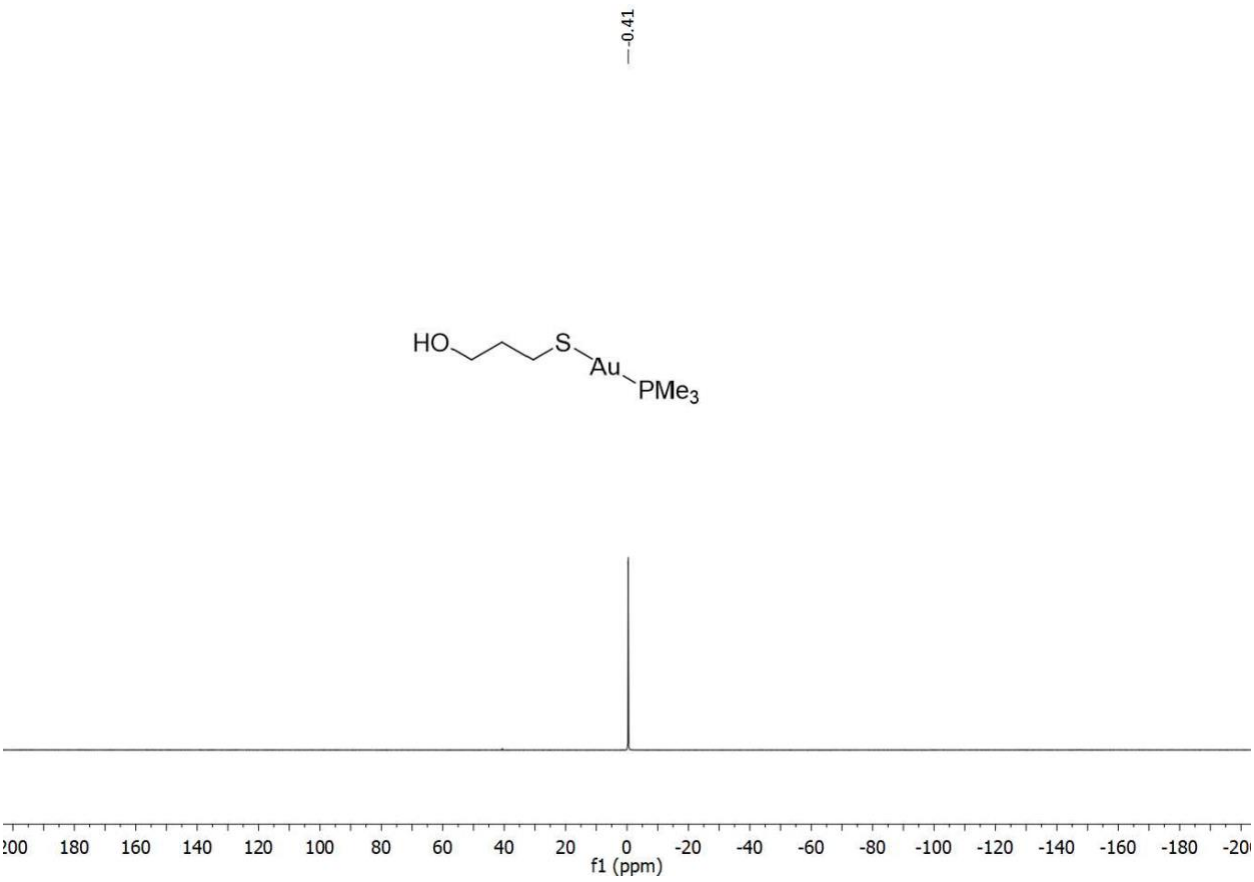

Figure A9. ^{31}P NMR spectrum of compound WB-19-HL4172 in $CDCl_3$.

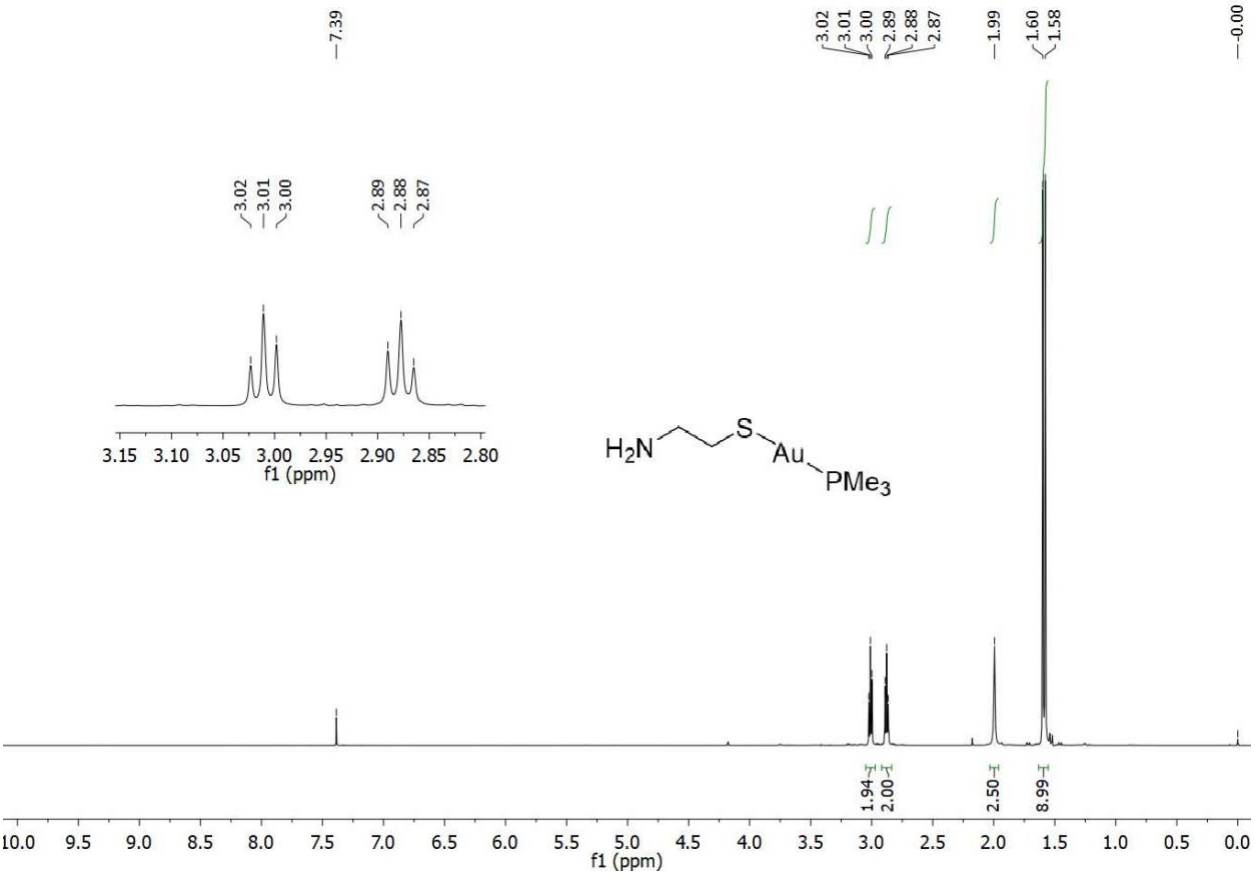

Figure A10. ^{1}H NMR spectrum of compound WB-19-HL4181 in $CDCl_3$.

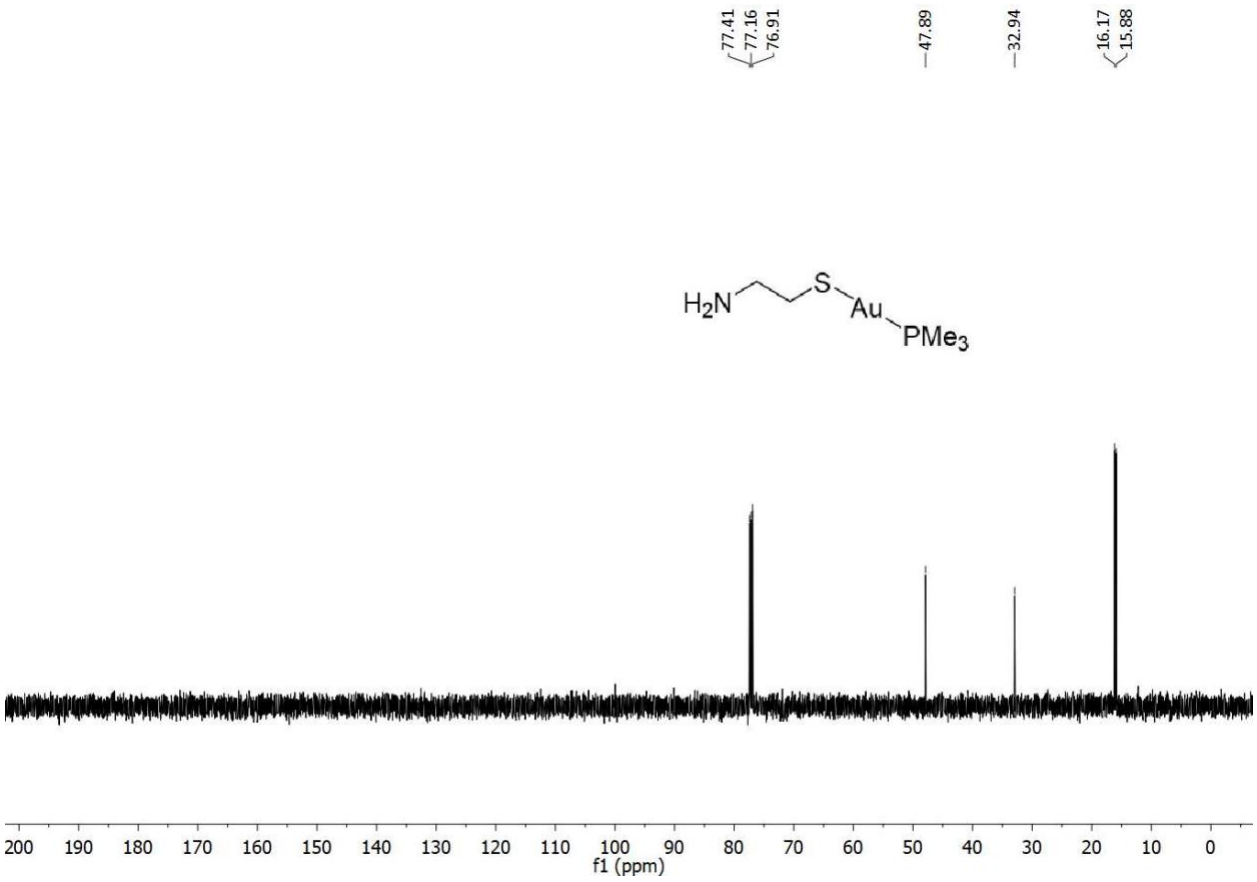

Figure A11. ^{13}C NMR spectrum of compound WB-19-HL4181 in $CDCl_3$.

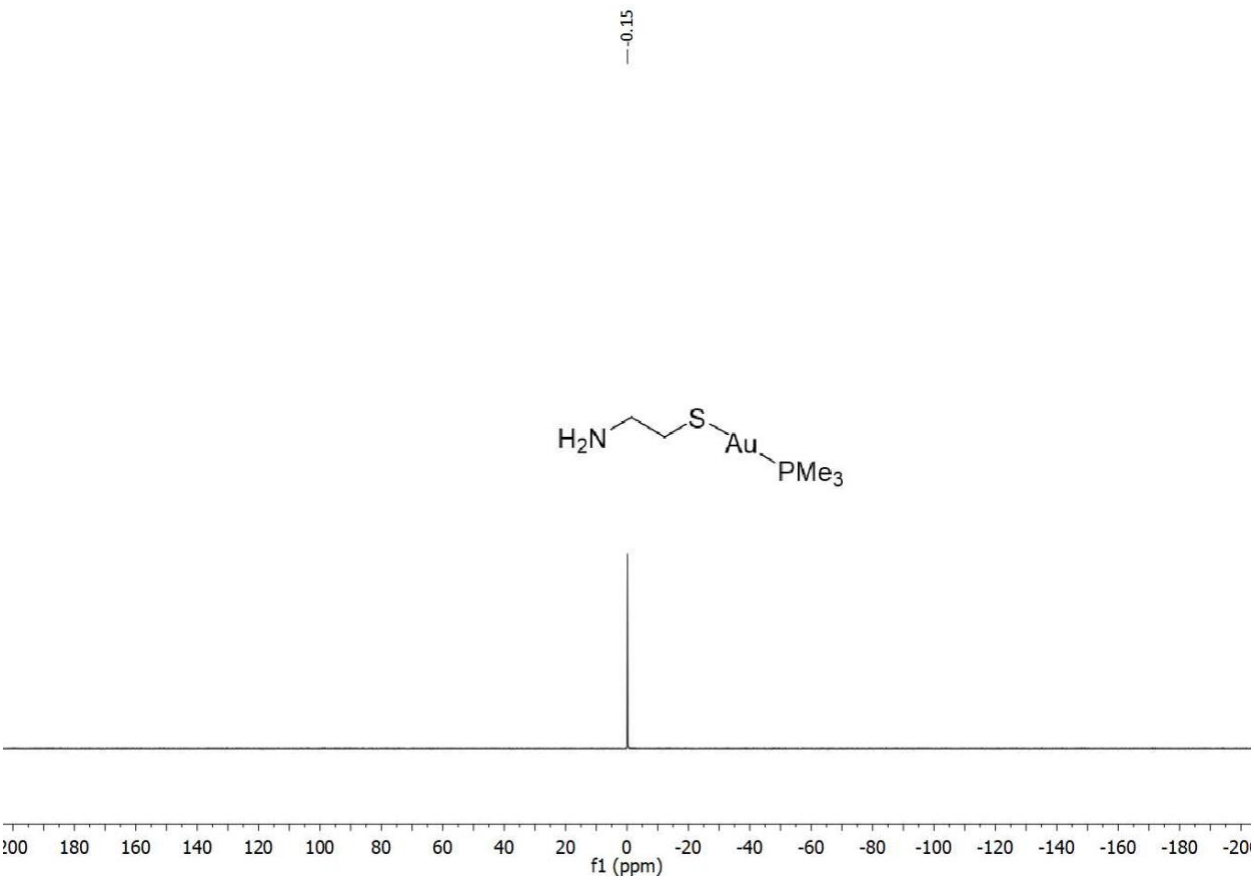

Figure A12. ^{31}P NMR spectrum of compound WB-19-HL4181 in $CDCl_3$.

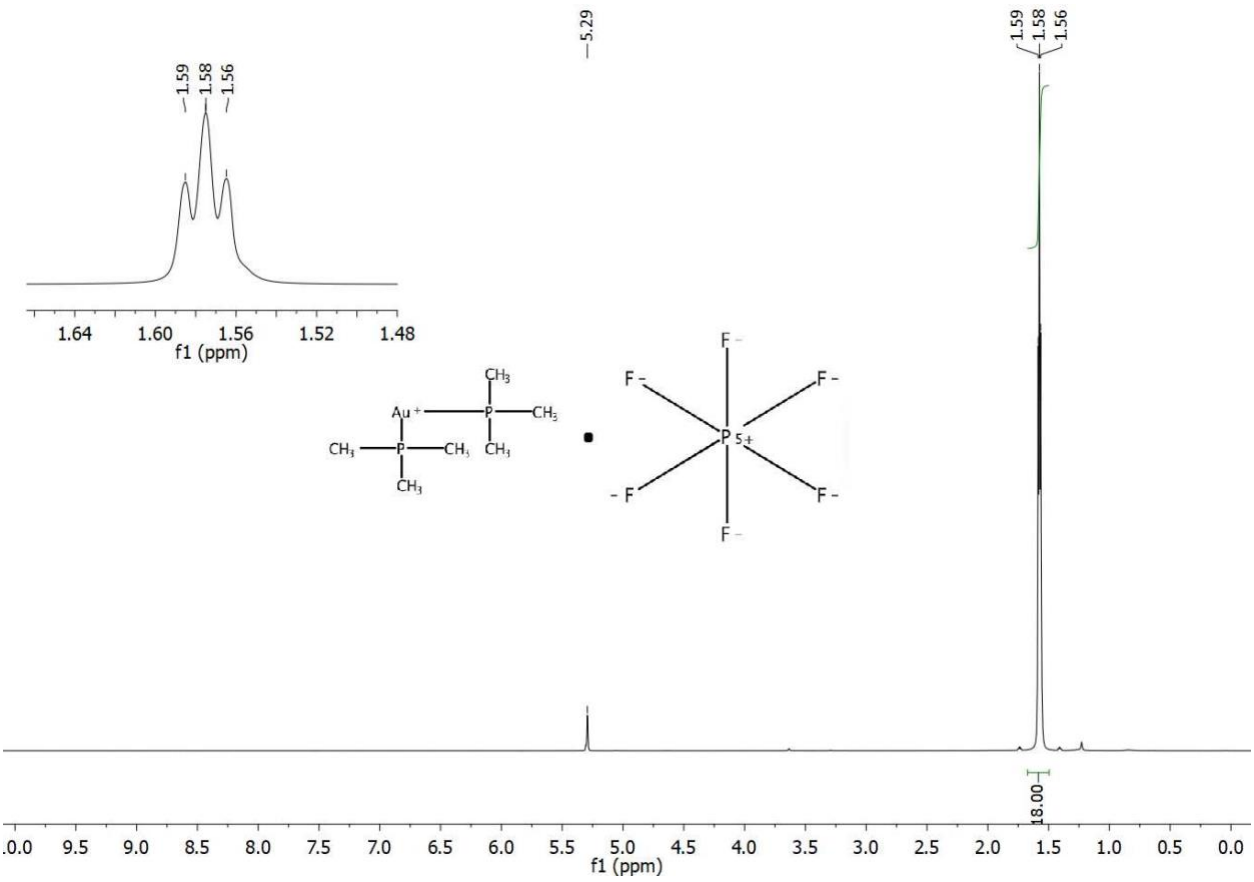

Figure A13. ^{1}H NMR spectrum of compound WB-19-HL4121a in CD_2Cl_2.

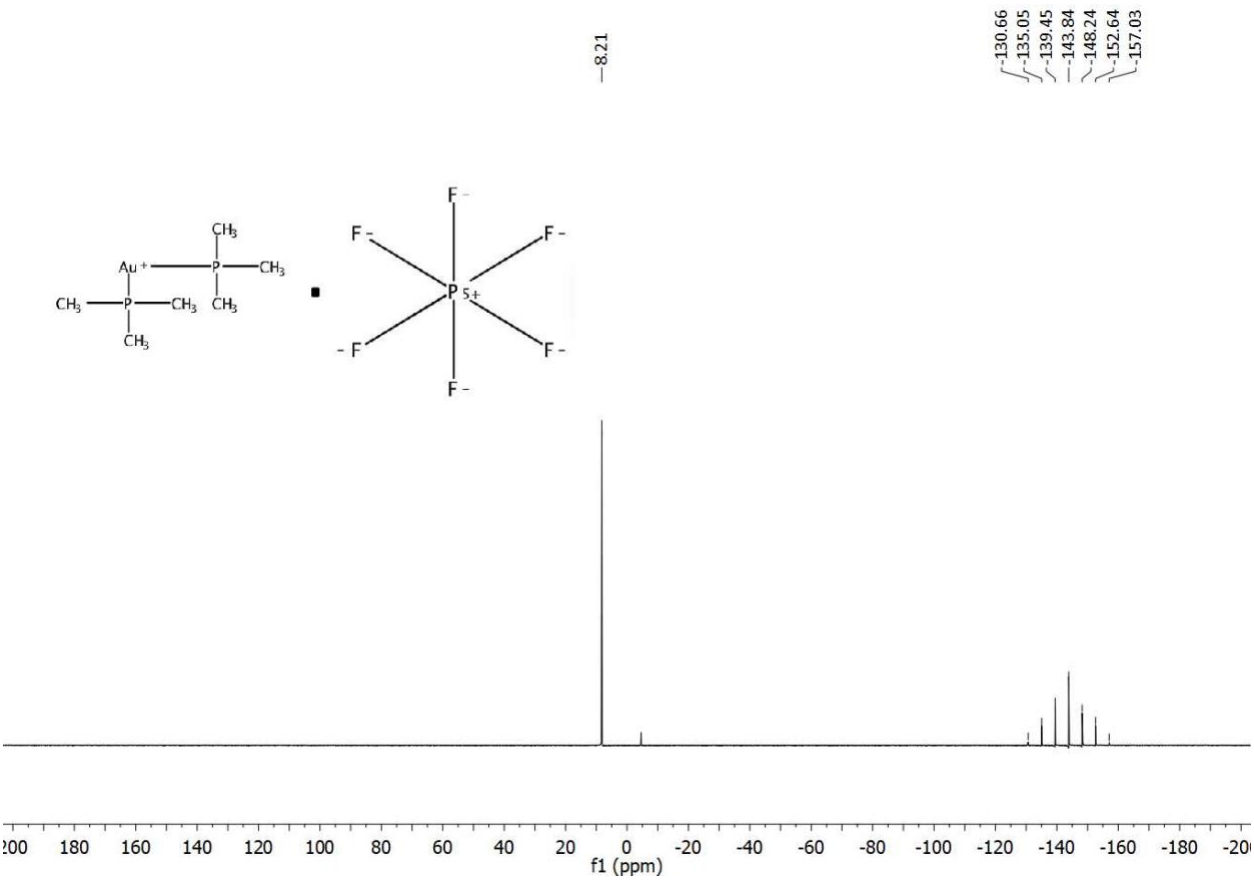

Figure A14. ^{31}P NMR spectrum of compound WB-19-HL4121a in CD_2Cl_2.

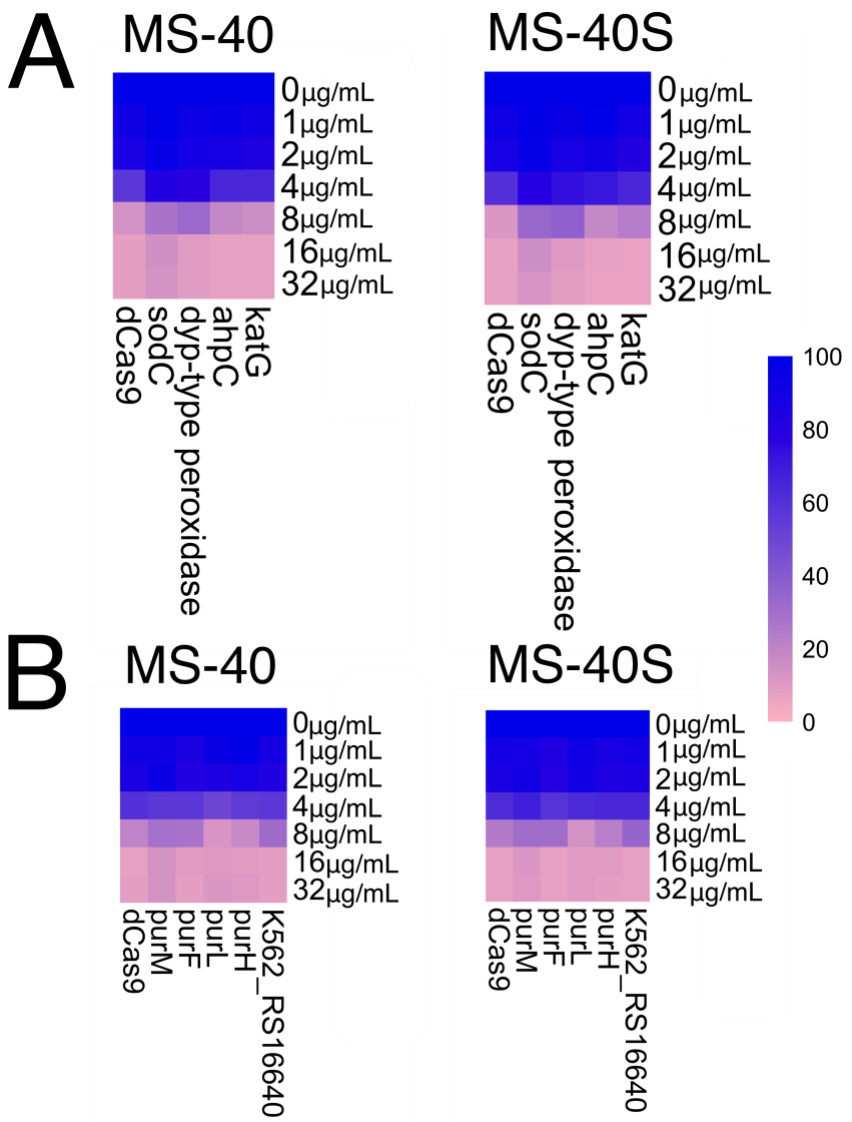

Figure A15. Susceptibility tests of CRISPRi mutants with MS-40 and MS-40S.

CRISPRi mutants of ROS related genes (**A**) and purine related genes (**B**) were exposed to a concentration gradient of MS-40 and MS-40S ranging from 32 µg/mL to 1 µg/mL in LB Tp100 and 30.5 mM rhamnose. Percent growth is shown with 100% being dark blue and 0% being pink.

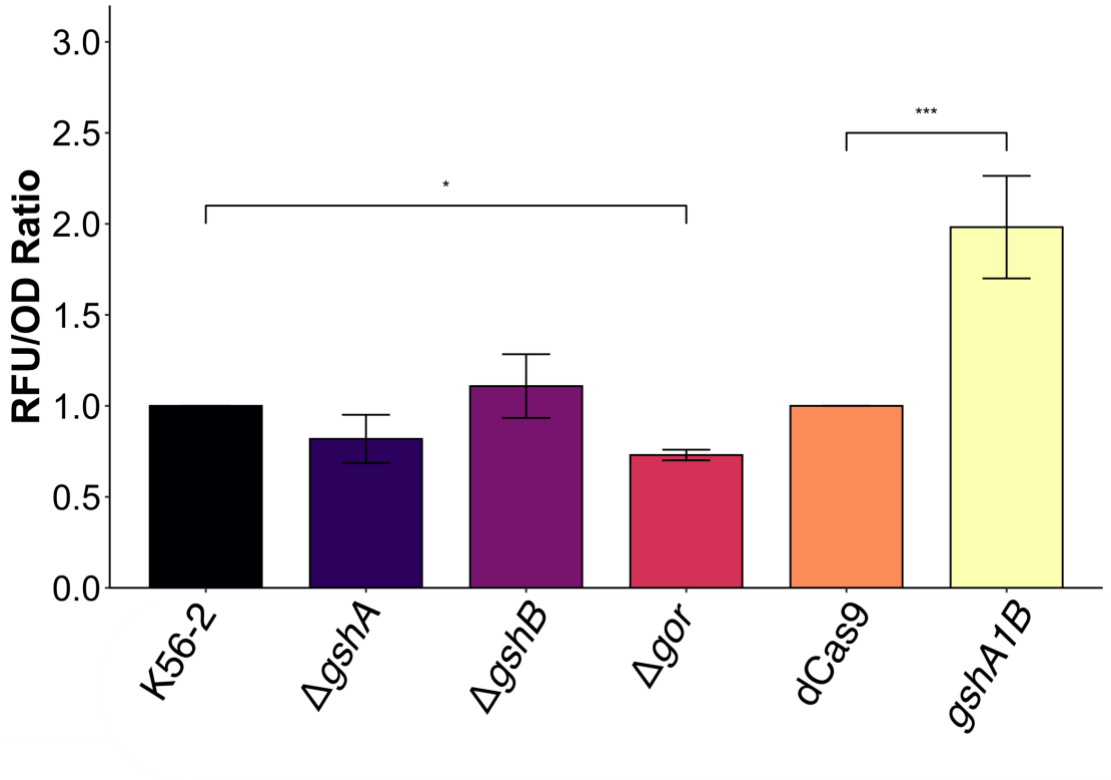

Figure A16. ROS detection of glutathione related mutants.

ROS detection of glutathione deletion mutants, Δ*gshA,* Δ*gshB,* and Δ*gor* and *gshA1B* CRISPRi mutant. Cells at a concentration of OD_{600nm} of 0.3 were incubated with H_2DCFDA for 45 mins at 37˚C. Fluorescence was measured on a synergy two plate reader with three biological replicates. * indicates $P < 0.05$ and *** indicates $P < 0.0001$ from a one-way ANOVA and Dunnett post-hoc.

REFERENCES

AbdelKhalek, A., Abutaleb, N.S., Elmagarmid, K.A., and Seleem, M.N. 2018. Repurposing auranofin as an intestinal decolonizing agent for vancomycin-resistant enterococci. Sci Rep **8**(1): 8353. doi:10.1038/s41598-018-26674-0.

Abellon-Ruiz, J. 2023. Forward or backward, that is the question: phospholipid trafficking by the Mla system. Emerging Topics in Life Sciences **7**(1): 125–135. doi:10.1042/ETLS20220087.

Amini, S., and Tavazoie, S. 2011. Antibiotics and the post-genome revolution. Curr.Opin.Microbiol. **14(5)**(Journal Article): 515–518. doi:10.1016/j.mib.2011.07.017.

Apontoweil, P., and Berends, W. 1975. Isolation and initial characterization of glutathione-deficient mutants of Escherichia coli K12. Biochem. Biophys. Acta **399**: 22.

Aslund, F., Ehn, B., Miranda-Vizuete, A., Pueyo, C., and Holmgren, A. 1994. Two additional glutaredoxins exist in Escherichia coli: glutaredoxin 3 is a hydrogen donor for ribonucleotide reductase in a thioredoxin/glutaredoxin 1 double mutant. Proc Natl Acad Sci U S A **91**(21): 9813–9817.

Aubert, D.F., Hamad, M.A., and Valvano, M.A. 2014. A markerless deletion method for genetic manipulation of *Burkholderia cenocepacia* and other multidrug-resistant gram-negative bacteria. Methods Mol Biol **1197**: 311–327. doi:10.1007/978-1-4939-1261-2_18.

Bahar, A.A., Liu, Z., Totsingan, F., Buitrago, C., Kallenbach, N., and Ren, D. 2015. Synthetic dendrimeric peptide active against biofilm and persister cells of Pseudomonas aeruginosa. Appl Microbiol Biotechnol **99**(19): 8125–8135. doi:10.1007/s00253-015-6645-7.

Bahia, M.S., Khazanov, N., Zhou, Q., Yang, Z., Wang, C., Hong, J.S., Rab, A., Sorscher, E.J., Brouillette, C.G., Hunt, J.F., and Senderowitz, H. 2021. Stability Prediction for Mutations in the Cytosolic Domains of Cystic Fibrosis Transmembrane Conductance Regulator. J. Chem. Inf. Model. **61**(4): 1762–1777. doi:10.1021/acs.jcim.0c01207.

Balwan, A., Nicolau, D.P., Wungwattana, M., Zuckerman, J.B., and Waters, V. 2016. Clinafloxacin for Treatment of Burkholderia cenocepacia Infection in a Cystic Fibrosis Patient. Antimicrob. Agents Chemother. **60**(1): 1–5. doi:10.1128/AAC.01428-15.

Bazzini, S., Udine, C., and Riccardi, G. 2011. Molecular approaches to pathogenesis study of *Burkholderia cenocepacia*, an important cystic fibrosis opportunistic bacterium. Appl Microbiol Biotechnol **92**(5): 887–895. doi:10.1007/s00253-011-3616-5.

Behjati, S., and Tarpey, P.S. 2013. What is next generation sequencing? Arch Dis Child Educ Pract Ed **98**(6): 236–238. doi:10.1136/archdischild-2013-304340.

Ben Fekih, I., Zhang, C., Li, Y.P., Zhao, Y., Alwathnani, H.A., Saquib, Q., Rensing, C., and Cervantes, C. 2018. Distribution of Arsenic Resistance Genes in Prokaryotes. Front. Microbiol. **9**: 2473. doi:10.3389/fmicb.2018.02473.

Benet, L.Z., Hosey, C.M., Ursu, O., and Oprea, T.I. 2016. BDDCS, the Rule of 5 and drugability. Advanced Drug Delivery Reviews **101**: 89–98. doi:10.1016/j.addr.2016.05.007.

Bernardy, E.E., Petit, R.A., Raghuram, V., Alexander, A.M., Read, T.D., and Goldberg, J.B. 2020. Genotypic and Phenotypic Diversity of *Staphylococcus aureus* Isolates from Cystic Fibrosis Patient Lung Infections and Their Interactions with Pseudomonas aeruginosa. mBio **11**(3): e00735-20. doi:10.1128/mBio.00735-20.

Berners-Price, S.J., and Filipovska, A. 2011. Gold compounds as therapeutic agents for human diseases. Metallomics **3**(9): 863. doi:10.1039/c1mt00062d.
Bernier, S.P., Son, S., and Surette, M.G. 2018. The Mla pathway plays an essential role in the intrinsic resistance of *Burkholderia cepacia* complex species to antimicrobials and host innate components. J Bacteriol **200**(18): e00156-18. doi:10.1128/JB.00156-18.
Besier, S., Smaczny, C., von Mallinckrodt, C., Krahl, A., Ackermann, H., Brade, V., and Wichelhaus, T.A. 2007. Prevalence and Clinical Significance of *Staphylococcus aureus* Small-Colony Variants in Cystic Fibrosis Lung Disease. J Clin Microbiol **45**(1): 168–172. doi:10.1128/JCM.01510-06.
Bhagirath, A.Y., Li, Y., Somayajula, D., Dadashi, M., Badr, S., and Duan, K. 2016. Cystic fibrosis lung environment and Pseudomonas aeruginosa infection. BMC Pulm Med **16**(1): 174. doi:10.1186/s12890-016-0339-5.
Brauner, A., Fridman, O., Gefen, O., and Balaban, N.Q. 2016. Distinguishing between resistance, tolerance and persistence to antibiotic treatment. Nat Rev Microbiol **14**(5): 320–330. doi:10.1038/nrmicro.2016.34.
Burkholder, W.H. 1950. Sour skin, a bacterial rot of onion bulbs. Phytopathology **40**: 115–117.
Burns, J.L., Emerson, J., Stapp, J.R., Yim, D.L., Krzewinski, J., Louden, L., Ramsey, B.W., and Clausen, C.R. 1998. Microbiology of Sputum from Patients at Cystic Fibrosis Centers in the United States. CLIN INFECT DIS **27**(1): 158–163. doi:10.1086/514631.
Buroni, S., Pasca, M.R., Flannagan, R.S., Bazzini, S., Milano, A., Bertani, I., Venturi, V., Valvano, M.A., and Riccardi, G. 2009. Assessment of three Resistance-Nodulation-Cell Division drug efflux transporters of *Burkholderia cenocepacia* in intrinsic antibiotic resistance. BMC Microbiol. **9**: 200. doi:10.1186/1471-2180-9-200.
Cao, Y., Fanning, S., Proos, S., Jordan, K., and Srikumar, S. 2017. A Review on the Applications of Next Generation Sequencing Technologies as Applied to Food-Related Microbiome Studies. Front. Microbiol. **8**: 1829. doi:10.3389/fmicb.2017.01829.
Cardona, S.T., Selin, C., and Gislason, A.S. 2015. Genomic tools to profile antibiotic mode of action. Critical reviews in microbiology **4**: 465–472. doi:10.3109/1040841X.2013.866073.
Carmel-Harel, O., and Storz, G. 2000. Roles of the Glutathione- and Thioredoxin-Dependent Reduction Systems in the *Escherichia Coli* and *Saccharomyces Cerevisiae* Responses to Oxidative Stress. Annu. Rev. Microbiol. **54**(1): 439–461. doi:10.1146/annurev.micro.54.1.439.
Carney, D.A. 2008. Arsenic trioxide mechanisms of action – looking beyond acute promyelocytic leukemia. Leukemia & Lymphoma **49**(10): 1846–1851. doi:10.1080/10428190802464745.
Case, J.P. 2001. Old and New Drugs Used in Rheumatoid Arthritis. Am. J. Ther. **8**(2): 123–143.
Chalmers, J.D., van Ingen, J., van der Laan, R., and Herrmann, J.-L. 2021. Liposomal drug delivery to manage nontuberculous mycobacterial pulmonary disease and other chronic lung infections. Eur Respir Rev **30**(161): 210010. doi:10.1183/16000617.0010-2021.
Cheng, S.H., Gregory, R.J., Marshall, J., Paul, S., Souza, D.W., White, G.A., O'Riordan, C.R., and Smith, A.E. 1990. Defective intracellular transport and processing of CFTR is the molecular basis of most cystic fibrosis. Cell **63**(4): 827–834. doi:10.1016/0092-8674(90)90148-8.
Chong, P.A., Farber, P.J., Vernon, R.M., Hudson, R.P., Mittermaier, A.K., and Forman-Kay, J.D. 2015. Deletion of Phenylalanine 508 in the First Nucleotide-binding Domain of the

Cystic Fibrosis Transmembrane Conductance Regulator Increases Conformational Exchange and Inhibits Dimerization. Journal of Biological Chemistry **290**(38): 22862–22878. doi:10.1074/jbc.M115.641134.

Chua, S.M., and Fraser, J.A. 2020. Surveying purine biosynthesis across the domains of life unveils promising drug targets in pathogens. Immunol Cell Biol **98**(10): 819–831. doi:10.1111/imcb.12389.

Clinical and Laboratory Standards Institute CLSI. 2003. Susceptibility testing of mycobacteria, nocardiae, and other aerobic actinomycetes; approved standard. CLSI, Pennsylvania, USA.

Coenye, T., Vandamme, P., Govan, J.R.W., and LiPuma, J.J. 2001. Taxonomy and identification of the *Burkholderia cepacia* complex. J.Clin.Microbiol. **39**(10): 3427-3436.

Corona, F., and Martinez, J. 2013. Phenotypic Resistance to Antibiotics. Antibiotics **2**(2): 237–255. doi:10.3390/antibiotics2020237.

Corriveau, S., Sykes, J., and Stephenson, A.L. 2018. Cystic fibrosis survival: the changing epidemiology. Current Opinion in Pulmonary Medicine **24**(6): 574–578. doi:10.1097/MCP.0000000000000520.

Couto, N., Wood, J., and Barber, J. 2016. The role of glutathione reductase and related enzymes on cellular redox homoeostasis network. Free Radical Biology and Medicine **95**: 27–42. doi:10.1016/j.freeradbiomed.2016.02.028.

Coward, C., Dharmalingham, G., Abdulle, O., Avis, T., Beisken, S., Breidenstein, E., Carli, N., Figueiredo, L., Jones, D., Khan, N., Malara, S., Martins, J., Nagalingam, N., Turner, K., Wain, J., Williams, D., Powell, D., and Mason, C. 2020. High-density transposon libraries utilising outward-oriented promoters identify mechanisms of action and resistance to antimicrobials. FEMS Microbiology Letters **367**(22): fnaa185. doi:10.1093/femsle/fnaa185.

Cribbs, S.K., and Beck, J.M. 2017. Microbiome in the pathogenesis of cystic fibrosis and lung transplant-related disease. Translational Research **179**: 84–96. doi:10.1016/j.trsl.2016.07.022.

Cruz, L., Lopes, L., de Camargo Ribeiro, F., de Sá, N., Lino, C., Tharmalingam, N., de Oliveira, R., Rosa, C., Mylonakis, E., Fuchs, B., and Johann, S. 2018. Anti-Candida albicans Activity of Thiazolylhydrazone Derivatives in Invertebrate and Murine Models. JoF **4**(4): 134. doi:10.3390/jof4040134.

Cumming, R.C., Andon, N.L., Haynes, P.A., Park, M., Fischer, W.H., and Schubert, D. 2004. Protein Disulfide Bond Formation in the Cytoplasm during Oxidative Stress. Journal of Biological Chemistry **279**(21): 21749–21758. doi:10.1074/jbc.M312267200.

Dalle-Donne, I., Rossi, R., Colombo, G., Giustarini, D., and Milzani, A. 2009. Protein S-glutathionylation: a regulatory device from bacteria to humans. Trends in Biochemical Sciences **34**(2): 85–96. doi:10.1016/j.tibs.2008.11.002.

Darling, P., Chan, M., Cox, A.D., and Sokol, P.A. 1998. Siderophore production by cystic fibrosis isolates of *Burkholderia cepacia*. Infection and immunity **66**(2): 874–877.

De Soyza, A., Meachery, G., Hester, K.L.M., Nicholson, A., Parry, G., Tocewicz, K., Pillay, T., Clark, S., Lordan, J.L., Schueler, S., Fisher, A.J., Dark, J.H., Gould, F.K., and Corris, P.A. 2010. Lung transplantation for patients with cystic fibrosis and Burkholderia cepacia complex infection: A single-center experience. The Journal of Heart and Lung Transplantation **29**(12): 1395–1404. doi:10.1016/j.healun.2010.06.007.

Dupont, L. 2017. Lung transplantation in cystic fibrosis patients with difficult to treat lung infections. Curr Opin Pulm Med. doi:10.1097/MCP.0000000000000431.

Durão, P., Balbontín, R., and Gordo, I. 2018. Evolutionary Mechanisms Shaping the Maintenance of Antibiotic Resistance. Trends in Microbiology **26**(8): 677–691. doi:10.1016/j.tim.2018.01.005.

Eberl, L., and Vandamme, P. 2016. Members of the genus *Burkholderia*: good and bad guys. F1000Res **5**: 1007. doi:10.12688/f1000research.8221.1.

Edwards, B.D., Somayaji, R., Greysson-Wong, J., Izydorczyk, C., Waddell, B., Storey, D.G., Rabin, H.R., Surette, M.G., and Parkins, M.D. 2020. Clinical Outcomes Associated With Escherichia coli Infections in Adults With Cystic Fibrosis: A Cohort Study. Open Forum Infectious Diseases **7**(1): ofz476. doi:10.1093/ofid/ofz476.

Eichhorn, E., van der Ploeg, J.R., and Leisinger, T. 1999. Characterization of a Two-component Alkanesulfonate Monooxygenase from Escherichia coli. Journal of Biological Chemistry **274**(38): 26639–26646. doi:10.1074/jbc.274.38.26639.

Elborn, J.S. 2016. Cystic fibrosis. The Lancet **388**(10059): 2519–2531. doi:10.1016/S0140-6736(16)00576-6.

El-Halfawy, O.M., Naguib, M.M., and Valvano, M.A. 2017. Novel antibiotic combinations proposed for treatment of *Burkholderia cepacia* complex infections. Antimicrob Resist Infect Control **6**(1): 120. doi:10.1186/s13756-017-0279-8.

El-Halfawy, O.M., and Valvano, M.A. 2014. Putrescine reduces antibiotic-induced oxidative stress as a mechanism of modulation of antibiotic resistance in *Burkholderia cenocepacia*. Antimicrob. Agents Chemother. **58**(7): 4162–4171. doi:10.1128/AAC.02649-14.

El-Laboudi, A.H., Etherington, C., Whitaker, P., Clifton, I.J., Conway, S.P., Denton, M., and Peckham, D.G. 2009. Acute Burkholderia cenocepacia pyomyositis in a patient with cystic fibrosis. Journal of Cystic Fibrosis **8**(4): 273–275. doi:10.1016/j.jcf.2009.04.007.

Epstein, T.D., Wu, B., Moulton, K.D., Yan, M., and Dube, D.H. 2019. Sugar-Modified Analogs of Auranofin Are Potent Inhibitors of the Gastric Pathogen *Helicobacter pylori*. ACS Infect. Dis. **5**(10): 1682–1687. doi:10.1021/acsinfecdis.9b00251.

Ezelarab, H.A.A., Abbas, S.H., Hassan, H.A., and Abuo-Rahma, G.E.-D.A. 2018. Recent updates of fluoroquinolones as antibacterial agents. Arch. Pharm. Chem. Life Sci. **351**(9): e1800141. doi:10.1002/ardp.201800141.

Ezraty, B., Gennaris, A., Barras, F., and Collet, J.-F. 2017. Oxidative stress, protein damage and repair in bacteria. Nat Rev Microbiol **15**(7): 385–396. doi:10.1038/nrmicro.2017.26.

Fàbrega, A., Madurga, S., Giralt, E., and Vila, J. 2009. Mechanism of action of and resistance to quinolones: Mechanism of action of and resistance to quinolones. Microbial Biotechnology **2**(1): 40–61. doi:10.1111/j.1751-7915.2008.00063.x.

Ferroni, A., Guillemot, D., Moumile, K., Bernede, C., Le Bourgeois, M., Waernessyckle, S., Descamps, P., Sermet-Gaudelus, I., Lenoir, G., Berche, P., and Taddei, F. 2009. Effect of mutator *P. aeruginosa* on antibiotic resistance acquisition and respiratory function in cystic fibrosis. Pediatr. Pulmonol. **44**(8): 820–825. doi:10.1002/ppul.21076.

Fields, F.R., Lee, S.W., and McConnell, M.J. 2016. Using bacterial genomes and essential genes for the development of new antibiotics. Biochemical pharmacology. doi:S0006-2952(16)30463-4 [pii].

Flannagan, R.S., Linn, T., and Valvano, M.A. 2008. A system for the construction of targeted unmarked gene deletions in the genus *Burkholderia*. Environmental microbiology **10**(6): 1652–1660. doi:10.1111/j.1462-2920.2008.01576.x.

Flórez, L.V., and Kaltenpoth, M. 2017. Symbiont dynamics and strain diversity in the defensive mutualism between *Lagria* beetles and *Burkholderia*: Prevalence of *Burkholderia* symbionts in *Lagria* beetles. Environ Microbiol **19**(9): 3674–3688. doi:10.1111/1462-2920.13868.

Flórez, L.V., Scherlach, K., Gaube, P., Ross, C., Sitte, E., Hermes, C., Rodrigues, A., Hertweck, C., and Kaltenpoth, M. 2017. Antibiotic-producing symbionts dynamically transition between plant pathogenicity and insect-defensive mutualism. Nat Commun **8**(1): 15172. doi:10.1038/ncomms15172.

Gallagher, L.A., Shendure, J., and Manoil, C. 2011. Genome-scale identification of resistance functions in *Pseudomonas aeruginosa* using Tn-seq. MBio **2**(1): e00315-10. doi:10.1128/mBio.00315-10.

Gawronski, J.D., Wong, S.M.S., Giannoukos, G., Ward, D.V., and Akerley, B.J. 2009. Tracking insertion mutants within libraries by deep sequencing and a genome-wide screen for *Haemophilus* genes required in the lung. PNAS **106**(38): 16422–16427. National Academy of Sciences. doi:10.1073/pnas.0906627106.

Geisinger, E., Mortman, N.J., Dai, Y., Cokol, M., Syal, S., Farinha, A., Fisher, D.G., Tang, A.Y., Lazinski, D.W., Wood, S., Anthony, J., van Opijnen, T., and Isberg, R.R. 2020. Antibiotic susceptibility signatures identify potential antimicrobial targets in the *Acinetobacter baumannii* cell envelope. Nature Communications **11**(1): 4522. Nature Publishing Group. doi:10.1038/s41467-020-18301-2.

Geisinger, E., Vargas-Cuebas, G., Mortman, N.J., Syal, S., Dai, Y., Wainwright, E.L., Lazinski, D., Wood, S., Zhu, Z., Anthony, J., Opijnen, T. van, and Isberg, R.R. 2019. The landscape of phenotypic and transcriptional responses to ciprofloxacin in *Acinetobacter baumannii*: acquired resistance alleles modulate drug-induced SOS response and prophage replication. mBio **10**(3): e01127-19. American Society for Microbiology. doi:10.1128/mBio.01127-19.

Gilchrist, F.J., Webb, A.K., Bright-Thomas, R.J., and Jones, A.M. 2012. Successful treatment of cepacia syndrome with a combination of intravenous cyclosporin, antibiotics and oral corticosteroids. Journal of cystic fibrosis : official journal of the European Cystic Fibrosis Society **11**(5): 458–460. doi:10.1016/j.jcf.2012.04.002 [doi].

Gislason, A.S., Turner, K., Domaratzki, M., and Cardona, S.T. 2017. Comparative analysis of the *Burkholderia cenocepacia* K56-2 essential genome reveals cell envelope functions that are uniquely required for survival in species of the genus *Burkholderia*. Microb Genom **3**(11): e000140. doi:10.1099/mgen.0.000140.

Goerke, C., and Wolz, C. 2010. Adaptation of *Staphylococcus aureus* to the cystic fibrosis lung. International Journal of Medical Microbiology **300**(8): 520–525. doi:10.1016/j.ijmm.2010.08.003.

Goodman, A.L., McNulty, N.P., Zhao, Y., Leip, D., Mitra, R.D., Lozupone, C.A., Knight, R., and Gordon, J.I. 2009. Identifying genetic determinants needed to establish a human gut symbiont in its habitat. Cell host & microbe **6**(3): 279–289. doi:10.1016/j.chom.2009.08.003.

Grossman, T.H. 2016. Tetracycline Antibiotics and Resistance. Cold Spring Harb Perspect Med **6**(4): a025387. doi:10.1101/cshperspect.a025387.

Guglierame, P., Pasca, M.R., Rossi, E.D., Buroni, S., Arrigo, P., Manina, G., and Riccardi, G. 2006. Efflux pump genes of the resistance-nodulation-division family in *Burkholderia cenocepacia* genome. BMC microbiology **6**: 66. doi:10.1186/1471-2180-6-66.

Hainfeld, J.F., Liu, W., and Barcena, M. 1999. Gold-ATP. J. Struct. Biol. **127**: 120–134.

Hamad, M.A., Skeldon, A.M., and Valvano, M.A. 2010. Construction of aminoglycoside-sensitive *Burkholderia cenocepacia* strains for use in studies of intracellular bacteria with the gentamicin protection assay. Applied and Environmental Microbiology **76**(10): 3170–3176. doi:10.1128/AEM.03024-09.

Harbut, M.B., Vilchèze, C., Luo, X., Hensler, M.E., Guo, H., Yang, B., Chatterjee, A.K., Nizet, V., Jacobs, W.R., Schultz, P.G., and Wang, F. 2015. Auranofin exerts broad-spectrum bactericidal activities by targeting thiol-redox homeostasis. Proc. Natl. Acad. Sci. U.S.A. **112**(14): 4453–4458. doi:10.1073/pnas.1504022112.

Hoeksema, M., Brul, S., and Ter Kuile, B.H. 2018. Influence of Reactive Oxygen Species on De Novo Acquisition of Resistance to Bactericidal Antibiotics. Antimicrob Agents Chemother **62**(6). doi:10.1128/AAC.02354-17.

Hogan, A.M., Rahman, A.S.M.Z., Lightly, T.J., and Cardona, S.T. 2019. A broad-host-range CRISPRi toolkit for silencing gene expression in *Burkholderia*. ACS Synth. Biol. **8**(10): 2372–2384. doi:10.1021/acssynbio.9b00232.

Hogan, A.M., Rahman, A.S.M.Z., Motnenko, A., Natarajan, A., Maydaniuk, D.T., León, B., Batun, Z., Palacios, A., Bosch, A., and Cardona, S.T. 2023. Profiling cell envelope-antibiotic interactions reveals vulnerabilities to β-lactams in a multidrug-resistant bacterium. Nat Commun **14**(1): 4815. Nature Publishing Group. doi:10.1038/s41467-023-40494-5.

Hogan, A.M., Scoffone, V.C., Makarov, V., Gislason, A.S., Tesfu, H., Stietz, M.S., Brassinga, A.K.C., Domaratzki, M., Li, X., Azzalin, A., Biggiogera, M., Riabova, O., Monakhova, N., Chiarelli, L.R., Riccardi, G., Buroni, S., and Cardona, S.T. 2018. Competitive fitness of essential gene knockdowns reveals a broad-spectrum antibacterial inhibitor of the cell division protein FtsZ. Antimicrob Agents Chemother **62**(12): e01231-18. doi:10.1128/AAC.01231-18.

Holden, M.T., Seth-Smith, H.M., Crossman, L.C., Sebaihia, M., Bentley, S.D., Cerdeno-Tarraga, A.M., Thomson, N.R., Bason, N., Quail, M.A., Sharp, S., Cherevach, I., Churcher, C., Goodhead, I., Hauser, H., Holroyd, N., Mungall, K., Scott, P., Walker, D., White, B., Rose, H., Iversen, P., Mil-Homens, D., Rocha, E.P., Fialho, A.M., Baldwin, A., Dowson, C., Barrell, B.G., Govan, J.R., Vandamme, P., Hart, C.A., Mahenthiralingam, E., and Parkhill, J. 2009. The genome of *Burkholderia cenocepacia* J2315, an epidemic pathogen of cystic fibrosis patients. Journal of Bacteriology **191**(1): 261–277. doi:10.1128/JB.01230-08.

Horcajada, J.P., Montero, M., Oliver, A., Sorlí, L., Luque, S., Gómez-Zorrilla, S., Benito, N., and Grau, S. 2019. Epidemiology and Treatment of Multidrug-Resistant and Extensively Drug-Resistant *Pseudomonas aeruginosa* Infections. Clin Microbiol Reviews **32**(4): e00031-19, /cmr/32/4/CMR.00031-19.atom. doi:10.1128/CMR.00031-19.

Huang, Y.J., and LiPuma, J.J. 2016. The Microbiome in Cystic Fibrosis. Clinics in Chest Medicine **37**(1): 59–67. doi:10.1016/j.ccm.2015.10.003.

Hughes, D., and Andersson, D.I. 2017. Evolutionary Trajectories to Antibiotic Resistance. Annu. Rev. Microbiol. **71**(1): 579–596. doi:10.1146/annurev-micro-090816-093813.

Huse, H.K., Lee, M.J., Wootton, M., Sharp, S.E., Traczewski, M., LiPuma, J.J., and Jorth, P. 2021. Evaluation of antimicrobial susceptibility testing methods for *Burkholderia cenocepacia* and *Burkholderia multivorans* isolates from cystic fibrosis patients. J Clin Microbiol **59**(12): e0144721. doi:10.1128/JCM.01447-21.

Hwang, J., and Kim, H.S. 2015. Cell Wall Recycling-Linked Coregulation of AmpC and PenB β-Lactamases through *ampD* Mutations in Burkholderia cenocepacia. Antimicrob. Agents Chemother. **59**(12): 7602–7610. doi:10.1128/AAC.01068-15.

Imlay, J.A. 2003. Pathways of Oxidative Damage. Annu. Rev. Microbiol. **57**(1): 395–418. Annual Reviews. doi:10.1146/annurev.micro.57.030502.090938.

Imlay, J.A. 2008. Cellular Defenses against Superoxide and Hydrogen Peroxide. Annu. Rev. Biochem. **77**(1): 755–776. doi:10.1146/annurev.biochem.77.061606.161055.

Imlay, J.A. 2015. Transcription Factors That Defend Bacteria Against Reactive Oxygen Species. Annu. Rev. Microbiol. **69**(1): 93–108. doi:10.1146/annurev-micro-091014-104322.

Infield, D.T., Strickland, K.M., Gaggar, A., and McCarty, N.A. 2021. The molecular evolution of function in the CFTR chloride channel. Journal of General Physiology **153**(12): e202012625. doi:10.1085/jgp.202012625.

Kahl, B.C. 2010. Impact of Staphylococcus aureus on the pathogenesis of chronic cystic fibrosis lung disease. International Journal of Medical Microbiology **300**(8): 514–519. doi:10.1016/j.ijmm.2010.08.002.

Kaltenpoth, M., and Flórez, L.V. 2020. Versatile and Dynamic Symbioses Between Insects and *Burkholderia* Bacteria. Annu. Rev. Entomol. **65**(1): 145–170. doi:10.1146/annurev-ento-011019-025025.

Kaplan, E., Greene, N.P., Crow, A., and Koronakis, V. 2018. Insights into bacterial lipoprotein trafficking from a structure of LolA bound to the LolC periplasmic domain. Proc Natl Acad Sci USA **115**(31): E7389–E7397. doi:10.1073/pnas.1806822115.

Karp, P.D., Billington, R., Caspi, R., Fulcher, C.A., Latendresse, M., Kothari, A., Keseler, I.M., Krummenacker, M., Midford, P.E., Ong, Q., Ong, W.K., Paley, S.M., and Subhraveti, P. 2019. The BioCyc collection of microbial genomes and metabolic pathways. Brief Bioinform **20**(4): 1085–1093. Oxford Academic. doi:10.1093/bib/bbx085.

Kean, W.F., Hart, L., and Buchanan, W.W. 1997. Auranofin. Br J Rheumatol **36**: 560–572.

Kedrowski, B.L., Gutow, J.H., Stock, G., Smith, M., Jordan, C., and Masterson, D.S. 2014. Glutathione reductase activity with an oxidized methylated glutathione analog. Journal of Enzyme Inhibition and Medicinal Chemistry **29**(4): 491–494. doi:10.3109/14756366.2013.805757.

Keith, K.E., and Valvano, M.A. 2007. Characterization of SodC, a periplasmic superoxide dismutase from *Burkholderia cenocepacia*. Infection and immunity **75**(5): 2451–2460. doi:10.1128/IAI.01556-06.

Kikuchi, Y., and Fukatsu, T. 2014. Live imaging of symbiosis: spatiotemporal infection dynamics of a GFP -labelled *B urkholderia* symbiont in the bean bug *R iptortus pedestris* . Molecular Ecology **23**(6): 1445–1456. doi:10.1111/mec.12479.

Kikuchi, Y., and Yumoto, I. 2013. Efficient Colonization of the Bean Bug Riptortus pedestris by an Environmentally Transmitted Burkholderia Symbiont. Appl Environ Microbiol **79**(6): 2088–2091. doi:10.1128/AEM.03299-12.

Kitt, H., Lenney, W., and Gilchrist, F.J. 2016. Two case reports of the successful eradication of new isolates of *Burkholderia cepacia* complex in children with cystic fibrosis. BMC pharmacology & toxicology **17**: 14-016-0054–0. doi:10.1186/s40360-016-0054-0 [doi].

Kohanski, M.A., Dwyer, D.J., and Collins, J.J. 2010. How antibiotics kill bacteria: from targets to networks. Nat.Rev.Microbiol. **8**(6): 423–435. doi:10.1038/nrmicro2333.

Kohanski, M.A., Dwyer, D.J., Hayete, B., Lawrence, C.A., and Collins, J.J. 2007. A common mechanism of cellular death induced by bactericidal antibiotics. Cell **130**(5): 797–810. doi:10.1016/j.cell.2007.06.049.

Kumar, N., Su, C.-C., Chou, T.-H., Radhakrishnan, A., Delmar, J.A., Rajashankar, K.R., and Yu, E.W. 2017. Crystal structures of the *Burkholderia multivorans* hopanoid transporter HpnN. Proc. Natl. Acad. Sci. U.S.A. **114**(25): 6557–6562. doi:10.1073/pnas.1619660114.

Kwon, Y.M., Ricke, S.C., and Mandal, R.K. 2016. Transposon sequencing: methods and expanding applications. Appl Microbiol Biotechnol **100**(1): 31–43. doi:10.1007/s00253-015-7037-8.

Lazarus, J.E., Warr, A.R., Westervelt, K.A., Hooper, D.C., and Waldor, M.K. 2021. A genome-scale antibiotic screen in *Serratia marcescens* identifies YdgH as a conserved modifier of cephalosporin and detergent susceptibility. Antimicrob Agents Chemother **65**(12): e0078621. doi:10.1128/AAC.00786-21.

Leitao, J.H., Sousa, S.A., Cunha, M.V., Salgado, M.J., Melo-Cristino, J., Barreto, M.C., and Sa-Correia, I. 2008. Variation of the antimicrobial susceptibility profiles of *Burkholderia cepacia* complex clonal isolates obtained from chronically infected cystic fibrosis patients: a five-year survey in the major Portuguese treatment center. European journal of clinical microbiology & infectious diseases : official publication of the European Society of Clinical Microbiology **27**(11): 1101–1111. doi:10.1007/s10096-008-0552-0; 10.1007/s10096-008-0552-0.

Lepuschitz, S., Weinmaier, T., Mrazek, K., Beisken, S., Weinberger, J., and Posch, A.E. 2020. Analytical Performance Validation of Next-Generation Sequencing Based Clinical Microbiology Assays Using a K-mer Analysis Workflow. Front. Microbiol. **11**: 1883. doi:10.3389/fmicb.2020.01883.

Lesniak, J. 2002. Structural and functional characterization of the Pseudomonas hydroperoxide resistance protein Ohr. The EMBO Journal **21**(24): 6649–6659. doi:10.1093/emboj/cdf670.

Liao, X., Yang, F., Li, H., So, P.-K., Yao, Z., Xia, W., and Sun, H. 2017. Targeting the Thioredoxin Reductase–Thioredoxin System from *Staphylococcus aureus* by Silver Ions. Inorg. Chem. **56**(24): 14823–14830. doi:10.1021/acs.inorgchem.7b01904.

LiPuma, J.J. 2010. The Changing Microbial Epidemiology in Cystic Fibrosis. Clin Microbiol Rev **23**(2): 299–323. doi:10.1128/CMR.00068-09.

Liu, Y., Lu, Y., Xu, Z., Ma, X., Chen, X., and Liu, W. 2022. Repurposing of the gold drug auranofin and a review of its derivatives as antibacterial therapeutics. Drug Discovery Today: S1359644622000691. doi:10.1016/j.drudis.2022.02.010.

Loewen, P.C. 1979. Levels of glutathione in *Escherichia coli*. Can. J. Biochem **57**: 107–111.

Los-Arcos, I., Len, O., Martín-Gómez, M.T., González-López, J.J., Saéz-Giménez, B., Deu, M., Nuvials, X., Ferrer, R., Román, A., and Gavaldà, J. 2019. Lung transplantation in two cystic fibrosis patients infected with previously pandrug-resistant Burkholderia cepacia complex treated with ceftazidime–avibactam. Infection **47**(2): 289–292. doi:10.1007/s15010-018-1261-y.

Loutet, S. 2011. Extreme antimicrobial peptide and polymyxin B resistance in the genus *Burkholderia*. Front. Cell. Inf. Microbio. **1**. doi:10.3389/fcimb.2011.00006.

Loutet, S.A., Flannagan, R.S., Kooi, C., Sokol, P.A., and Valvano, M.A. 2006. A complete lipopolysaccharide inner core oligosaccharide is required for resistance of *Burkholderia cenocepacia* to antimicrobial peptides and bacterial survival *in vivo*. Journal of Bacteriology **188**(6): 2073–2080. doi:188/6/2073 [pii]; 10.1128/JB.188.6.2073-2080.2006 [doi].

Lu, J., and Holmgren, A. 2014. The thioredoxin antioxidant system. Free Radical Biology and Medicine **66**: 75–87. doi:10.1016/j.freeradbiomed.2013.07.036.

Lu, J., Vlamis-Gardikas, A., Kandasamy, K., Zhao, R., Gustafsson, T.N., Engstrand, L., Hoffner, S., Engman, L., and Holmgren, A. 2013. Inhibition of bacterial thioredoxin reductase: an antibiotic mechanism targeting bacteria lacking glutathione. FASEB j. **27**(4): 1394–1403. doi:10.1096/fj.12-223305.

Mahenthiralingam, E., Urban, T.A., and Goldberg, J.B. 2005. The multifarious, multireplicon *Burkholderia cepacia* complex. Nature Reviews Microbiology **3**(2): 144–156.

Malhotra, S., Hayes, D., and Wozniak, D.J. 2019. Cystic Fibrosis and Pseudomonas aeruginosa: the Host-Microbe Interface. Clin Microbiol Rev **32**(3): e00138-18. doi:10.1128/CMR.00138-18.

Massip, C., Mathieu, C., Gaudru, C., Miaut, V., Floch, P., Oswald, E., Segonds, C., and Guet-Revillet, H. 2019. *In vitro* activity of seven β-lactams including ceftolozane/tazobactam and ceftazidime/avibactam against *Burkholderia cepacia* complex, *Burkholderia gladioli* and other non-fermentative Gram-negative bacilli isolated from cystic fibrosis patients. Journal of Antimicrobial Chemotherapy **74**(2): 525–528. doi:10.1093/jac/dky423.

Melnyk, R.A., Youngblut, M.D., Clark, I.C., Carlson, H.K., Wetmore, K.M., Price, M.N., Iavarone, A.T., Deutschbauer, A.M., Arkin, A.P., and Coates, J.D. 2015. Novel Mechanism for Scavenging of Hypochlorite Involving a Periplasmic Methionine-Rich Peptide and Methionine Sulfoxide Reductase. mBio **6**(3): e00233-15. doi:10.1128/mBio.00233-15.

Metzker, M.L. 2010. Sequencing technologies - the next generation. Nature reviews.Genetics **11**(1): 31–46. doi:10.1038/nrg2626.

Moore, R.A., and Hancock, R.E. 1986. Involvement of outer membrane of *Pseudomonas cepacia* in aminoglycoside and polymyxin resistance. Antimicrob Agents Chemother **30**(6): 923–926.

Morin, M., Pierce, E.C., and Dutton, R.J. 2018. Changes in the genetic requirements for microbial interactions with increasing community complexity. eLife **7**: e37072. doi:10.7554/eLife.37072.

Munita, J.M., and Arias, C.A. 2016. Mechanisms of Antibiotic Resistance. Virulence Mechanisms of Bacterial Pathogens, Fifth Edition **4**(2): 481–511. doi:10.1128/microbiolspec.VMBF-0016-2015.

Naguib, M.M., and Valvano, M.A. 2018. Vitamin E Increases Antimicrobial Sensitivity by Inhibiting Bacterial Lipocalin Antibiotic Binding. mSphere **3**(6): e00564-18, /msphere/3/6/mSphere564-18.atom. doi:10.1128/mSphere.00564-18.

Narayanaswamy, V.P., Duncan, A.P., LiPuma, J.J., Wiesmann, W.P., Baker, S.M., and Townsend, S.M. 2019. In Vitro Activity of a Novel Glycopolymer against Biofilms of Burkholderia cepacia Complex Cystic Fibrosis Clinical Isolates. Antimicrob. Agents Chemother. doi:10.1128/AAC.00498-19.

Narayanaswamy, V.P., Giatpaiboon, S., Baker, S.M., Wiesmann, W.P., LiPuma, J.J., and Townsend, S.M. 2017. Novel glycopolymer sensitizes Burkholderia cepacia complex

isolates from cystic fibrosis patients to tobramycin and meropenem. PLoS ONE **12**(6): e0179776. doi:10.1371/journal.pone.0179776.

Nunvar, J., Kalferstova, L., Bloodworth, R.A., Kolar, M., Degrossi, J., Lubovich, S., Cardona, S.T., and Drevinek, P. 2016. Understanding the Pathogenicity of *Burkholderia contaminans*, an Emerging Pathogen in Cystic Fibrosis. PloS one **11**(8): e0160975. doi:10.1371/journal.pone.0160975 [doi].

Ogata, F.T., Branco, V., Vale, F.F., and Coppo, L. 2021. Glutaredoxin: Discovery, redox defense and much more. Redox Biology **43**: 101975. doi:10.1016/j.redox.2021.101975.

Okoliegbe, I.N., Hijazi, K., Cooper, K., Ironside, C., and Gould, I.M. 2021. Trends of Antimicrobial Resistance and Combination Susceptibility Testing of Multidrug-Resistant Pseudomonas aeruginosa Isolates from Cystic Fibrosis Patients: a 10-Year Update. Antimicrob Agents Chemother **65**(6): e02483-20. doi:10.1128/AAC.02483-20.

Oliver, A. 2010. Mutators in cystic fibrosis chronic lung infection: Prevalence, mechanisms, and consequences for antimicrobial therapy. International Journal of Medical Microbiology **300**(8): 563–572. doi:10.1016/j.ijmm.2010.08.009.

Oliver, A., Cantón, R., Campo, P., Baquero, F., and Blázquez, J. 2000. High Frequency of Hypermutable *Pseudomonas aeruginosa* in Cystic Fibrosis Lung Infection. Science **288**(5469): 1251–1253. doi:10.1126/science.288.5469.1251.

Ong, Y.C., and Gasser, G. 2020. Organometallic compounds in drug discovery: Past, present and future. Drug Discovery Today: Technologies **37**: 117–124. doi:10.1016/j.ddtec.2019.06.001.

Opijnen, T. van, Bodi, K.L., and Camilli, A. 2009. Tn-seq: high-throughput parallel sequencing for fitness and genetic interaction studies in microorganisms. Nature methods **6**(10): 767–772. doi:10.1038/nmeth.1377.

Ostermann, M.F., Neubauer, H., Frickmann, H., and Hagen, R.M. 2016. Correlation of *rpsU* gene sequence clusters and biochemical properties, GC—MS spectra and resistance profiles of clinical *Burkholderia* spp. isolates. European Journal of Microbiology and Immunology **6**(1): 25–39. doi:10.1556/1886.2016.00002.

Pal, G., Saxena, S., Kumar, K., Verma, A., Sahu, P.K., Pandey, A., White, J.F., and Verma, S.K. 2022. Endophytic Burkholderia: Multifunctional roles in plant growth promotion and stress tolerance. Microbiological Research **265**: 127201. doi:10.1016/j.micres.2022.127201.

Pang, Z., Raudonis, R., Glick, B.R., Lin, T.-J., and Cheng, Z. 2019. Antibiotic resistance in Pseudomonas aeruginosa: mechanisms and alternative therapeutic strategies. Biotechnology Advances **37**(1): 177–192. doi:10.1016/j.biotechadv.2018.11.013.

Parr, J.T., Moore, R.A., Moore, L.V., and Hancock, R.E. 1987. Role of porins in intrinsic antibiotic resistance of *Pseudomonas cepacia*. Antimicrob Agents Chemother **31**(1): 121–123. doi:10.1128/AAC.31.1.121.

Pedley, A.M., and Benkovic, S.J. 2017. A New View into the Regulation of Purine Metabolism: The Purinosome. Trends in Biochemical Sciences **42**(2): 141–154. doi:10.1016/j.tibs.2016.09.009.

Peeters, E., Sass, A., Mahenthiralingam, E., Nelis, H., and Coenye, T. 2010. Transcriptional response of Burkholderia cenocepacia J2315 sessile cells to treatments with high doses of hydrogen peroxide and sodium hypochlorite. BMC Genomics **11**(1): 90. doi:10.1186/1471-2164-11-90.

Pierce, E.C., Morin, M., Little, J.C., Liu, R.B., Tannous, J., Keller, N.P., Pogliano, K., Wolfe, B.E., Sanchez, L.M., and Dutton, R.J. 2021. Bacterial–fungal interactions revealed by genome-wide analysis of bacterial mutant fitness. Nature Microbiology **6**(1): 87–102. Nature Publishing Group. doi:10.1038/s41564-020-00800-z.

Podnecky, N.L., Rhodes, K.A., and Schweizer, H.P. 2015. Efflux pump-mediated drug resistance in *Burkholderia*. Front. Microbiol. **6**: 305. doi:10.3389/fmicb.2015.00305.

Potamitou, A., Holmgren, A., and Vlamis-Gardikas, A. 2002. Protein Levels of Escherichia coli Thioredoxins and Glutaredoxins and Their Relation to Null Mutants, Growth Phase, and Function. Journal of Biological Chemistry **277**(21): 18561–18567. doi:10.1074/jbc.M201225200.

Pöther, D.-C., Liebeke, M., Hochgräfe, F., Antelmann, H., Becher, D., Lalk, M., Lindequist, U., Borovok, I., Cohen, G., Aharonowitz, Y., and Hecker, M. 2009. Diamide Triggers Mainly S Thiolations in the Cytoplasmic Proteomes of Bacillus subtilis and Staphylococcus aureus. JB **191**(24): 7520–7530. doi:10.1128/JB.00937-09.

Qin, D. 2019. Next-generation sequencing and its clinical application. Cancer Biol Med **16**(1): 4–10.

Rafeeq, M.M., and Murad, H.A.S. 2017. Cystic fibrosis: current therapeutic targets and future approaches. J Transl Med **15**(1): 84. doi:10.1186/s12967-017-1193-9.

Rahal, A., Kumar, A., Singh, V., Yadav, B., Tiwari, R., Chakraborty, S., and Dhama, K. 2014. Oxidative Stress, Prooxidants, and Antioxidants: The Interplay. BioMed Research International **2014**: 1–19. doi:10.1155/2014/761264.

Rajagopal, M., Martin, M.J., Santiago, M., Lee, W., Kos, V.N., Meredith, T., Gilmore, M.S., and Walker, S. 2016. Multidrug intrinsic resistance factors in *Staphylococcus aureus* identified by profiling fitness within high-diversity transposon libraries. MBio **7**(4). doi:10.1128/mBio.00950-16.

Ratjen, F., Bell, S.C., Rowe, S.M., Goss, C.H., Quittner, A.L., and Bush, A. 2015. Cystic fibrosis. Nat Rev Dis Primers **1**(1): 1–19. Nature Publishing Group. doi:10.1038/nrdp.2015.10.

Rees, V.E., Deveson Lucas, D.S., López-Causapé, C., Huang, Y., Kotsimbos, T., Bulitta, J.B., Rees, M.C., Barugahare, A., Peleg, A.Y., Nation, R.L., Oliver, A., Boyce, J.D., and Landersdorfer, C.B. 2019. Characterization of Hypermutator Pseudomonas aeruginosa Isolates from Patients with Cystic Fibrosis in Australia. Antimicrob Agents Chemother **63**(4): e02538-18. doi:10.1128/AAC.02538-18.

Rehman, A., Patrick, W.M., and Lamont, I.L. 2019. Mechanisms of ciprofloxacin resistance in *Pseudomonas aeruginosa*: new approaches to an old problem. Journal of Medical Microbiology **68**(1): 1–10. doi:10.1099/jmm.0.000873.

Rhodes, K.A., and Schweizer, H.P. 2016. Antibiotic resistance in *Burkholderia* species. Drug Resistance Updates **28**: 82–90. doi:10.1016/j.drup.2016.07.003.

Rinaldi, F., Hanieh, P.N., Sennato, S., Santis, F.D., Forte, J., Fraziano, M., Casciardi, S., Marianecci, C., Bordi, F., and Carafa, M. 2021. Rifampicin–Liposomes for Mycobacterium abscessus Infection Treatment: Intracellular Uptake and Antibacterial Activity Evaluation. : 13.

Ronaghi, M., Karamohamed, S., Pettersson, B., Uhlén, M., and Nyrén, P. 1996. Real-Time DNA Sequencing Using Detection of Pyrophosphate Release. Analytical Biochemistry **242**(1): 84–89. doi:10.1006/abio.1996.0432.

Rosales-Reyes, R., Sánchez-Gómez, C., Ortiz-Navarrete, V., and Santos-Preciado, J.I. 2018. *Burkholderia cenocepacia* Induces Macropinocytosis to Enter Macrophages. BioMed Research International **2018**: 1–8. doi:10.1155/2018/4271560.

Ross, B.N., Myers, J.N., Muruato, L.A., Tapia, D., and Torres, A.G. 2018. Evaluating New Compounds to Treat Burkholderia pseudomallei Infections. Front Cell Infect Microbiol **8**. doi:10.3389/fcimb.2018.00210.

Rothberg, J.M., and Leamon, J.H. 2008. The development and impact of 454 sequencing. Nat.Biotechnol. **26**(10): 1117–1124. doi:10.1038/nbt1485.

Roy, P.H., Tetu, S.G., Larouche, A., Elbourne, L., Tremblay, S., Ren, Q., Dodson, R., Harkins, D., Shay, R., Watkins, K., Mahamoud, Y., and Paulsen, I.T. 2010. Complete genome sequence of the multiresistant taxonomic outlier *Pseudomonas aeruginosa* PA7. PLOS ONE **5**(1): e8842. doi:10.1371/journal.pone.0008842.

Sáenz, J.P., Grosser, D., Bradley, A.S., Lagny, T.J., Lavrynenko, O., Broda, M., and Simons, K. 2015. Hopanoids as functional analogues of cholesterol in bacterial membranes. Proc. Natl. Acad. Sci. U.S.A. **112**(38): 11971–11976. doi:10.1073/pnas.1515607112.

Salizzoni, S., Pilewski, J., and Toyoda, Y. 2014. Lung Transplant for a Patient With Cystic Fibrosis and Active *Burkholderia cenocepacia* Pneumonia. Exp Clin Transplant **12**(5): 487–489.

Sanger, F., and Coulson, A.R. 1975. A Rapid Method for Determining Sequences in DNA by Primed Synthesis with DNA Polymerase. J. Mol. Biol. **94**: 441–448. doi:10.1016/0022-2836(75)90213-2.

Sanger, F., Nicklen, S., and Coulson, A.R. 1977. DNA sequencing with chain-terminating inhibitors. Proceedings of the National Academy of Sciences **74**(12): 5463–5467. doi:10.1073/pnas.74.12.5463.

Santiago, M., Lee, W., Fayad, A.A., Coe, K.A., Rajagopal, M., Do, T., Hennessen, F., Srisuknimit, V., Müller, R., Meredith, T.C., and Walker, S. 2018. Genome-wide mutant profiling predicts the mechanism of a Lipid II binding antibiotic. Nature Chemical Biology **14**(6): 601–608. doi:10.1038/s41589-018-0041-4.

Sawana, A., Adeolu, M., and Gupta, R.S. 2014. Molecular signatures and phylogenomic analysis of the genus *Burkholderia*: proposal for division of this genus into the emended genus *Burkholderia* containing pathogenic organisms and a new genus *Paraburkholderia* gen. nov. harboring environmental species. Front. Genet. **5**. doi:10.3389/fgene.2014.00429.

Schmerk, C.L., Bernards, M.A., and Valvano, M.A. 2011. Hopanoid Production Is Required for Low-pH Tolerance, Antimicrobial Resistance, and Motility in Burkholderia cenocepacia. J Bacteriol **193**(23): 6712–6723. doi:10.1128/JB.05979-11.

Schmerk, C.L., and Valvano, M.A. 2013. *Burkholderia multivorans* survival and trafficking within macrophages. J Med Microbiol **62**(Pt 2): 173–184. doi:10.1099/jmm.0.051243-0.

Schmidt, S., Blom, J.F., Pernthaler, J., Berg, G., Baldwin, A., Mahenthiralingam, E., and Eberl, L. 2009. Production of the antifungal compound pyrrolnitrin is quorum sensing-regulated in members of the *Burkholderia cepacia* complex. Environ. Microbiol. **11**(6): 1422–1437. doi:10.1111/j.1462-2920.2009.01870.x.

Scoffone, V.C., Chiarelli, L.R., Trespidi, G., Mentasti, M., Riccardi, G., and Buroni, S. 2017. *Burkholderia cenocepacia* infections in cystic fibrosis patients: drug resistance and therapeutic approaches. Front Microbiol **8**: 1592. doi:10.3389/fmicb.2017.01592.

Selin, C., Stietz, M.S., Blanchard, J.E., Gehrke, S.S., Bernard, S., Hall, D.G., Brown, E.D., and Cardona, S.T. 2015. A pipeline for screening small molecules with growth inhibitory

activity against *Burkholderia cenocepacia*. PLoS ONE **10**(6): e0128587. doi:10.1371/journal.pone.0128587.
Sengupta, R., and Holmgren, A. 2014. Thioredoxin and glutaredoxin-mediated redox regulation of ribonucleotide reductase. **5**(1): 68–74.
Serata, M., Iino, T., Yasuda, E., and Sako, T. 2012. Roles of thioredoxin and thioredoxin reductase in the resistance to oxidative stress in Lactobacillus casei. Microbiology **158**(4): 953–962. doi:10.1099/mic.0.053942-0.
Shan, Y., Brown Gandt, A., Rowe, S.E., Deisinger, J.P., Conlon, B.P., and Lewis, K. 2017. ATP-Dependent Persister Formation in *Escherichia coli*. mBio **8**(1): e02267-16. doi:10.1128/mBio.02267-16.
Shen, S., Li, X.-F., Cullen, W.R., Weinfeld, M., and Le, X.C. 2013. Arsenic Binding to Proteins. Chem. Rev. **113**(10): 7769–7792. doi:10.1021/cr300015c.
Shendure, J., and Ji, H. 2008. Next-generation DNA sequencing. Nature biotechnology **26**(10): 1135–1145. doi:10.1038/nbt1486.
Shirley, M. 2018. Ceftazidime-Avibactam: A Review in the Treatment of Serious Gram-Negative Bacterial Infections. Drugs **78**(6): 675–692. doi:10.1007/s40265-018-0902-x.
Simpson, B.W., and Trent, M.S. 2019. Pushing the envelope: LPS modifications and their consequences. Nat Rev Microbiol **17**(7): 403–416. doi:10.1038/s41579-019-0201-x.
Slachmuylders, L., Van Acker, H., Brackman, G., Sass, A., Van Nieuwerburgh, F., and Coenye, T. 2018. Elucidation of the mechanism behind the potentiating activity of baicalin against Burkholderia cenocepacia biofilms. PLoS ONE **13**(1): e0190533. doi:10.1371/journal.pone.0190533.
Slatko, B.E., Gardner, A.F., and Ausubel, F.M. 2018. Overview of Next-Generation Sequencing Technologies. Current Protocols in Molecular Biology **122**(1): e59. doi:10.1002/cpmb.59.
Smirnova, G.V., and Oktyabrsky, O.N. 2005. Glutathione in bacteria. Biochemistry (Mosc) **70**(11): 1199–1211. doi:10.1007/s10541-005-0248-3.
Smith, A.M., Heisler, L.E., Mellor, J., Kaper, F., Thompson, M.J., Chee, M., Roth, F.P., Giaever, G., and Nislow, C. 2009. Quantitative phenotyping via deep barcode sequencing. Genome research **19**(10): 1836–1842. doi:10.1101/gr.093955.109; 10.1101/gr.093955.109.
Somprasong, N., Yi, J., Hall, C.M., Webb, J.R., Sahl, J.W., Wagner, D.M., Keim, P., Currie, B.J., and Schweizer, H.P. 2021. Conservation of Resistance-Nodulation-Cell Division Efflux Pump-Mediated Antibiotic Resistance in Burkholderia cepacia Complex and Burkholderia pseudomallei Complex Species. Antimicrobial Agents and Chemotherapy **65**(9): e00920-21. American Society for Microbiology. doi:10.1128/AAC.00920-21.
Sonnabend, M.S., Klein, K., Beier, S., Angelov, A., Kluj, R., Mayer, C., Groß, C., Hofmeister, K., Beuttner, A., Willmann, M., Peter, S., Oberhettinger, P., Schmidt, A., Autenrieth, I.B., Schütz, M., and Bohn, E. 2020. Identification of drug resistance determinants in a clinical isolate of *Pseudomonas aeruginosa* by high-density transposon mutagenesis. Antimicrob Agents Chemother **64**(3): e01771-19. doi:10.1128/AAC.01771-19.
Sosnay, P.R., Siklosi, K.R., Van Goor, F., Kaniecki, K., Yu, H., Sharma, N., Ramalho, A.S., Amaral, M.D., Dorfman, R., Zielenski, J., Masica, D.L., Karchin, R., Millen, L., Thomas, P.J., Patrinos, G.P., Corey, M., Lewis, M.H., Rommens, J.M., Castellani, C., Penland, C.M., and Cutting, G.R. 2013. Defining the disease liability of variants in the cystic

fibrosis transmembrane conductance regulator gene. Nat Genet **45**(10): 1160–1167. doi:10.1038/ng.2745.

Stopnisek, N., Bodenhausen, N., Frey, B., Fierer, N., Eberl, L., and Weisskopf, L. 2014. Genus-wide acid tolerance accounts for the biogeographical distribution of soil *Burkholderia* populations: Preference of *Burkholderia* sp. for acid soils. Environ Microbiol **16**(6): 1503–1512. doi:10.1111/1462-2920.12211.

Sutton, B.M., McGusty, E., Walz, D.T., and DiMartino, M.J. 1972. Oral gold. Antiarthritic properties of alkylphosphinegold coordination complexes. J. Med. Chem. **15**(11): 1095–1098. doi:10.1021/jm00281a001.

Tajima, T., Yokota, N., Matsuyama, S., and Tokuda, H. 1998. Genetic analyses of the in vivo function of LolA, a periplasmic chaperone involved in the outer membrane localization of *Escherichia coli* lipoproteins. FEBS Letters **439**(1–2): 51–54. doi:10.1016/S0014-5793(98)01334-9.

Thangamani, S., Mohammad, H., Abushahba, M.F.N., Sobreira, T.J.P., Hedrick, V.E., Paul, L.N., and Seleem, M.N. 2016. Antibacterial activity and mechanism of action of auranofin against multi-drug resistant bacterial pathogens. Sci Rep **6**(1): 22571. doi:10.1038/srep22571.

Thangamani, S., Younis, W., and Seleem, M.N. 2015. Repurposing ebselen for treatment of multidrug-resistant staphylococcal infections. Sci Rep **5**(1): 11596. doi:10.1038/srep11596.

Tseng, S.-P., Tsai, W.-C., Liang, C.-Y., Lin, Y.-S., Huang, J.-W., Chang, C.-Y., Tyan, Y.-C., and Lu, P.-L. 2014. The contribution of antibiotic resistance mechanisms in clinical *Burkholderia cepacia* complex isolates: An emphasis on efflux pump activity. PLoS One **9**(8): e104986. doi:10.1371/journal.pone.0104986.

Tuggle, C.K., and Fuchs, J.A. 1985. Glutathione reductase is not required for maintenance of reduced glutathione in Escherichia coli K-12. J Bacteriol **162**(1): 448–450. doi:10.1128/jb.162.1.448-450.1985.

Valvano, M.A., and Lefebre, M.D. 2001. In vitro resistance of *Burkholderia cepacia* complex isolates to reactive oxygen species in relation to catalase and superoxide dismutase production. Microbiology **147**(1): 97–109. doi:10.1099/00221287-147-1-97.

Van Acker, H., Gielis, J., Acke, M., Cools, F., Cos, P., and Coenye, T. 2016. The Role of Reactive Oxygen Species in Antibiotic-Induced Cell Death in *Burkholderia cepacia* Complex Bacteria. PLoS ONE **11**(7): e0159837. doi:10.1371/journal.pone.0159837.

Van Dalem, A., Herpol, M., Echahidi, F., Peeters, C., Wybo, I., De Wachter, E., Vandamme, P., and Piérard, D. 2018. In Vitro Susceptibility of Burkholderia cepacia Complex Isolated from Cystic Fibrosis Patients to Ceftazidime-Avibactam and Ceftolozane-Tazobactam. Antimicrob Agents Chemother **62**(9). doi:10.1128/AAC.00590-18.

Vandamme, P., Holmes, B., Vancanneyt, M., Coenye, T., Hoste, B., Coopman, R., Revets, H., Lauwers, S., Gillis, M., Kersters, K., and Govan, J.R. 1997. Occurrence *Burkholderia cepacia* in cystic fibrosis patients and proposal of *Burkholderia multivorans* sp. nov. Int. J. Syst. Bacteriol. **47**(4): 1188–1200. doi:10.1099/00207713-47-4-1188.

Vandeplassche, E., Tavernier, S., Coenye, T., and Crabbé, A. 2019. Influence of the lung microbiome on antibiotic susceptibility of cystic fibrosis pathogens. Eur Respir Rev **28**(152): 190041. doi:10.1183/16000617.0041-2019.

Vitale, A., Pessi, G., Urfer, M., Locher, H.H., Zerbe, K., Obrecht, D., Robinson, J.A., and Eberl, L. 2020. Identification of Genes Required for Resistance to Peptidomimetic Antibiotics by Transposon Sequencing. Front. Microbiol. **11**: 1681. doi:10.3389/fmicb.2020.01681.

Waksman, G., Krishna, T.S.R., Jr., C.H.W., and Kuriyan, J. 1994. Crystal Structure of *Escherichia coli* Thioredoxin Reductase Refinded at 2 A Resolution. J. Mol. Bio. **236**(3): 800–816.

Wang, G., Alamuri, P., and Maier, R.J. 2006. The diverse antioxidant systems of *Helicobacter pylori*. Mol Microbiol **61**(4): 847–860. doi:10.1111/j.1365-2958.2006.05302.x.

Wang, H., Claveau, D., Vaillancourt, J.P., Roemer, T., and Meredith, T.C. 2011. High-frequency transposition for determining antibacterial mode of action. Nat.Chem.Biol. **7**(10): 720–729. doi:10.1038/nchembio.643.

Wetmore, K.M., Price, M.N., Waters, R.J., Lamson, J.S., He, J., Hoover, C.A., Blow, M.J., Bristow, J., Butland, G., Arkin, A.P., and Deutschbauer, A. 2015. Rapid quantification of mutant fitness in diverse bacteria by sequencing randomly bar-coded transposons. MBio **6**(3): e00306-00315. doi:10.1128/mBio.00306-15.

Wigfield, S.M., Rigg, G.P., Kavari, M., Webb, A.K., Matthews, R.C., and Burnie, J.P. 2002. Identification of an immunodominant drug efflux pump in *Burkholderia cepacia*. J.Antimicrob.Chemother. **49**(4): 619-624.

Wilmaerts, D., Windels, E.M., Verstraeten, N., and Michiels, J. 2019. General Mechanisms Leading to Persister Formation and Awakening. Trends in Genetics **35**(6): 401–411. doi:10.1016/j.tig.2019.03.007.

Wood, T.K., Knabel, S.J., and Kwan, B.W. 2013. Bacterial persister cell formation and dormancy. Appl.Environ.Microbiol. **79**(23): 7116–7121. doi:10.1128/AEM.02636-13.

Wu, B., Yang, X., and Yan, M. 2019. Synthesis and Structure–Activity Relationship Study of Antimicrobial Auranofin against ESKAPE Pathogens. J. Med. Chem. **62**(17): 7751–7768. doi:10.1021/acs.jmedchem.9b00550.

Yabuuchi, E., Kawamura, Y., Ezaki, T., Ikedo, M., Dejsirilert, S., Fujiwara, N., Naka, T., and Kobayashi, K. 2000. *Burkholderia uboniae* Sp. Nov., L -Arabinose-Assimilating but Different from *Burkholderia thailandensis* and *Burkholderia vietnamiensis*. Microbiology and Immunology **44**(4): 307–317. doi:10.1111/j.1348-0421.2000.tb02500.x.

Yabuuchi, E., Kosako, Y., Oyaizu, H., Yano, I., Hotta, H., Hashimoto, Y., Ezaki, T., and Arakawa, M. 1992. Proposal of *Burkholderia* gen. nov. and transfer of seven species of the genus *Pseudomonas* homology group II to the new genus, with the type species *Burkholderia cepacia* (Palleroni and Holmes 1981) comb. nov. Microbiology and Immunology **36**(12): 1251–1275. doi:10.1111/j.1348-0421.1992.tb02129.x.

Yang, J.H., Wright, S.N., Hamblin, M., McCloskey, D., Alcantar, M.A., Schrübbers, L., Lopatkin, A.J., Satish, S., Nili, A., Palsson, B.O., Walker, G.C., and Collins, J.J. 2019. A White-Box Machine Learning Approach for Revealing Antibiotic Mechanisms of Action. Cell **177**(6): 1649-1661.e9. doi:10.1016/j.cell.2019.04.016.

Yarlagadda, V., Akkapeddi, P., Manjunath, G.B., and Haldar, J. 2014. Membrane Active Vancomycin Analogues: A Strategy to Combat Bacterial Resistance. J. Med. Chem. **57**(11): 4558–4568. doi:10.1021/jm500270w.

Yasir, M., Turner, A.K., Bastkowski, S., Baker, D., Page, A.J., Telatin, A., Phan, M.-D., Monahan, L., Savva, G.M., Darling, A., Webber, M.A., and Charles, I.G. 2020. TraDIS-Xpress: a high-resolution whole-genome assay identifies novel mechanisms of triclosan action and resistance. Genome Res. **30**(2): 239–249. doi:10.1101/gr.254391.119.

Zeiser, E.T., Becka, S.A., Wilson, B.M., Barnes, M.D., LiPuma, J.J., and Papp-Wallace, K.M. 2019. “Switching partners”: piperacillin-avibactam is a highly potent combination against multidrug-resistant *Burkholderia cepacia* complex and *Burkholderia gladioli* cystic fibrosis isolates. Journal of Clinical Microbiology **57**(8): e00181-19. doi:10.1128/JCM.00181-19.

Zhanel, G.G., Wiebe, R., Dilay, L., Thomson, K., Rubinstein, E., Hoban, D.J., Noreddin, A.M., and Karlowsky, J.A. 2007. Comparative Review of the Carbapenems: Drugs **67**(7): 1027–1052. doi:10.2165/00003495-200767070-00006.

Zheng, E.J., Stokes, J.M., and Collins, J.J. 2020. Eradicating Bacterial Persisters with Combinations of Strongly and Weakly Metabolism-Dependent Antibiotics. Cell Chemical Biology: S2451945620303378. doi:10.1016/j.chembiol.2020.08.015.

Zheng, M., Åslund, F., and Storz, G. 1998. Activation of the OxyR Transcription Factor by Reversible Disulfide Bond Formation. Science **279**(5357): 1718–1722. doi:10.1126/science.279.5357.1718.